

Enhancement of a decellularized tracheal scaffold for tracheal tissue engineering



A Dissertation Submitted in Partial Fulfillment of the Requirements
for the Degree of Doctor of Philosophy in Medical Sciences
Faculty Of Medicine
Chulalongkorn University
Academic Year 2023

การเพิ่มประสิทธิภาพของเนื้อเยื่อหลอดลมที่ปราศจากเซลล์สำหรับวิศวกรรมเนื้อเยื่อหลอดลม



วิทยานิพนธ์นี้เป็นส่วนหนึ่งของการศึกษาตามหลักสูตรปริญญาวิทยาศาสตรดุษฎีบัณฑิต
สาขาวิชาวิทยาศาสตร์การแพทย์
คณะแพทยศาสตร์ จุฬาลงกรณ์มหาวิทยาลัย
ปีการศึกษา 2566

เพื่อสุตา สมญา : การเพิ่มประสิทธิภาพของเนื้อเยื่อหลอดลมที่ปราศจากเซลล์สำหรับวิศวกรรมเนื้อเยื่อหลอดลม. (Enhancement of a decellularized tracheal scaffold for tracheal tissue engineering) อ.ที่ปรึกษาหลัก : ผศ. ดร.สุพรรณษา ยอดเมือง, อ.ที่ปรึกษาร่วม : รศ. ทพ.ดร.โจวแอล นู๋ แอนดร้าตรี ริคิเซ พิเรียร์

การสร้างหลอดลมทดแทนเพื่อใช้รักษาหลอดลมที่ได้รับบาดเจ็บในปัจจุบันยังไม่มีแนวทางปฏิบัติที่เป็นมาตรฐาน เนื่องจากความซับซ้อนของโครงสร้างและการทำงานของหลอดลม การรักษาโดยใช้เซลล์และเนื้อเยื่อของผู้ป่วยมาเพาะเลี้ยงบนสารเคลือบเซลล์ (extracellular matrix, ECM) เป็นหนึ่งในทางเลือกของการรักษาโดยใช้หลักการวิศวกรรมเนื้อเยื่อ วัตถุประสงค์ของการศึกษานี้เพื่อพัฒนาโครงเลี้ยงเซลล์จากหลอดลมที่ปราศจากเซลล์ โดยการใช้หลอดลมสุนัขเป็นแบบจำลองในการศึกษากระบวนการล้างเซลล์และการสร้างโครงสร้างบรรจุเซลล์ซึ่งสามารถนำมาปรับใช้กับหลอดลมมนุษย์ต่อไป หลอดลมสุนัขถูกล้างเซลล์ด้วยวิธี vacuum-assisted decellularization (VAD) และถูกพัฒนาไปเป็นโครงสร้างบรรจุเซลล์ 2 ชนิด คือ หลอดลมที่ปราศจากเซลล์ (dTracheal scaffold) และไฮโดรเจลจากเนื้อเยื่อหลอดลมที่ปราศจากเซลล์ (dECM hydrogel) จากการตรวจวิเคราะห์ด้วย Histology และ Biochemistry assay พบว่าเซลล์ในหลอดลมถูกล้างออกอย่างมีประสิทธิภาพ เห็นได้จากปริมาณ DNA และโมเลกุล Major Histocompatibility complex (MHC) class II ลดลงอย่างมีนัยสำคัญทางสถิติ และยังคงรักษาปริมาณสารเคลือบเซลล์ไว้หลังจากผ่านกระบวนการล้างเซลล์ กล้องจุลทรรศน์อิเล็กตรอนแบบส่องกราดแสดงให้เห็นโครงสร้างเส้นใยของสารเคลือบเซลล์ ผลการทดสอบความเป็นพิษต่อเซลล์พบว่าหลอดลมที่ปราศจากเซลล์มีความเข้ากันได้ทางชีวภาพกับเซลล์เยื่อบุผิว และพบว่าเซลล์ต้นกำเนิดมีเซนไคม์ของมนุษย์มีชีวิตรอดในไฮโดรเจลที่พัฒนาขึ้นหลังจากเพาะเลี้ยงเป็นเวลา 3 วัน นอกจากนี้ได้ทำการศึกษาบทบาทของไฟโบรบลาสต์ต่อการสร้างเนื้อเยื่อบุผิวของหลอดลมในหลอดทดลอง โดยใช้การเพาะเลี้ยงสองเซลล์ร่วมกัน (co-culture) ระหว่างเซลล์เยื่อบุผิว และไฟโบรบลาสต์ บนพื้นผิวด้านในของหลอดลมที่ปราศจากเซลล์ พบว่ามีการก่อตัวของเซลล์เยื่อบุผิวบนชั้นเยื่อเมือกหลังจากเพาะเลี้ยงเซลล์ร่วมกันเป็นเวลา 21 วัน เมื่อเปรียบเทียบกับ การเพาะเลี้ยงที่ไม่มีไฟโบรบลาสต์ร่วมด้วยพบว่าเซลล์เยื่อบุผิวแทรกลงไปในพื้นที่เยื่อเมือก ส่วนการเพาะเลี้ยงสามเซลล์ร่วมกัน (Tri-culture) ระหว่างเซลล์เยื่อบุผิว เซลล์ไฟโบรบลาสต์ และเซลล์ต้นกำเนิดมีเซนไคม์ของมนุษย์ พบว่ามีการก่อตัวของเซลล์เยื่อบุผิวบนชั้นเยื่อเมือกเช่นเดียวกับการเพาะเลี้ยงสองเซลล์ร่วมกัน นอกจากนี้เซลล์ต้นกำเนิดมีเซนไคม์ของมนุษย์ที่ผสมกับไฮโดรเจลที่พัฒนาขึ้น มีความสามารถเปลี่ยนแปลงเป็นเนื้อเยื่อที่มีลักษณะคล้ายกระดูกอ่อนบนพื้นผิวด้านนอกของหลอดลม โดยยืนยันได้จาก การย้อมติดสีฟ้าของ Alcian blue ซึ่งแสดงให้เห็นถึงการสร้างไกลโคซามิโนไกลแคน (sGAG) และตรวจพบ Collagen type II การเพาะเลี้ยงสามเซลล์ร่วมกันพบการแสดงออกของโปรตีนที่เกี่ยวข้องกับการก่อตัวของเซลล์เยื่อบุผิว เช่น epithelial tight junction, ciliation, และ mucin production ตามที่ประเมินด้วยวิธี Immunostaining นอกจากนี้การวิเคราะห์โปรตีนโอมิกส์ระบุการเพิ่มขึ้นของโปรตีน alpha-tubulin, beta-tubulin, vimentin, collagen type VI และ tenascin-C ในการเพาะเลี้ยงสามเซลล์ร่วมกัน การศึกษาทั้งหมดนี้แสดงให้เห็นถึงข้อมูลเชิงลึกของหลอดลมที่ปราศจากเซลล์และไฮโดรเจลที่พัฒนาขึ้นจากเนื้อเยื่อหลอดลมที่ปราศจากเซลล์ทั้งในด้านโครงสร้างและชีวเคมี บทบาทของไฟโบรบลาสต์ในการสร้างเยื่อบุผิว การพัฒนาและเปลี่ยนแปลงของเซลล์ต้นกำเนิดมีเซนไคม์ของมนุษย์ไปเป็นเนื้อเยื่อกระดูกอ่อน รวมทั้งแสดงให้เห็นว่าโครงสร้างเนื้อเยื่อหลอดลมที่เหมาะสม อาจนำไปสู่การพัฒนาไปเป็นเนื้อเยื่อที่ทำงานได้ การศึกษานี้ได้สร้างองค์ความรู้ที่มีศักยภาพนำไปสู่การสร้างหลอดลมทดแทนในอนาคต

สาขาวิชา วิทยาศาสตร์การแพทย์
ปีการศึกษา 2566

ลายมือชื่อนิสิต
ลายมือชื่อ อ.ที่ปรึกษาหลัก
ลายมือชื่อ อ.ที่ปรึกษาร่วม

6271003330 : MAJOR MEDICAL SCIENCES

KEYWORD: Decellularized trachea, re-epithelization, extracellular matrix, hydrogels, cartilage formation, airway tissue formation

Pensuda Sompunga : Enhancement of a decellularized tracheal scaffold for tracheal tissue engineering.

Advisor: Asst. Prof. SUPANSA YODMUANG, Ph.D. Co-advisor: Assoc. Prof. JOAO NUNO ANDRADE REQUICHA

FERREIRA, D.D.S.,MSc.,Ph.D.

Development of tracheal substitutions currently lacks a standard protocol due to the complexity of trachea structure and function. Tissue-based treatments using patient's cells grown on an extracellular matrix (ECM) from donor tissue are promising approach in tissue engineering. The aim of this study was to develop canine dECM-based tissue engineered tracheal constructs, which serve as tissue model to develop decellularization process and cell carriers. Canine tracheas were performed vacuum-assisted decellularization (VAD) to create dual cell carrier systems, which are a decellularized tracheal scaffold (dTracheal scaffold) and a dECM hydrogel. The results from histology and biochemistry assay found that dTracheal scaffolds were effectively decellularized, resulting in a significantly low level of DNA content and Major histocompatibility complex class II. However, decellularization process preserved ECM components. Scanning electron micrographs revealed a fibrous structure of ECM network. The cytotoxicity testing demonstrated the biocompatibility with epithelial cells. Moreover, hMSCs encapsulated in ECM-rich hydrogel for 3 days showed excellent viability. Furthermore, the effects of fibroblasts on epithelial tissue formation *in vitro* were evaluated by a co-culture system between epithelial cells and fibroblasts, cultured on the luminal surface of the dTracheal scaffold. The H&E staining demonstrated a ciliated epithelial formation on the mucosa layer after co-culture for 21 days, while an epithelial cell monoculture group could observe the epithelial cell infiltration in the submucosa layer. The tri-culture system between epithelial cells, fibroblasts, and human mesenchymal stem cells (hMSCs) exhibited a ciliated epithelial formation on the mucosa layer similar to co-culture construct. Moreover, hMSCs encapsulated in dECM hydrogel demonstrated a chondrogenic differentiation to cartilage-like tissue, which confirms by Alcian blue staining of sGAG and detection of collagen type II. The tri-culture construct found the expression of proteins associated with epithelium tissue formation, such as epithelial tight junctions, ciliation, and mucin production, as assessed by immunostaining. Furthermore, proteomics analysis identified the increase of proteins such as alpha-tubulin, beta-tubulin, vimentin, collagen type VI, and tenascin-C in the tri-culture construct. This study highlights an insightful information of structure and biochemistry of the decellularized trachea scaffold and the hydrogel, an influence of fibroblasts on epithelial layer formation and chondrogenic differentiation of hMSCs. Furthermore, this study provides a proof-of-concept for creating a well-structured trachea that can effectively function. Additionally, it contributes to the formation of knowledge and sets the stage for the future development of tracheal substitutes.

Field of Study: Medical Sciences

Academic Year: 2023

Student's Signature

Advisor's Signature

Co-advisor's Signature

ACKNOWLEDGEMENTS

I would like to express my sincere thanks to my thesis advisor, Assistance Prof. Dr. Supansa Yodmuang for her invaluable help and constant encouragement throughout the course of this research. I am most grateful for her teaching and advice, not only the research methodologies but also many other methodologies in life. I would not have achieved this far, and this thesis would not have been completed without all the support that I have always received from her.

I would like to extend my heartfelt appreciation to my co-advisor, Associate Prof. Dr. Joao Nuno Andrade Requicha Ferreira for his invaluable assistance and unwavering support throughout this research. His expertise and insights greatly enriched the quality of this work. I am sincerely grateful for his mentorship, which extended beyond academics and encompassed various aspects of life. His guidance has been instrumental in reaching this point, and this thesis would not have been possible without their continuous encouragement and contributions.

I would like to gratitude to Mrs. Athitaya Rungwong from the Department of Anatomy, Faculty of Medicine, Chulalongkorn University, and Mr. Kittipot Kongsonthana from the Department of Anatomy, Faculty of Veterinary Science, Chulalongkorn University for invaluable advice on histological work and training.

Many thanks to SY laboratory members: Sonthikan Sitthisang, Panitporn Laowpanitchakorn, Trúc Nguyễn Thanh, Nattapak Darumas, Sairash Yousaf, Naree Sompao, Yamin Oo and other workers in the laboratory of Assistance Prof. Dr. Supansa Yodmuang and Associate Prof. Dr. Joao Ferreira for assistant, guidance, and suggestion about laboratory work. My research would not have been possible without their support.

Finally, I would also like to thank my parents, sister, and brother for always supporting and encouraging me with their best wishes.

Pensuda Sompunga

TABLE OF CONTENTS

	Page
ABSTRACT (THAI)	iii
ABSTRACT (ENGLISH)	iv
ACKNOWLEDGEMENTS	v
TABLE OF CONTENTS	vi
LIST OF TABLES	10
LIST OF FIGURES	11
CHAPTER I INTRODUCTION.....	13
1.1 Background and Rationale.....	13
1.2 Objectives	14
1.3. Research questions	14
1.4. Hypothesis.....	15
1.5. Keywords.....	15
1.6. Conceptual framework.....	16
1.7. Research Design.....	17
CHAPTER II LITERATURE REVIEWS	19
2.1 Anatomy of Trachea	19
2.2 Tracheal diseases	22
2.3 Tracheal tissue engineering.....	23
2.3.1 Decellularized tracheal matrix scaffold	26
2.3.2 Re-epithelization and regeneration of tracheal cartilage	28
2.3.3 Decellularized extracellular matrix (dECM)-derived hydrogels	29

CHAPTER III METERIALS AND METHODS.....	31
3.1 Part I: Preparation of decellularized trachea.....	31
3.1.1 Chemicals and reagents.	31
3.1.2. Harvesting canine trachea tissue	31
3.1.3. Decellularization process of tracheal tissue	31
3.1.4. Histology and immunohistochemistry.....	34
3.1.5. Biomechanical assessment.....	35
3.1.6. Biochemical assay.....	35
3.1.7 Re-epithelization and cytocompatibility.....	36
3.1.8. Micromorphological assessment of dTrachea	36
3.2 Part II: Development of decellularized extracellular matrix (dECM)-derived hydrogels	37
3.2.1 Decellularization of canine trachea	37
3.2.2 Preparation of dECM hydrogel.....	37
3.2.3 Gelation kinetic of decellularized extracellular matrix (dECM).....	38
3.2.4 Characterization of dECM solution.....	38
3.2.5 Micromorphological assessment of dECM hydrogel.....	39
3.2.6 Human mesenchymal stem cells viability on dECM hydrogel	39
3.2.6.1 Cell culture.....	39
3.2.6.2 Evaluation of cell viability on dECM hydrogel	40
3.2.7 Endothelial cell tube formation <i>in vitro</i> study.	40
3.2.8 Assessment of injectable dECM hydrogel for cartilage formation	41
3.3 Part III: Effects of fibroblasts on tracheal tissue formation.....	42
3.3.1 Cell culture and dTracheal scaffold preparation.....	42

3.3.2 Co-culture and tri-culture of epithelial cells, fibroblasts and hMSCs embedded canine dECM-fibrin hydrogel.....	43
3.3.3 Formation of co-culture system.....	45
3.3.3.1 Phase 1: Cell expansion.....	46
3.3.3.2 Phase 2: Fibroblasts seeding.....	46
3.3.3.3 Phase 3: Re-epithelialization.....	46
3.3.3.4 Phase 4: Epithelial cell differentiation (air-liquid interphase culture, ALI).....	47
3.3.4 Formation of tri-culture system.....	48
3.3.4.1 Phase 1: Cell expansion.....	49
3.3.4.2 Phase 2: hMSCs seeding.....	49
3.3.4.3 Phase 3: Fibroblasts seeding.....	49
3.3.4.4 Phase 4: Re-epithelialization.....	49
3.3.4.5 Phase 5: Epithelial cell differentiation (air-liquid interphase culture, ALI).....	50
3.3.5 TEER measurements.....	50
3.3.6 Histological and Immunofluorescence analysis.....	51
3.3.7 Protein quantitation using mass spectrometry.....	53
3.3.8 Bioinformatic analysis of proteomics data.....	53
3.4 Data Analysis and Statistics.....	54
CHAPTER IV RESULTS.....	55
4.1 The presence of decellularized trachea scaffold (VAD).....	55
4.2 Biomechanical characteristics of decellularized trachea (dTrachea).....	58
4.3 Biochemical qualification of decellularized trachea and dECM solution.....	59
4.4 The evaluation of re-epithelization in decellularized trachea.....	60

4.5 Characterization and gelation process of the dECM solution.....	62
4.6 The microarchitectural features of dECM hydrogel	63
4.7 Cytocompatibility of dECM hydrogel	64
4.8 Viability and tube formation assay of HUVECs.....	66
4.9 Histological analysis of chondrogenic differentiation of hMSCs in dTracheal scaffold	67
4.10 Fibroblasts support epithelium tissue formation and ciliated epithelial cell differentiation on decellularized tracheal scaffold (dTracheal scaffold).....	70
4.10.1 Histoarchitecture.....	70
4.10.2 Cartilage formation.....	73
4.10.3 Protein expression proves epithelium differentiation and function by immunofluorescence staining.....	76
4.11. Evaluation of barrier function.....	80
4.12. Proteomics analysis	81
4.12.1 Protein composition of dTracheal scaffold and dECM hydrogel.....	81
4.12.2 Protein profiling of tri-culture construct	84
CHAPTER V Discussion and conclusion	88
Ethical Consideration	99
Tabulation of research activities and timeline	100
Funding	102
Supplementary data	103
Supplementary data (preliminary data).....	119
REFERENCES	147
VITA.....	149

LIST OF TABLES

Table 1 Human airway epithelial cell marker genes and proposed function	20
Table 2 The list of cells and mediums used in the experiment.....	43
Table 3 The series of primary and secondary antibodies in immunofluorescence staining.....	52
Table 4 The mechanical parameters of unwashed trachea and decellularized trachea.	58



LIST OF FIGURES

Figure 1 Structure of trachea.....	21
Figure 2 Blood supply to trachea.....	22
Figure 3 The therapeutic options of tracheal replacement.	24
Figure 4 Graft types of trachea in clinical applications.....	26
Figure 5 Schematic diagram of the vacuum-assisted decellularization (VAD) of trachea.	33
Figure 6 Experimental designs in co-culture and tri-culture system	44
Figure 7 The overview of experimental design divided into 4 phases. Cell expansion, fibroblasts seeding, re-epithelialization and epithelial differentiation.	45
Figure 8 The overview of experimental design divided into 5 phases. Cell expansion, hMSC seeding, fibroblasts seeding,.....	48
Figure 9 Histological evaluation of decellularized tracheas. A) Hematoxylin and eosin (H&E) staining; B) Pentachrome staining; C) Immunostaining of the MHC-II.	57
Figure 10 Immunofluorescence detection of laminin and fibronectin in decellularized tracheas. A) laminin and B) fibronectin in decellularized trachea (dTrachea) compared to the unwashed trachea (Control).....	57
Figure 11 DNA contents and extracellular matrix composition of decellularized trachea.....	59
Figure 12 Re-epithelialization of decellularized trachea.....	61
Figure 13 Characterization of extracellular matrix-derived solution (dECM solution)..	63
Figure 14 Characterization of extracellular matrix-derived hydrogel (dECM hydrogel) 64	
Figure 15 In vitro cytotoxicity evaluation of dECM hydrogels.....	65
Figure 16 HUVEC viability and tube formation.....	67
Figure 17 Histological analysis.....	69

Figure 18 Comparison of co-culture system pre- and post-differentiation stained with H&E staining.	71
Figure 19 Comparison of tri-culture system pre- and post-differentiation stained with H&E staining.	72
Figure 20 Comparison of tri-culture system pre- and post-differentiation stained with H&E staining.	74
Figure 21 Histological analysis of study in tri-culture system: the appearance of the tracheal cartilage stained with Alcian blue and Immunohistochemistry staining post-differentiation.	75
Figure 22 Immunofluorescence staining of co-culture and tri-culture system in pre- and post-differentiation.....	77
Figure 23 Immunofluorescence staining of E-cadherin in pre-and post-differentiation.	79
Figure 24 Immunofluorescence staining against A) actin, B) E-cadherin, C) alpha-tubulin and D) mucin on cross sections of tri-culture constructs at 21 days (post-differentiation).....	80
Figure 25 Functional assessment of the epithelial barrier properties for each in vitro model.....	81
Figure 26 The proteomics dataset analyzed for biological significance of dTracheal scaffold and dECM hydrogel.	83
Figure 27 Gene Ontology Enrichment Analysis of dTracheal scaffold and dECM hydrogel by ShinyGO v0.74.	84
Figure 28 The proteomics dataset analyzed for biological significance of tri-culture. A) Sampling of tri-culture constructs for proteomics analysis.	86
Figure 29 Gene Ontology Enrichment Analysis of tri-culture constructs by ShinyGO v0.77.	87

CHAPTER I INTRODUCTION

1.1 Background and Rationale

Tracheobronchial injury and tracheal diseases are a cause of mortality worldwide such as tracheal stenosis, chronic obstructive pulmonary disease (COPD), cystic fibrosis (CF), trauma and tracheal, bronchial, and other lung cancers [1]. Currently, tracheal resection with direct end-to-end anastomosis is mostly used for treatment. However, this treatment is difficult for tracheal reconstruction in the case of 30% of the total length in children and longer than 6 cm in adults [2]. Thus, tracheal reconstruction would be achieved in a case with long-segment tracheal (longer than 6 cm) [3] through trachea transplantation with tracheal substitutes.

Tissue engineering offers the creation of functional tissue from cells in the laboratory. Tissue engineering has evolved from the field of biomaterials development and refers to the practice of combining scaffold or biomaterial, cells, and biologically active molecules into functional tissues [4]. The role of tissue engineering is to assemble functional constructs that restore, maintain, or improve damaged tissues or whole organs. Tubular structure, natural extracellular matrix components, appropriate mechanical strength, and good biocompatibility are indicated to biologic decellularized tracheal scaffold that is the best option for the development of trachea substitutes [2]. The several decellularization methods of trachea have been established for the removal of cells and immunogenic material by physical, chemical and enzymatic methods or combinative methods. Numerous studies mostly employed chemical and enzymatic methods, especially the detergent enzymatic decellularization (DED) and its modifications [5]. Recently, vacuum-assisted decellularization (VAD) which is a combinative method can enable chemical agents to reach the whole tissue resulting in accelerated scaffold production and reduces the associated costs [6-8]. This could be an alternative approach to preparing the tracheal scaffold for tracheal transplantation. Decellularized tracheal scaffolds could be systematically investigated under the concept of structure, leading to function. Nonetheless, tracheal tissue engineering

is currently no gold standard for tracheal replacement.

Unfortunately, few studies have been carried out on canine decellularized tracheal matrix scaffold. There is no previous report about decellularized extracellular matrix (dECM)-derived hydrogels develop from trachea of canine. Ideally, canine tracheal hold similar mechanical and dimensional characteristics to human trachea [9]. This is because the lateral diameter and anterior-posterior of canine trachea are approximately human trachea, which considers an outstanding animal model for trachea research. Accordingly, the present study attempts to establish that canine trachea would be a strong ideal of tracheal scaffold to regenerate trachea tissues which includes decellularization, re-epithelization, cartilage formation and development of injectable-derived extracellular matrix hydrogel to support the superlative of tracheal scaffolds for tracheal tissue engineering.

1.2 Objectives

Primary objective

To develop canine dECM-based tissue engineered tracheal constructs *in vitro* as viable tissue substitutes for human tracheal defects

Secondary objectives

1. To evaluate decellularized tissue outcomes of the trachea by vacuum-assisted decellularization (VAD) for re-epithelialization
2. To develop dECM-derived hydrogels for cartilage tissue formation and tracheal revascularization *in vitro*
3. To investigate biological effects of fibroblasts on epithelial tissue formation using co- and tri-culture system

1.3. Research questions

Primary question

Can the dECM scaffold support tracheal tissue formation *in vitro*?

Secondary question

1. Can the vacuum-assisted decellularization (VAD) method preserves biochemical cues of tissue and supports re-epithelialization?
2. Can the dECM-derived hydrogel promotes cartilage tissue formation and supports blood vessel formation *in vitro*?
3. Can fibroblasts enhance epithelial tissue formation and induce ciliated epithelial cell differentiation *in vitro*?

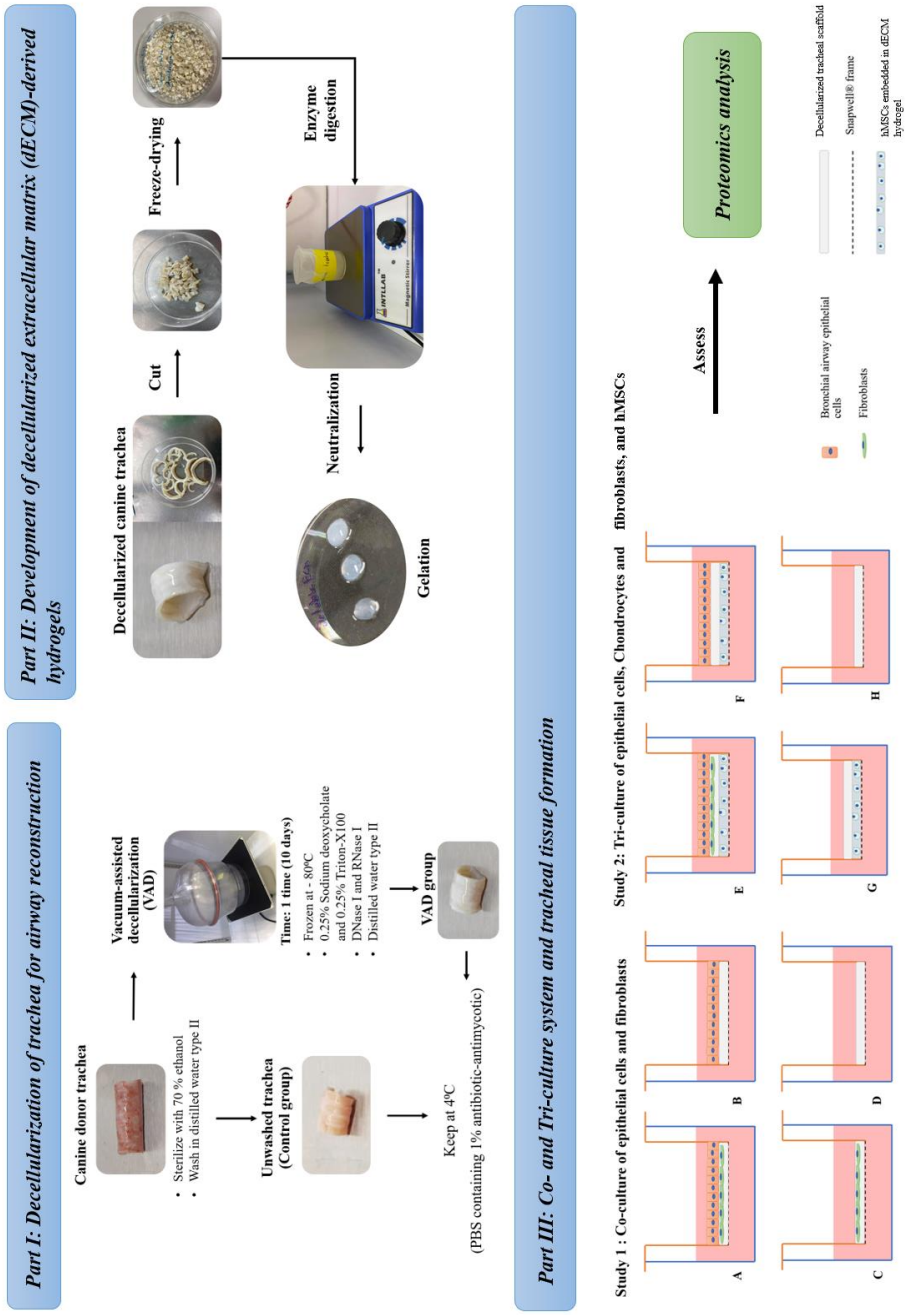
1.4. Hypothesis

1. Decellularized trachea obtained from the VAD method retains biochemical components and promotes re-epithelialization.
2. Hydrogel developed from decellularized tracheal scaffold promotes cartilage tissue formation and supports blood vessel formation *in vitro*.
3. Co-culture with fibroblasts can enhance epithelial tissue formation and induce ciliated epithelial cell differentiation *in vitro*.

1.5. Keywords

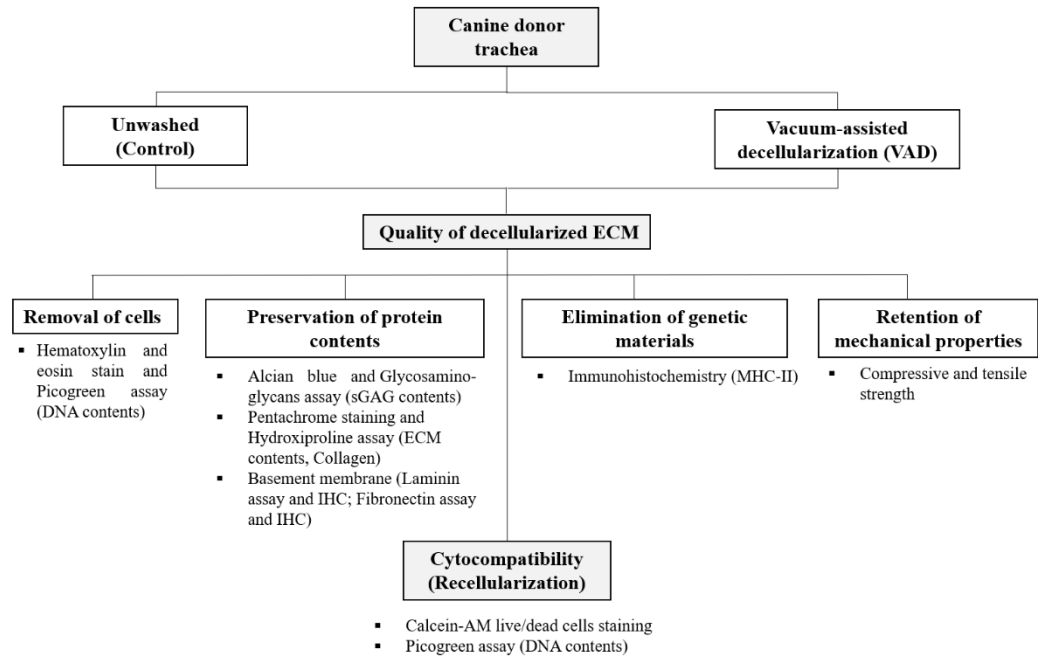
Decellularized trachea, re-epithelization, extracellular matrix, hydrogels, cartilage formation, airway tissue formation

1.6. Conceptual framework

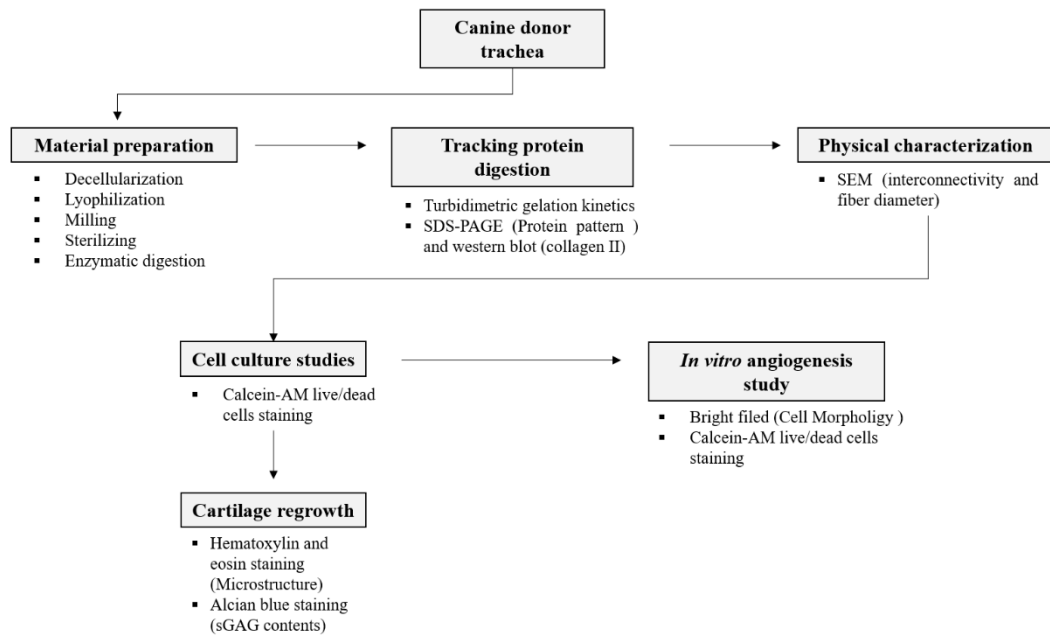


1.7. Research Design

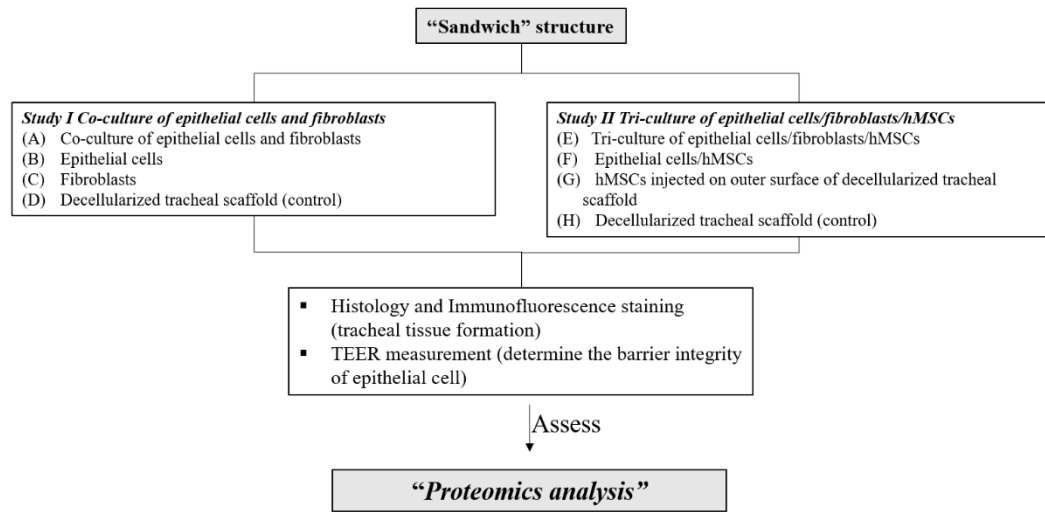
Part I: Preparation of decellularized trachea



Part II: Development of decellularized extracellular matrix (dECM)-derived hydrogels



Part III: Effects of fibroblasts on for tracheal tissue formation



CHAPTER II LITERATURE REVIEWS

2.1 Anatomy of Trachea

The trachea (windpipe) in human is the lower main airway to the lungs that is further divided into the right and left bronchi, where gas exchange occurs. The trachea defines the beginning from the cricoid cartilage and extends to the carina at the level of the fifth thoracic vertebra (8). The trachea is a cartilaginous tubular structure that consists of 18-22 C-shape hyaline cartilaginous rings covered with fibrous tissue and bridged by smooth muscle (**Fig. 1**). The average length of the trachea is 11.8 cm, with a normal range of 10 to 13 cm in males, while the trachea length in females is shorter. The height and the wall thickness average of each tracheal ring are about 4 mm and 3mm, respectively. Moreover, the average external diameter of the trachea is 2.3 cm [10, 11].

The wall of the trachea involves four distinct tissue layers (figure 1). The luminal mucosa is a first layer including lined with pseudostratified columnar ciliated epithelium with goblet cells where is complex in terms of cell type and function. Cell types include ciliated columnar cells, mucous (goblet) cells, basal/progenitor cells (BSCs), and brush cells. Thus, the epithelium is a multilayered tissue. Goblet cells and ciliated cells are essentially responsible for the defense mechanism. Because goblet cells secrete mucus, and cilia act in partnership to trap and expel particles or microorganisms that enter the airway. Furthermore, the mucus covers many mucins involved in the host-response defense, including response to infection, inflammation and the presence of foreign particles [12, 13]. BSCs act as resident stem cells for the trachea and proximal airway. Moreover, these cells are capable of repopulation of the pseudostratified columnar ciliated epithelium during hemostasis and after injury [14]. In addition, the summary of key markers in each cell type and proposed function of human airway are shown in **Table 1**. A deep layer to the mucosa is the submucosa, which encloses a loose meshwork of connective tissue, containing large blood vessels, nerves, and the seromucous gland. The seromucous secretes glycoprotein that is a combination of water and mucus to the luminal

surface through ducts. The external to submucosa is a cartilaginous layer containing C-shaped hyaline cartilage. This layer provides flexibility and maintains patency of lumen. The trachea is underlined with heterogeneous mesenchymal cell lineages which includes cartilage around the trachea, smooth muscle and interstitial fibroblasts, and which act as niche-supporting cells to regulate the regenerative response of airway epithelium after injury [14]. The adventitia is the outer layer of a band of loose connective tissue binding the trachea to the esophagus and other nearby organs [15].

Table 1 Human airway epithelial cell marker genes and proposed function [14]

Cell type	Marker genes	Proposed function
Basal cells	TRP63, KRT5	Progenitor cells for the airway epithelia
Secretory (club) cells	SCGB1A1, SCGB3A2	Produce various factors with protective and immunomodulatory functions, and serve in detoxification of harmful substances
Multiciliated cells	FOXJ1, TUBB3	Expel the mucus together with the entrapped particulates
Goblet cells	MUC5AC, MUC5B	Secrete mucus to entrap inhaled particulates
Pulmonary neuroendocrine cells (PNECs)	CALCA, ASCL1	Involve solitary in clusters known as neuroendocrine bodies that act as probe the microenvironment to influence smooth muscle tone and regulate immune responses.
Brush cells	IL-25, TSLP	Immune and taste sensor, leukotriene synthesis, links to type 2 immunity
Airway smooth muscle cells	ACTA2, LGR6	Control airway caliber and resist the airflow of the entire tracheobronchial tree
Fibroblast cells	GLI1, AXIN2	Role for the interstitial lung fibroblasts in lung wound repair and regeneration (unclear of transcriptional signature, phenotypic identity, and biological dynamic activities)

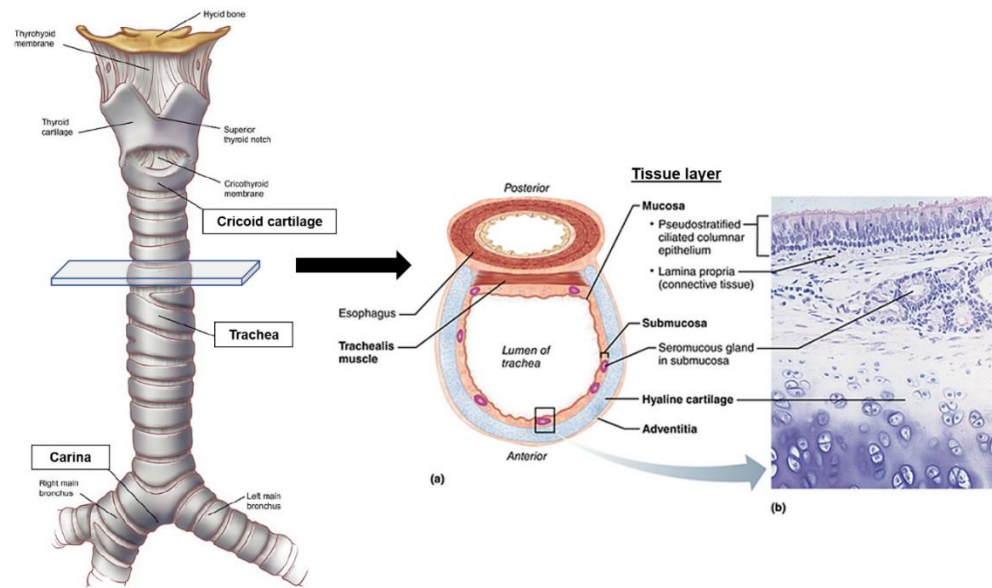


Figure 1 Structure of trachea. The cross-section of the trachea consists of four tissue layers including mucosa, submucosa, hyaline cartilage and adventitia (a and b) [10].

Normally, the blood supply to the trachea from arterial divides into two parts including the upper (cervical) and lower (thoracic) trachea. The superior, middle and inferior bronchial arteries bring blood directly from the aorta to the trachea and carina. The segmental arteries supplying approach the lateral tracheal wall and branch in a longitudinal forming anastomosis with the segmental arteries above and below [10]. Within the intercartilaginous ligaments, the tracheal arteries again branch into anterior and posterior branches that travel circumferentially within the tracheal wall where they anastomose with the corresponding tracheal arteries from the contralateral side. This segmental arrangement of blood flow limits circumferential tracheal dissection to no more than 1–2 cm on either side of a tracheal anastomosis due to the risk of devascularization and ischemia with larger dissections. The understanding of tracheal blood supply is a major issue for the high safety and success rate for tracheal dissection. To avoid tracheal ischemia, tracheal dissection can result in tracheal stenosis and anastomotic breakdown. Especially, the arteries feeding the trachea approach the lateral wall of the trachea and vascularize the trachea in a segmental fashion along with its longitudinal access (Fig. 2).

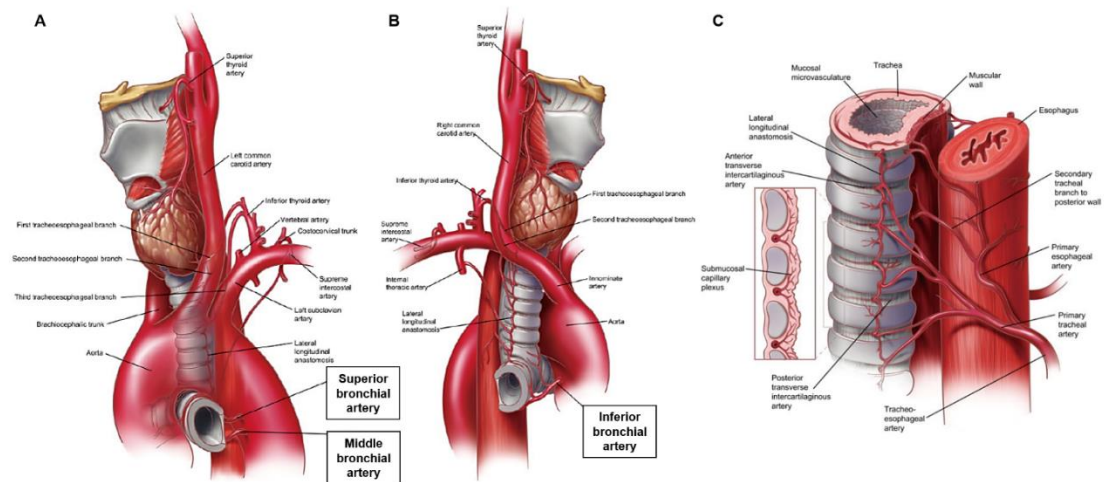


Figure 2 Blood supply to trachea. (A) Left anterior view; (B) right anterior view. (C) Association between the trachea and esophagus focuses attention on the segmental tracheal blood supply [10].

2.2 Tracheal diseases

Tracheal diseases are a significant challenge to clinical tracheal repair. The most common tracheal disorders are tracheal stenosis and tracheomalacia. Tracheal stenosis is a narrowing of the trachea such as external injuries (trauma), tumors, inflammation, autoimmune disorders (such as amyloidosis, pulmonary sarcoidosis, Wegener's granulomatosis), radiation therapy and congenital malformation (inborn defects) [11, 16]. Moreover, prolonged intubation or tracheostomy when a tube is used to assist with breathing via a medical ventilator can cause tracheal stenosis. Recently, it has been reported in post-intubation tracheal stenosis in COVID-19 patients [17, 18]. On the other hand, tracheomalacia is characterized by damage of cartilaginous wall tissue such as surgical injuries, chronic infection of used tracheostomy long-term, gastroesophageal reflux disease, polychondritis (inflammation of cartilage in the trachea) and inhaling irritants or toxic chemicals. These lead to scarring and narrowing of the trachea and collapsing of the trachea. Normally, the evaluation includes a computed tomography (CT) scan and bronchoscopy. The option treatment of tracheal disorders is laser bronchoscopy, a

balloon or rigid bronchoscopic dilation, ablation, stent placement, and direct end-to-end anastomosis. When the surgical treatment of extensive lesions, tracheal resection with primary anastomosis is not possible or is associated with a high rate of morbidity and mortality. Patients with these lesions are only offered palliative care [19]. Tracheal reconstruction would be an option for resection of extended lesions. Moreover, the tracheal defect is longer than 6 cm in adults (30% of the total length in children), it is difficult to achieve tracheal reconstruction by direct anastomosis [2, 3, 20]. Therefore, tracheal replacement with substitutes is imperative to achieve the reconstruction of the trachea.

2.3 Tracheal tissue engineering

Tissue engineering is the development of tissue or organs to replace or support the function of defective or injured body parts. To regenerate tissues or organs, the key components of tissue engineering are scaffold or biomaterial, cells, and signaling molecules. Furthermore, tissue engineering permits fabrication of tracheal tissues *in vitro* or *in vivo* by using a condition of a three-dimensional matrix, stem cells cultivated *in vitro* and originating from the patient [2]. Tracheal tissue engineering is the regeneration of the trachea by applying the principle of tissue engineering. The ideal tracheal replacement would be non-immunogenic, biocompatible, durable, and assess growth potential, which can all be achieved with tissue engineering [21]. Tracheal tissue engineering is an inherent challenge with airway reconstruction and neo-tissue formation. First, the cartilaginous rings receive their nutrients and avascular nature of hyaline cartilage that is challenged by poor regenerative ability. Second, the airway was exposed to the air during breathing, so it is not a sterile environment. Third, orthotopic graft failure or compromise results in morbidity in terms of airway obstruction, respiratory distress and death [21]. Forth, the potential of epithelial cells are protected mechanical shear from using stents, and the relatively hypoxic phase occurs during grafts revascularization [22]. Thus, tracheal scaffolds should be designed for epithelial formation; meanwhile, there also remains structural integrity to prevent airway collapse.

Substitutes for tracheal replacement can be classified into five types including

synthetic prosthesis, allografts, tracheal transplantation, autologous tissue composite and tissue engineering (Fig. 3). However, each option has benefits and disadvantages in terms of time, risk of rejection, risk of contamination, and complications. Clinical applications of allografts and autografts are limited because of the lack of healthy donors and the high probability of immune rejection. The substitute characteristics of ideal tracheal replacement are lateral rigidity and stiffness, longitudinal flexibility, airtight lumen, no need for immunosuppression, appropriate mechanical strength, feasibility, reproductive technique and biocompatibility [2, 23].

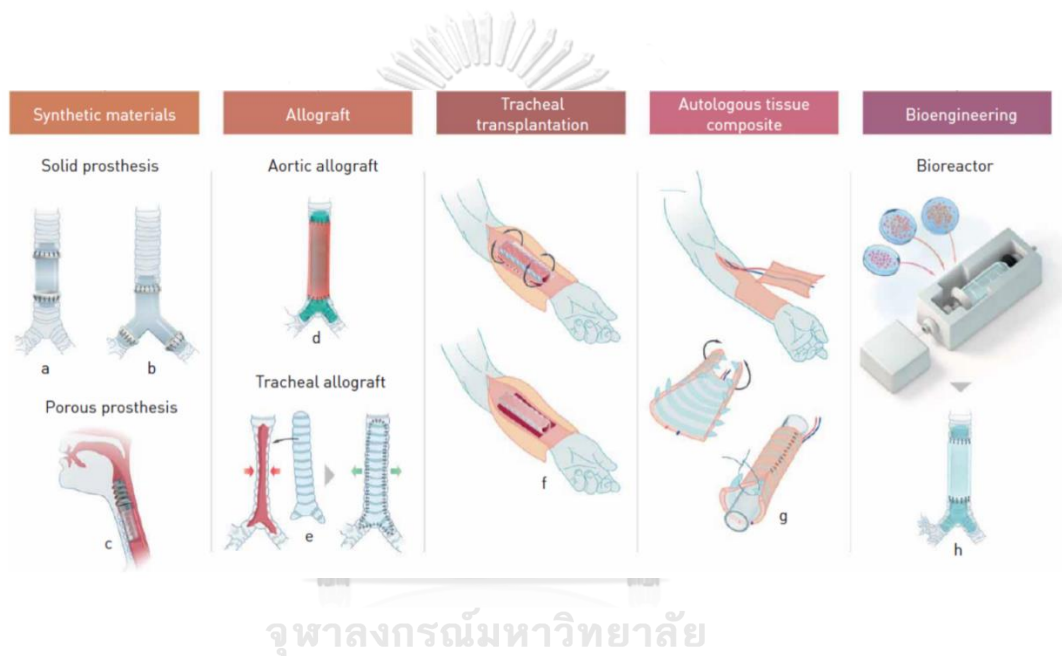


Figure 3 The therapeutic options of tracheal replacement. a-c) Synthetic materials; straight solid or bifurcated solid prosthesis, and porous titanium prosthesis after laryngectomy. This approach is limited to the proximal part of the trachea associated with the larynx. (d) Aortic allograft with a stent to maintain lateral rigidity. (e) Long tracheal stenosis treated by a tracheal allograft. (f) Positioning of the tracheal graft on the forearm to promote vascularization and viability before transplantation in the orthotopic position. (g) Free fascio-cutaneous flap from the forearm reinforced by cartilage struts. (h) Stem cells seeding in the bioreactor before implantation of the bioengineered trachea [2].

In century years, researchers and clinicians have been designing trachea grafts with advancing material fabrication techniques, surgical procedures and understanding of trachea mechanics and physiology. The tracheal scaffold firstly came using cadaveric human tracheal allografts in 1980 [24]. Nevertheless, these grafts did not support cellular ingrowth, leading to stenosis and malacia after implantation. Recently, 290 patient cases were published who received long-segment and circumferential tracheal replacement grafts [25]. The reported treatment conditions are as follow: 171 (60.4%) tumor invasion; 22 (7.8%) critical airway stenosis; 19 (6.7%) airway trauma; 17 (6.0%) congenital stenosis; 11 (3.9%) tuberculosis; 11 (3.9%) prolonged intubation; and 32 (11.3%) other conditions (**Fig. 4A**). The scaffold types were applied in clinical applications and reported follow-up of tracheal replacement as shown in **figures 4B and 4C**, respectively. Currently, heterotopic/orthotopic allotransplantation is the trend in tracheal replacement defined with maximum follow-up and the most to the patients. However, limitations of this protocol are multiple wound sites, a long-time procedure, and systemic immunosuppression. Another modern allotransplantation is decellularized allograft, which removes all cellular components from cadaveric tracheas using decellularization techniques. The method is biocompatible and non-immunogenic.

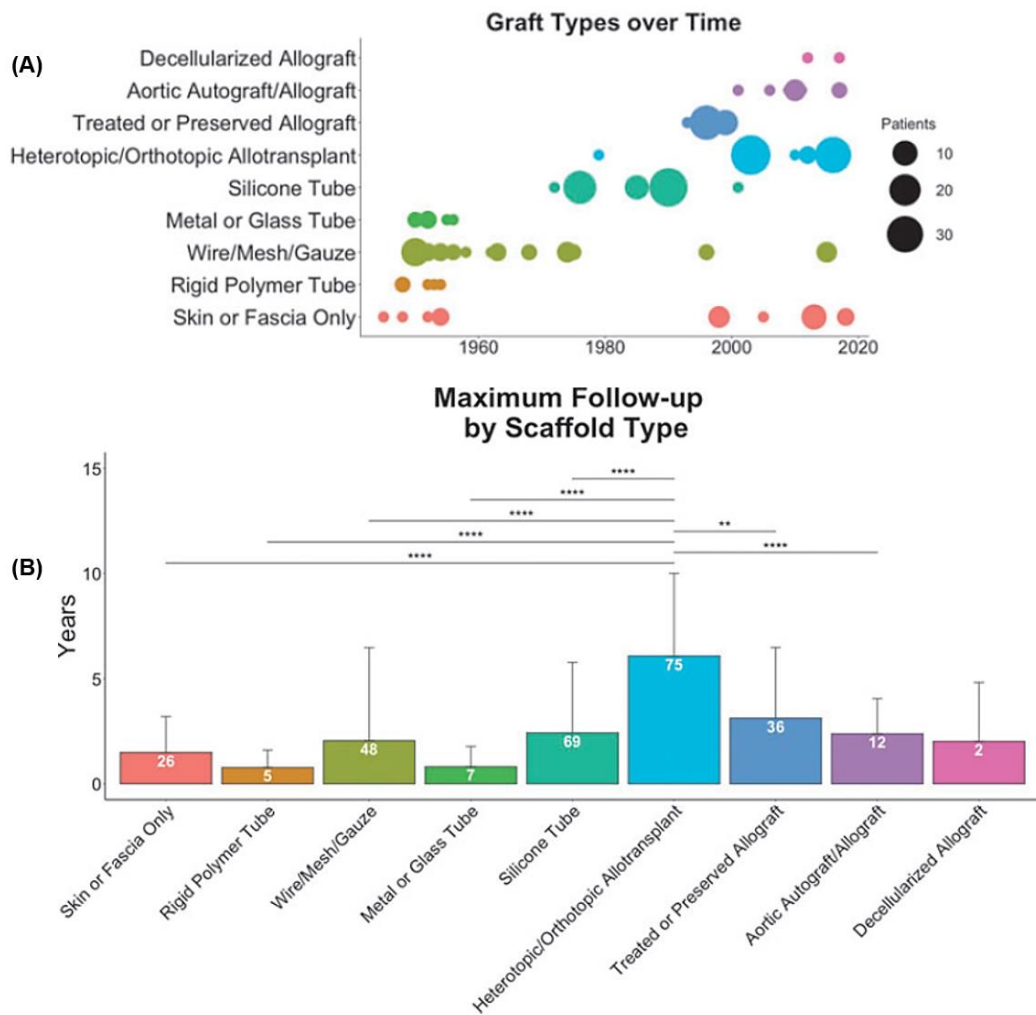


Figure 4 Graft types of trachea in clinical applications. (A) Dot plot of the number of patients who received long-tracheal each graft type. (B) The follow-up report of each graft type [25] showed the number of patients per condition on data bars (white color).

2.3.1 Decellularized tracheal matrix scaffold

Tissue engineered scaffolds designed to support structure, maintain an open airway and mimic the biological and mechanical function of the native ECM. Moreover, scaffolds provide as a template for the stem cells until they have proliferated, regenerated, and stabilized the damaged area [26]. Scaffold fabrication has difference techniques such as freeze-drying (spongy porous), electrospinning (nano or micro fibrous mesh), Thermally induced phase separation (film or

membrane), solvent casting/particulate leaching (porous film), foaming method (spongy porous), decellularization (ECM-based graft) and 3D printing (3D structure) [11]. The classification of tracheal scaffolds is a synthetic scaffold and biologic decellularized tracheal matrix scaffold (DTM). The decellularized scaffolds are widely used due to their good biomechanical properties, functional extracellular matrix (ECM), and removes the possibility of an immune response by eliminating major histocompatibility complexes class I and II [26]. In contrast, synthetic scaffolds are frequently development and composed of modified polymer and/or combination with biological elements. However, the synthetic tubular scaffold of the trachea is challenging for its complex structure with such high morbidity and mortality, solid prostheses are not a long-term viable option for extensive tracheal replacement [2].

Decellularization is the removal of cell and immunogenic material processes from a tissue that would preserve intact the extracellular matrix (ECM) and the biomechanical properties. The biomechanical properties of the trachea ECM are primarily related to collagen, glycosaminoglycans, and elastin [5]. The tracheal cartilage plays a main role in the mechanical function of trachea, which directly affects its physical respiratory function. The various trachea decellularization methods of trachea have been established by using physical, chemical and enzymatic treatment. The previous studies mostly used chemical and enzymatic method, specifically the detergent enzymatic method (DEM) and its modifications by the repeated detergent exposure [8, 27-30]. The main detergents of DEM method are sodium deoxycholate, deoxyribonuclease (DNase) enzyme and distilled water. Sodium deoxycholate is used to solubilize cellular membranes, where major histocompatibility complex antigens reside [31, 32]. DNase enzyme is effective the cellular DNA removal that is a part of some commercial decellularization processes. Distilled water removes residual reagents by repeated rinsing. Furthermore, physical methods apply to use in trachea decellularization such as thermal shock, ultrasonic, snap freeze or freeze thawing and vacuum. These methods are normally accustomed to complement chemical and enzymatic techniques and increase the decellularization effects. Newly, it has been reported that vacuum-assisted decellularization (VAD) can enable chemical agents to reach the whole tissue

resulting in accelerated scaffold production and reduced the associated costs [6-8, 33, 34]. Moreover, the modification of the VAD method was established increasing DNase concentration from 2 KU/ml to 6 KU/ml or up to 50 kU/ml, which is more effective to reduce the time decellularization [7, 33]. This technique could become a new trend for the preparation of decellularized tracheal matrix scaffolds.

2.3.2 Re-epithelization and regeneration of tracheal cartilage

Cells are an important role in improving the functional clinical outcome after trachea implantation. Several studies have been focused on attempts made to the pseudostratified ciliated columnar epithelium and chondrocytes that are two main cells types as in the native trachea structure. Pseudostratified ciliated columnar epithelium cells provide the function of the native airway, while chondrocytes form to support the trachea structure. Many cell types have been applied alone or in combination on tracheal scaffolds such as epithelial cells, chondrocytes, mesenchymal stromal cells, human bone marrow mononuclear cells, human embryonic lung fibroblasts, fibroblasts, and adipose tissue [21]. Epithelial cells are mainly applied for improved tracheal tissue regeneration. In contrast, scaffolds seeded with chondrocytes enhanced biomechanical strength, but chondrocytes cannot be capable of living after implantation. Therefore, co-culture is an alternative option to reenerate the full function of trachea tissue. It has been reported that human epithelial cell co-culture with articular chondrocytes in fibrin glue scaffolds shows the fully function of *in vitro* tissue construct [35]. Co-culturing of nasal epithelial cell and chondrocytes *in vivo* condition fully grown pseudostratified ciliated columnar epithelium layer and collagenous tissue-engineered graft [36, 37]. In addition, previous research has shown that fibroblast cells have effect on epithelial migration, differentiation and regeneration [38, 39]. The cell density is also significant to reconstruct a functioning trachea by cell-cell and cell-matrix communication. The cell density at 10^6 cells/ml is useful to yield a suitable graft for lifelong implantation.

Scaffolds, cells and signal molecules (growth factors) interact with each other to regenerate tissue in a specific way. Numerous types of signaling

molecules have been used in tracheal tissue engineering such as epithelial growth factor (EGF), basic fibroblast growth factor (bFGF), platelet-derived growth factor (PDGF), vascular epithelial growth factor (VEGF), transforming growth factor (TGF), insulin-like growth factor (IGF), granulocyte colony-stimulating factor (G-CSF) and bone morphogenetic protein (BMP) [11].

2.3.3 Decellularized extracellular matrix (dECM)-derived hydrogels

To guideline regenerate cells layer, the three-dimensional surfaces of the airway wound bed are needed to restore as the native trachea form. This strategy has been successfully used to regenerate the entire skin surface using epidermal cells applied on a fibrin carrier in a child with a severe blistering skin disorder [40], and to improve host epithelial repair and/or contribute directly to mucosal regeneration on collagen I based-sheet *in vivo* rabbit model [22]. Additionally, previous research has shown that Matrigel can be regenerate 3D spheroids “Bronchospheres” of airway basal cells, but the origin of gel is murine sarcoma; therefore, it is not appropriate for clinical transplantation [41]. Newly, it has been presented that upregulation of oncogenic markers and pathways aberrant of cancer were expressed in Matrigel compared to organoids formed in dECM hydrogel for human airway organoid culture [42].

Injectable extracellular matrix (ECM) hydrogel can potentially adapt to various three-dimensional shapes and be delivered to a specific site with minimal invasiveness surgery technique. The acellular ECM of xenogenes has become a major theme of today’s tissue repair technology research. The ECM proteins are a complex network of macromolecular substances that are generally secreted and synthesized innumerable tissues and cells, for example, fibroblast, mesenchymal cells, and epithelial cells. ECM has an important role on cell behavior which includes adhesion, differentiation, proliferation, migration and functional expression [43]. In particularly, ECM play a significant impact on tissue development, hemostasis and disease [44]. Animal tissue sources have been widely used to develop dECM hydrogel such as the lung, bladder, heart and cartilage of pigs, tendons of cattle, lung and kidney of goat and liver and lungs of rats [45]. More recent studies have confirmed that dECM

hydrogel can promote the repair of several damaged tissues and cell culture *in vitro*. The different tissue source may affect the composition, gelation, degradation rate and mechanical properties of dECM hydrogel [46]. Therefore, tracheal tissue engineering strong and through animal trials should be performed and precisely studied before transition to human subjects.

The formation of ECM hydrogel is based on the collagen-based self-assembly process and is regulated by the presence of glycosaminoglycans, proteoglycans, and ECM proteins. Polymerization kinetics are influenced by native biochemical profile of source tissue and of remaining proteins after decellularization and solubilization. Hydrogel formation includes two key steps which are solubilization of ECM material into protein monomeric components and temperature-and/or pH-controlled neutralization to induce spontaneous reformation of intramolecular bonds of the monomeric components into a homogeneous gel. Pepsin enzyme is mostly used to cleave the telopeptide bonds of the collagen triple helix structure along with hydrochloric acid or acetic acid as a base medium to unravel collagen fibril aggregation. Solubilized ECM or ECM digestion forms gel when liquid solution is neutralized to physiologic pH, salt concentration (ECM pre-gel) and temperature *in vitro* (ECM hydrogel) in an entropy-driven process dominated by collagen kinetics. In a self-assembly process, there is an increase of entropy when collagen monomers lose water, form aggregates, and bury surface-exposed hydrophobic residues within the fibril *in vitro* [9].

CHAPTER III MATERIALS AND METHODS

3.1 Part I: Preparation of decellularized trachea

3.1.1 Chemicals and reagents.

Phosphate buffered saline powder, Sodium deoxycholate, DNase I (750KU), Triton X-100 were purchased from Sigma-Aldrich (St. Louis, MO). Antibiotic/antimycotic solution (100X) and Ambion® RNase I (100 U/μL) were purchased from Gibco and Invitrogen (Thermo Fisher Scientific Inc., PA, USA), respectively. Proteinase K and Papain were purchased from Worthington biochemical corporation (Lakewood, NJ).

3.1.2. Harvesting canine trachea tissue

Canine tracheas were obtained in sterile environment from canine donors kindly supported from the Faculty of veterinary science, Chulalongkorn university, Thailand. The uses of cadaveric samples, which do not apply to the Institutional Animal Care and Use Committee (IACUC) approval. Donor tracheas (n=6) were immediately rinsed in 40 ml of phosphate buffered saline (PBS) containing 1% antibiotic/antimycotic solution and surrounding tissue was dissected away. Each trachea was divided into two segments evenly along the transverse plane. Each segment contains 5-6 cartilage rings. The first segment of trachea was performed by vacuum-assisted decellularization VAD methods. The second segment served as the native trachea, defining name as the unwashed trachea (control).

3.1.3. Decellularization process of tracheal tissue

Tracheal tissues were conducted by vacuum-assisted decellularization (VAD) method that removes cells from pre-frozen tissue under vacuum conditions (Fig. 5). Briefly, tracheas were sterilized with 70 % ethanol overnight on a rotating shaker at 4 °C and washed in distilled water type II for 72 hours at 4 °C to remove ethanol. Tracheas were frozen at -80 °C for 24 hours, thawed at room temperature and rinsed with PBS. All steps in VAD were taken place in a vacuum chamber in conjunction

with detergent and enzymatic treatment. All solutions will be supplemented with 1% antibiotic-antimycotic. The trachea was incubated in a detergent solution containing 0.25% sodium deoxycholate and 0.25% Triton X-100 in PBS and then placed inside the vacuum chamber for 24 hours at 37°C on a rocker. Afterward, the tracheas were rinsed twice in distilled water type II for 2 hours and incubated for another 44 hours in distilled water type II at 4 °C. At enzymatic treatment, the tissues were incubated in an enzymatic solution containing 2 KU/ml DNase I and 4 U/ml RNase I at 37 °C for 24 hours and washed with distilled water type II at 4 °C for 24 hours. This enzymatic treatment step was performed again. Finally, tracheas were washed with distilled water type II for 48 hours and stored at 4 °C in PBS containing 1% antibiotic-antimycotic until use.



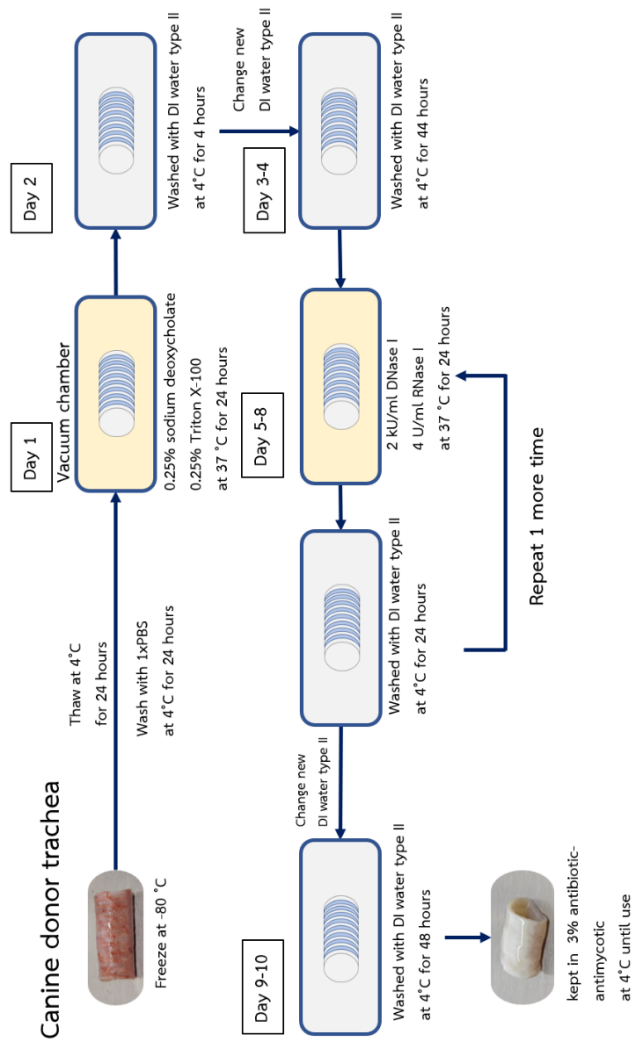


Figure 5 Schematic diagram of the vacuum-assisted decellularization (VAD) of trachea. The canine trachea underwent a vacuum chamber washing process for a duration of 10 days, with various solutions being used. On the first day, the trachea was immersed in a detergent solution and subsequently rinsed with DI water type I. From day 5 to 8, DNase I and RNase I solutions were employed to remove nucleic acid materials from the trachea. Following decellularization, the trachea was stored in a 3% antibiotic-antimycotic solution at 4 °C until use.

3.1.4. Histology and immunohistochemistry

The unwashed trachea (control) and decellularized trachea (dTrachea) samples (n=3) were fixed with 4% paraformaldehyde in PBS, embedded in paraffin, and sectioned to 3 μm thickness. The sections were stained with hematoxylin and eosin (H&E) to assess cell nuclei and general tissue histoarchitecture. The extracellular matrix components (i.e. collagen, elastin, muscle, mucin and fibrin) were examined using Movat pentachrome stain kit (Modified Russell-Movat). The presence of a major histocompatibility complex (MHC-II) marker was evaluated using immunohistochemistry. The MHC class II marker was labeling by monoclonal mouse anti-human HLA-DP, DQ, DR antibody [CR3/43] at 1:100 dilution (M0775, Dako). Horse anti-mouse IgG antibody (H+L) biotinylated at 1:200 dilution (BA-2000-1.5, Vector Laboratories) was used as secondary antibody. Then, sections were incubated with ImmPACT DAB substrate kit (Vector Laboratories) according to the manufacturer's instructions and finally counterstained with hematoxylin.

To detect laminin and fibronectin, the control and dTrachea samples (n=3) were embedded in Cryo-gel (Leica Biosystems, USA), and the sections were cut at 18 μm thickness. Following the blocking step, the sections were incubated with 2.5% horse serum for 1 hour at room temperature and then washed with 1xPBS for 3 minutes. Subsequently, the sections were incubated with primary antibodies at a 1:200 dilution overnight at 4°C. The primary antibodies used were rabbit polyclonal antibody to laminin (ab11575) and anti-fibronectin antibody [IST-9] - BSA and Azide free (ab6328) from Abcam (Cambridge, United Kingdom). After the overnight incubation, the sections were washed with 1xPBS for 3 minutes and then incubated with secondary antibodies at a 1:200 dilution. The secondary antibodies used were goat polyclonal antibody to rabbit IgG (IR, Texas red; ab6719) or goat polyclonal antibody to mouse IgG (FITC; ab97239), both from Abcam. This incubation with secondary antibodies was performed for 2 hours in the dark at room temperature. Finally, the samples were washed with 1xPBS and stained with DAPI using Fluroshield Mounting medium with DAPI (ab104139, Abcam).

All sections were observed under an optical microscope (Nikon, Tokyo, Japan) using a NIS-Elements BR imaging software (vD4.10.02; Nikon Instruments, NY, USA).

3.1.5. Biomechanical assessment

Decellularized trachea (dTrachea) and the unwashed trachea (control) were analyzed for mechanical properties: compression test (n = 4) and tensile tests (n = 4) using the Universal testing machine (Hounsfield-H10KM, USA). Length and wall thickness measurements of both the unwashed trachea and the dTrachea samples were recorded and are presented in **Supplementary Table S1**.

The trachea samples underwent compression in the anterior-posterior direction at a speed of 5 mm/min until the diameter decreased to 50% of its initial diameter. The calculation of Young's Modulus was performed by determining the slope of the linear region of the stress-strain curve. This calculation was conducted using ASTM C 165 compressive properties software from Tinius Olsen (Kongsberg, Norway).

During the tensile testing, two fixtures were inserted into the lumen of the trachea. Each sample was subjected to tensile testing at a rate of 50 mm/min. The tensile strength, ultimate tensile strength, and percent elongation were calculated using the ASTM D 882 Simplified Tensile & Break software from Tinius Olsen (Kongsberg, Norway).

3.1.6. Biochemical assay

The unwashed trachea and dTrachea were digested in 1 ml of proteinase K buffer (1 mg/ml Proteinase K and 0.88 mg/ml papain), incubated at 60 °C overnight and centrifuged at 6,000 rpm at 4 °C for 20 minutes. The supernatant was transferred to new tubes to quantify DNA, Sulfated glycosaminoglycan (sGAG) and collagen contents. The DNA content was measured using the Quant-iT PicoGreen® dsDNA Assay Kit (Life Technologies, Grand Island, NY). Sulfated glycosaminoglycan (sGAG) content was determined by DMMB dye-binding assay and the total collagen content was measured using an Ortho-hydroxyproline (OHP) colorimetric assay [47]. This assay involved the reaction of chloramine T and dimethyl-amino benzaldehyde to quantify the amount of collagen present in the sample. DNA, sGAG and collagen contents were normalized to tissue wet weight (n=4). In addition, the compositions of laminin (ab119572) and fibronectin (ab108849) were measured (n=4) using ELISA kits from

Abcam (Cambridge, United Kingdom). The measurements were carried out following the instructions provided by the manufacturer.

3.1.7 Re-epithelization and cytocompatibility

3.1.7.1 Cell culture and cell seeding

Primary human bronchial epithelial cells (HBEpC) obtained from Promocell GmbH (Heidelberg, Germany) were cultured and expanded in airway epithelial cell growth medium also provided by Promocell GmbH. The cells were maintained in a 5% CO₂ environment at 37 °C, with regular medium changes every 2 days. For the experiments, 1x10⁶ HBEpCs in 200 µl of growth medium were directly seeded onto the luminal side of dTrachea disks measuring 5 mm in diameter. The cell-seeded constructs were placed in a 96-well plate from NUNC (Fisher Scientific GTF, Sweden) and incubated in a 5% CO₂ environment at 37 °C overnight to allow for cell attachment. Subsequently, the growth medium was replaced every 48 hours for a period of 3 and 7 days. Non-seeded dTrachea samples were used as a control group in the experiment.

3.1.7.2 Cytocompatibility

Following ISO standard 10993-5:2009, dTrachea was assessed using cytotoxicity by LIVE/DEAD® Viability/Cytotoxicity Kit (Thermo Fisher Scientific). At day 3, the cell-seeded constructs were incubated in a solution of 200 µl PBS containing 2 µM Calcein AM and 4 µM Ethidium homodimer-1 (EthD-1) for 45 minutes at 37 °C and 5% CO₂. After the incubation period, the constructs were washed twice with PBS and examined under a fluorescent microscope to visualize the cells. Furthermore, all the constructs were collected for analysis of DNA content using the Quant-iT PicoGreen® dsDNA Assay.

3.1.8. Micromorphological assessment of dTrachea

The non-seeded dTrachea and cell-seeded constructs were fixed using a solution of 2.5% glutaraldehyde in 1xPBS at 4 °C overnight, washed three times with

1xPBS for 10 minutes each at room temperature and rinsed with distilled water. Next, constructs were dehydrated using a series of ethanol concentrations ranging from 30% to 100% ethanol. Subsequently, they were subjected to evaporation using a critical point dryer (Leica EM CPD300). Once dried, the constructs were coated with a layer of Gold (Au) using a sputter-coater (BALZERS SCD 040). Finally, the samples were visualized using a scanning electron microscope (SEM) at magnifications of 10,000X and 3000X, and energy dispersive X-ray spectrometer (JSM-IT500HR, JEOL Group Companies, Japan) was used for analysis.

3.2 Part II: Development of decellularized extracellular matrix (dECM)-derived hydrogels

3.2.1 Decellularization of canine trachea

Cadaveric canine tracheas were obtained from the Faculty of veterinary science, Chulalongkorn University, Thailand.

The tracheas were chopped into small pieces (~8 mm) and cleaned using DI type II containing a 3X concentration of antibiotic/antimycotic solution. The tracheal cartilage of canine trachea was decellularized by the VAD method following the protocol in section 9.1.3. To determine the amounts of DNA and sGAG present, Quant-iT PicoGreen® dsDNA Assay and DMMB dye-binding assay were employed. The samples were rapidly frozen at -80°C, subjected to freeze drying for 2 days, milled using a grinder machine, sterilized through gamma irradiation (15 kGy for 5 hours), and stored at -80°C until use.

3.2.2 Preparation of dECM hydrogel

Decellularized canine trachea was enzymatically digested as previously described [9, 46]. Briefly, 20 mg/ml of decellularized canine trachea were added in 0.5 M acetic acid (pH 3.0) containing a final pepsin concentration of 627U/mg of tissue (P7000-100G; Sigma). Enzyme digestion was performed at 25°C under constant stir bar agitation. The digested samples were collected at 4, 12, 24, 48, 72 hours, and centrifuged at 10,000 rpm for 15 min, 4°C to remove undigested particles. The

supernatant, the soluble dECM, were collected. The supernatant was dialyzed for 2 days against 0.01 M acetic acid at 4°C in MWCO 3500 dialysis tubing, as modified from published protocols [48, 49]. To polymerize solubilized dECM solutions were neutralized pH ~7.4 with 1 M NaOH (pepsin activity is deactivated above pH 6) and balanced salt concentration with a one-ninth volume of 10xPBS. dECM solution and chemical reagents were chilled on ice before neutralization. Gelation of dECM solution was induced under 37 °C incubator. All solutions were sterile-filtered and all steps were performed in a biosafety cabinet.

3.2.3 Gelation kinetic of decellularized extracellular matrix (dECM)

To determine effects of digestion time on gelation of dECM, turbidimetric gelation kinetics and calculation parameters were determined as previously described [46]. The 50 µL of dECM solution was transferred to a 96-well plate in triplicate, and kept in 4°C. The dECM solution was incubated at 37 °C and recorded the absorbance every 5 min for 60 min at 405 nm. The normalized absorbance (NA) was calculated at each digestion time point using equation (1)

$$NA = (A_t - A_0) / (A_{max} - A_0) \text{ ----- (1)}$$

Where A_t is the absorbance at time point t , A_0 is the initial time point t_0 , and A_{max} is the maximum absorbance value.

3.2.4 Characterization of dECM solution

dECM solution were determined by the protein size distribution using SDS-PAGE and western blot to detect specific protein (collagen II).

Twenty microliters (5 µg of protein) of the dECM solutions were load on a 4-15% Mini-Protein TGX gels (Bio-rad Laboratories, California, USA). Electrophoresis was conducted at 120V for 65 min. Then, proteins on SDS-PAGE were transferred on Immun-Blot PVDF membrane (Bio-rad Laboratories, California, USA) at 4°C, 100 V for 2 hours.

The membrane was blocked with 3% BSA in 0.1% Tris-buffered saline with 0.1% Tween® 20 Detergent (TBST) at 4 °C for overnight with rotator, rinsed with 0.1%

TBST for 3 times, incubated with rabbit polyclonal antibody collagen type II (ab34712, Abcam) at dilution of 1:5000 in 3%BSA containing 0.1% TBST at 4 °C for 2 hours, and rinsed with 0.1% TBST for 3 times. The membrane was then incubated with goat anti-rabbit IgG H&L HRP (1:5000, ab205718, Abcam) for 2 hours and 4 °C and rinsed with 0.1% TBST for 3 times. The western blotting detection reagent (Amersham ECL Prime, GE healthcare) was added on the membrane and the signals were detected by Visionworks software on UVP GelStudio imaging system (Analytik Jena GmbH, USA).

3.2.5 Micromorphological assessment of dECM hydrogel

Hydrogels prepared from dECM digested at 24, 48, or 72 hrs were fixed in 2.5% glutaraldehyde in PBS at 4 °C overnight, washed with 1xPBS for 3 times and then dehydrated in a series of graded ethanol solutions by following protocol in 9.1.8. ECM fibrous network and its interconnectivity were investigated using SEM, with three selected fields of views at each time point. The dry hydrogel constructs were sputter-coated with Gold (Au) (BALZERS SCD 040) and visualized by a scanning electron microscope (SEM) and energy dispersive x-ray spectrometer at 5,000X magnification (JSM-IT500HR, JEOL Group Companies, Japan). Three fields of SEM images in each sample measured the diameter of 12 fibers using Image J software (National Institutes of Health, NIH), as described previously [50]. For a total number of branching fibers, 12 dECM fibers in branching points were recorded and divided by the combined area ($6.25 \mu\text{m}^2$) to calculate as [interconnections/ μm^2].

3.2.6 Human mesenchymal stem cells viability on dECM hydrogel

3.2.6.1 Cell culture

Human mesenchymal stem cells (hMSCs) from bone marrow (hMSCs, C-12972; Promocell GmbH, Heidelberg, Germany) were cultured in hMSC medium (alpha-MEM medium containing 4% FBS, 1% antibiotic-antimycotic, 1% Glutamax, 1% HEPES buffer, and 1 ng/mL recombinant human basic fibroblast growth factor; bFGF). Cells were maintained in 5% CO₂ at 37 °C, with medium change every 2 days.

3.2.6.2 Evaluation of cell viability on dECM hydrogel

A volume of 400 μL of dECM solutions, prepared by peptic digestion of decellularized trachea from 24, 48, and 72 hours according to method 9.2.2, was added to a 24-well plate and incubated at 37 °C for 1 hour to allow gel formation.

Following the guidelines of ISO standard 10993-5:2009, the resulting dECM hydrogels were incubated with 2 ml of serum free alpha-MEM medium for 24 hours to prepare extracts from the dECM hydrogel. The hMSCs (hMSC, C-12972; Promocell GmbH, Heidelberg, Germany) were seeded in 96-well plate at a density of 30,000 cells / cm^2 and incubated at 37 °C, 5% CO_2 for 24 hours to enable cell attachment. The hMSC medium was replaced with the dECM hydrogel's extract solution. The metabolic activity of cells was evaluated using PrestoBlue™ according to the manufacturer's instructions. The hMSC medium and 100% DMSO were used as positive and negative controls, respectively.

For the cell viability assessment, hMSCs 100,000 cells were mixed with 500 μL of dECM solution, transferred to a 24-well plate, incubated at 37°C, 5% CO_2 for 1 hour to allow gelation, and cultured for 3 days in hMSC medium. The LIVE/DEAD® assay was used to assess and visualized by a confocal microscope Zeiss LSM 800 (ZEISS, Oberkochen, Germany).

3.2.7 Endothelial cell tube formation *in vitro* study.

Human umbilical vein endothelial cells (HUVECs) were obtained from PromoCell (Heidelberg, Germany) to examine the formation of capillary-like structures *in vitro*. The HUVECs were cultured in Endothelial Cell Growth Media-2 (EGM-2, PromoCell) and maintained at 37 °C with 5% CO_2 and 95% humidified air. In a 96-well plate, 20,000 cells were directly seeded onto 50 μL of dECM hydrogels, which were prepared by subjecting the decellularized trachea to peptic digestion for 72 hours. The HUVEC-hydrogel samples were inculcated at 37 °C with 5% CO_2 and visualized under light microscopy (SA115B-05V, Olympus, China) at 0, 4, and 24 hours.

The viability of HUVECs was determined at 24 hours using LIVE/DEAD® staining. The stained samples were visualized under fluorescence microscopy (Nikon;

ECLIPSE: Ti-U, Tokyo, Japan), and the NIS-Elements BR imaging software (vD4.10.02; Nikon Instruments, NY, USA) was used for analysis. Control hydrogels, such as Matrigel[®], and fibrin gel [51] were employed as comparison benchmarks.

3.2.8 Assessment of injectable dECM hydrogel for cartilage formation

To prepare injectable canine dECM-fibrinogen hydrogel, gelatin (G6411), fibrinogen (F8630), and glycerol (G2025) were purchased from Sigma-Aldrich (St. Louis, MO). Briefly, the glycerol (10% v/v) was dissolved in 1xPBS containing 3% antimitotic-antibiotic by stirring the solution at room temperature for 1 hour. Gelatin (40 mg/ml) was then added to the solution, stirring for 5 minutes, and left to stand for 10 minutes. Next, the mixture was incubated in a water bath at 37°C for 10 minutes until the gelatin completely dissolved. The mixture solution was transferred to a tube, and fibrinogen (20 mg/ml) was gently added and mixed by inverting the tube until the fibrinogen dissolved in the solution. The mixture solution was sterilized by filtration through a 0.45- μ m syringe filter.

The dECM solution (20 mg/ml) obtained from 72 hours peptic digestion was neutralized and filter through a 0.45- μ m. The sterile dECM solution was mixed with fibrinogen/gelatin/glycerol solution in a volume ratio of 1:1, resulted in the dECM-fibrin solution containing final concentrations of gelatin (20 mg/ml), fibrinogen (10 mg/ml), glycerol (5% v/v), and dECM solution (10 mg/ml). The dECM-fibrin solution was kept at -20°C until further use.

hMSCs of 1×10^6 cells/ml were gently mixed with warm dECM-fibrinogen solution after incubated in a water bath at 37 °C for 15 min. The mixture was cross-linked by the addition of a thrombin solution (20 UI/ml, T4648, Sigma-Aldrich) for 30 min at room temperature.

Two types of decellularized tracheal scaffold (dTracheal scaffold) sized 8 mm in diameter were prepared: the dTracheal scaffold with intact cartilage ring (n=3) and the dTracheal scaffold with punched cartilage rings (n=3). The dTracheal scaffold with punched cartilage rings was prepared by punching tiny holes in cartilage rings using a needle sized 20Gx1" (0.9x25mm).

The experiment was performed in a 48-well plate and coated 200 μ l in each

well with 2% agarose gel. The luminal surface of all scaffolds was positioned to face downwards, while the top view displayed the tracheal cartilage.

The cells/dECM-fibrin hydrogel (200 μ l) was injected onto the outer surface of dTracheal scaffold sized 8 mm in diameter. After hydrogel injection, dTracheal scaffold and punched dTracheal scaffolds were incubated at 37 °C with 5% CO₂ for 2 hours to allow hydrogel completely attachment with dTracheal scaffold, and then add 250 μ l of chondrogenic medium into each well, with medium change every 3 days. All scaffolds were cultured for 3 weeks.

The scaffolds were evaluated for cartilage formation using the frozen tissue section technique (method in 3.1.4). Sections were subsequently stained with H&E and Alcian Blue to observe cell morphology and to assess the secretion of sGAG, respectively. Samples were observed under bright-field microscopy (Nikon; ECLIPSE: *Ti-U*, Tokyo, Japan), and the NIS-Elements BR imaging software (vD4.10.02; Nikon Instruments, NY, USA).

3.3 Part III: Effects of fibroblasts on tracheal tissue formation

3.3.1 Cell culture and dTracheal scaffold preparation

The human primary cells (Promocell GmbH, Germany) were maintained in media, shown in **Table 2**. Growth medium (Promocell GmbH, Germany) was changed every 3 days. Sub-culturing was performed using TrypLE™ Express when cells reached 80% confluency.

The decellularized tracheal scaffold (dTracheal scaffold) was prepared for seeding platforms in several steps. First, decellularized tracheas were punched with a 10-mm diameter biopsy punch (Acuderm, Netherland) to create the dTracheal scaffold, and then disinfected scaffolds with 70% ETOH at 4°C overnight. Second, the dTracheal scaffolds were washed 2 times with 1xPBS containing 3X antibiotic-antimitotic for 16 hours with rotating. After sterilization under UV light for 2 hours, scaffolds were incubated with hMSCs culture medium for 4 days at 37°C, 5% CO₂. Finally, dTracheal scaffolds were dried on filter paper at 37°C, 5% CO₂, for 4 days to set a dried dTracheal scaffold.

Table 2 The list of cells and mediums used in the experiment

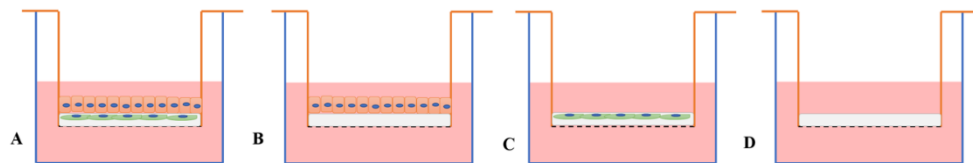
Cells	Media
1. Primary human bronchial epithelial cells (HBEpCs; C-12640) (Promocell GmbH, Germany)	1.1 Airway epithelial cell growth medium (Promocell GmbH, Germany), containing 1% antibiotic/antimycotic solution 1.2 Epithelium differentiation medium (PneumaCult™-ALI Medium, Stemcell™ Technologies, Canada), containing 1% antibiotic/antimycotic solution, 0.02% (v/v) heparin and 500 ng/mL of hydrocortisone (Sigma)
2. Primary human pulmonary fibroblasts cells (HPFs; C-12360) (Promocell GmbH, Germany)	2. Fibroblast growth medium (Promocell GmbH, Germany), containing 1% antibiotic/antimycotic solution
3. Primary human mesenchymal stem cells from bone marrow (hMSCs; C-12974) (Promocell GmbH, Germany)	3.1 hMSCs medium consist of alpha MEM medium, containing 4% FBS, 1% antibiotic/antimycotic solution, 1X HEPES, 1X Glutamax and 1 ng/ml bFGF. 3.2 Chondrogenic medium comprised of high glucose DMEM, 1% antibiotic/antimycotic solution, 1x HEPES, 1X Insulin-Transferrin-Selenium-Ethanolamine (ITS-X), 6 µg/ml L-proline, 1 µM dexamethasone, 15 µg/ml ascorbic acid, and 5 ng/ml TGF-β3.

3.3.2 Co-culture and tri-culture of epithelial cells, fibroblasts and hMSCs embedded canine dECM-fibrin hydrogel

Primary human brachial epithelial cells were cultured with or without primary human pulmonary fibroblast cells as study designs shown in **Figure 6**. The effects of fibroblasts on epithelial cells maturation and differentiation of ciliated cells were investigated by co-culturing of epithelial cells with fibroblasts (**Fig. 6, study 1: co-**

culture system). For tri-culturing, chondrogenic differentiation of hMSCs located was pre-cultured with fibroblasts. The hMSCs were differentiating on the outer layer of dTracheal scaffold, fibroblasts were seeded on a luminal surface of dTracheal scaffold and epithelial cells were seeded on the fibroblasts layers (**Fig. 6, study 2: tri-culture system**). Each condition was performed in four replicates.

Study 1 : Co-culture of epithelial cells and fibroblasts



Study 2: Tri-culture of epithelial cells, fibroblasts and hMSCs

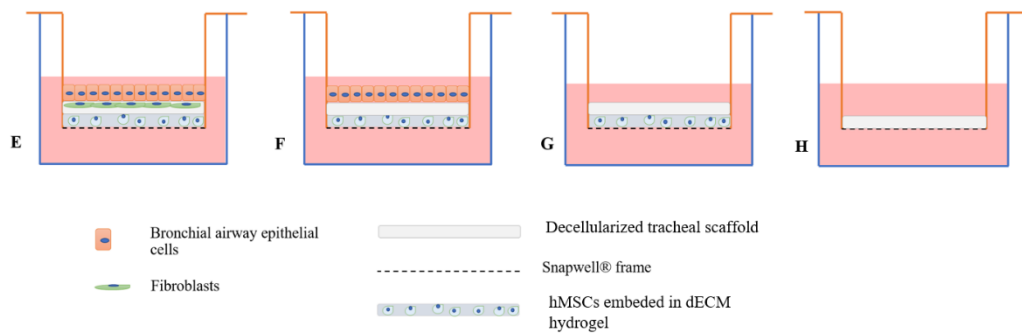


Figure 6 Experimental designs in co-culture and tri-culture system

Study 1: Co-culture of epithelial cells and fibroblasts. Fibroblasts were seeded in decellularized scaffolds, followed by seeding epithelial cells on the top layer (A). Separate cultures of epithelial cells (B), fibroblasts (C), and decellularized tracheal scaffold (D).

Study 2: Tri-culture of epithelial cells/fibroblasts/chondrogenic differentiation of hMSCs. hMSCs/dECM-fibrin hydrogel mixture was injected into the outer layers of a dTracheal scaffold and placed on a cell insert. Fibroblasts were cultured on the luminal surface and thereafter tri-cultured with epithelial cells (E). Epithelial cells and cultured with chondrogenic differentiation of hMSCs (F), chondrogenic differentiation of hMSCs (G), and decellularized tracheal scaffold (H).

3.3.3 Formation of co-culture system

The experiments were divided into 4 phases as shown in figure 7.

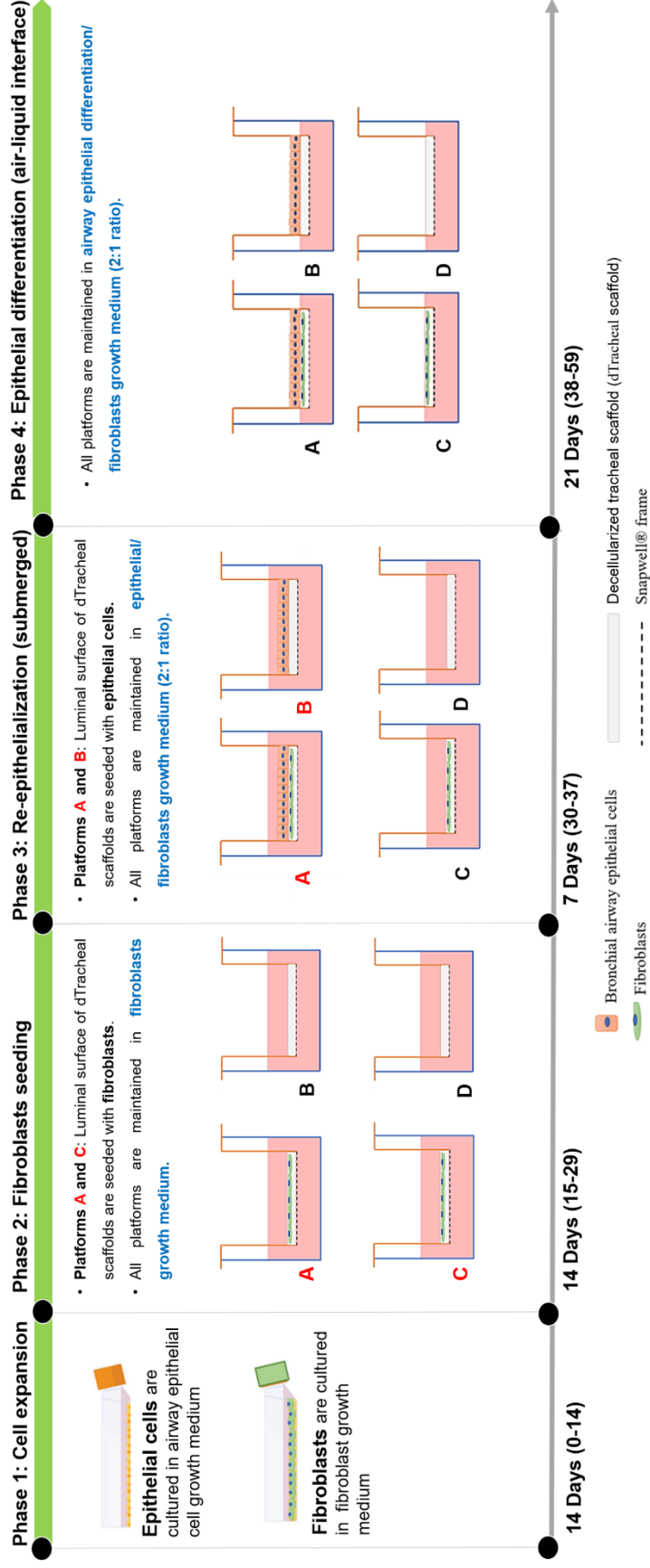


Figure 7 The overview of experimental design divided into 4 phases. Cell expansion, fibroblasts seeding, re-epithelialization and epithelial differentiation.

3.3.3.1 Phase 1: Cell expansion

The HBEpCs, and HPFs were expanded in growth media in **Table 2** following the manufacturer's instructions. The cells were cultured at 37°C and 5% CO₂ and changed media every 2-3 days up to the confluency. Cell passage 6-12 were used in this study.

3.3.3.2 Phase 2: Fibroblasts seeding

The experimental was divided into four platforms including co-culture of epithelial cells (A), epithelial cells (B), fibroblasts (C), and decellularized tracheal scaffold (dTracheal scaffold) (D) (**Fig. 7**). A dTracheal scaffold was placed on polymeric membranes of the transwell insert with pore size of 0.4 µm used in a 12-well plate.

Fibroblasts were seeded on platform A and C at a density of 0.5×10^5 cells/cm² on days 1 and 4 of culture on the luminal surface of the scaffold [52] and incubated each time at 37 °C with 5% CO₂ for 2 hours to allow cell attachment. Fibroblast growth medium was added to all four platforms in the transwell insert (500 µl on the basolateral side and the apical side 500 µl) and then maintained for 14 days with medium changes every 3-4 days.

3.3.3.3 Phase 3: Re-epithelialization

Epithelial cells were seeded two times on days 1 and 4 in platform A and B at a seeding density of 0.5×10^5 cells/cm² and incubated for 2 hours at 37 °C with 5% CO₂. Then, the 500 µl of airway epithelial cell growth medium/fibroblast growth medium (2:1 ratio) was added on the basolateral side and another 500 µl at the apical side of the transwell insert to cover the scaffolds, and cultured for 7 days with medium changes every 3 days. Condition C and D are control groups without epithelial seeding.

3.3.3.4 Phase 4: Epithelial cell differentiation (air-liquid interphase culture, ALI)

The 500 μl and 200 μl of epithelial cell differentiation medium/fibroblast growth medium (2:1 ratio) were added to the basolateral and the apical sides of the transwell insert, respectively, in all platforms. The fresh medium was changed 3 times per week for 21 days. The samples were collected (n=2) from each condition at pre- and post-epithelium cell differentiation (pre-and post-phase 4) to determine tissue formation.



3.3.4 Formation of tri-culture system

The experiments were divided into 5 phases as shown in figure 8.

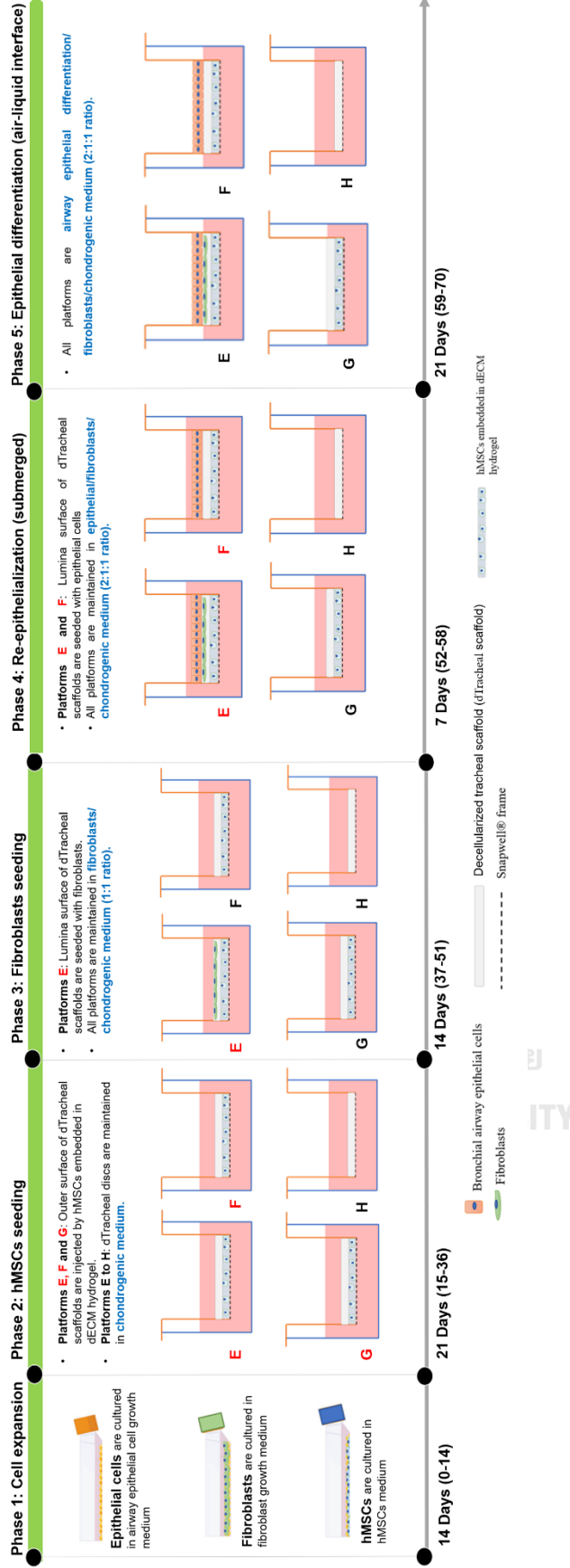


Figure 8 The overview of experimental design divided into 5 phases. Cell expansion, hMSC seeding, fibroblasts seeding, re-epithelialization and epithelial cell differentiation.

3.3.4.1 Phase 1: Cell expansion

The HBEpCs, HPFs and hMSCs were expanded in growth media in Table 2 following the manufacturer's instructions. The cells were cultured at 37°C and 5% CO₂ and changed media every 2-3 days up to the confluency. Cell passage 6-12 were used in this study.

3.3.4.2 Phase 2: hMSCs seeding

The experimental was divided into 4 platforms including tri-culture of epithelial cells, fibroblasts, and hMSCs (E), epithelial cells and hMSCs (F), hMSCs (G), and decellularized tracheal scaffold (H) (Fig. 8). dTracheal scaffolds were pinned at cartilage rings located at the outer surface using a 20Gx1" needle. The dTracheal scaffolds were placed on polymeric membranes of the transwell insert with pore size of 0.4 µm filled in a 12-well plate.

hMSCs at concentration of 1×10^6 cells/ml were mixed with 200 µl of dECM-fibrin hydrogel and injected onto the outer surface of scaffold with punched cartilage rings in platforms E, F and G. Platform H is a control groups. Chondrogenic differentiation medium were added on all platforms at 500 µl in both the basolateral and apical sides of the transwell insert and maintained for 3 weeks (21 days) with medium changes every 3-4 days.

3.3.4.3 Phase 3: Fibroblasts seeding

Fibroblasts were seeded on luminal surface of platforms E with a density of 0.5×10^5 cells/cm² on days 1 and 4 [52] and incubated each time at 37 °C with 5% CO₂ for 2 hours to allow cell attachment. Then, fibroblast growth medium/chondrogenic differentiation medium (1:1 ratio) were added in all platforms and maintained in the for 14 days with medium changes every 3-4 days.

3.3.4.4 Phase 4: Re-epithelialization

Epithelial cells were seeded two times on days 1 and 4 in conditions E and F at a seeding density of 0.5×10^5 cells/cm² and incubated for 2 hours at 37 °C

with 5% CO₂. Then, the 500 µl of airway epithelial cell growth medium/fibroblasts growth medium/chondrogenic differentiation medium (2:1:1 ratio) was added on the basolateral side and another 500 µl of medium on the apical side of the transwell insert to cover the scaffolds. Platform G is a control group without epithelial seeding and platform H is a control groups. Medium was maintained for 7 days with 3-4 days medium changes.

3.3.4.5 Phase 5: Epithelial cell differentiation (air-liquid interphase culture, ALI)

The 500 µl and 200 µl of epithelial cell differentiation medium/fibroblast growth medium/chondrogenic medium (2:1:1 ratio) were added to the basolateral and the apical sides of the transwell insert, respectively, in all platforms. The fresh medium was changed 3 times per week for 21 days. The samples were collected (n=2) from each condition at pre-and post- epithelium cell differentiation (pre-and post- phase 5) to determine tissue formation.

3.3.5 TEER measurements

Cultures were evaluated on the barrier integrity of the airway epithelium formation to measure the transepithelial electrical resistance (TEER) using an EVOM² Voltohmeter with STX2 Chopstick probes at days 7 and 21 during culturing. Chopstick probes were sterile with 70% ethanol for 15 minutes and washed with 1xPBS for 15 minutes at room temperature under a biosafety cabinet. Before measuring TEER value, chopstick probes were incubated with a warm culture medium for 5 minutes. Then, chopstick probes were put on the basolateral side and another probe on the apical side of the transwell insert. The TEER value was measured as ohms unit.

The TEER values reported as unit area resistance [$\Omega \cdot \text{cm}^2$] from the total resistance subtracted from the blank resistance (membrane without cells) and multiplied by the membrane surface area: TEER value ($\Omega \cdot \text{cm}^2$) = (Ω Total resistance - Ω blank resistance) x membrane surface area cm^2 [52].

3.3.6 Histological and Immunofluorescence analysis

Tissue constructs (n = 2) in each platform were fixed 30% sucrose in 1xPBS and embedded with Cryo-gel (Leica Biosystems, USA) for H&E, Alcian blue, immunohistochemistry and immunofluorescent staining. The frozen tissue section were cut at 18 µm thickness and stained with hematoxylin and eosin (H&E) to assess for tissue formation. The sections were stained with Alcian blue to evaluate sGAG secretion.

For immunofluorescent staining, the tissue sections were permeable with 0.25% Triton-X in PBS for 30 minutes at room temperature. Next, samples were incubated with 2.5% horse serum for 1 hour at room temperature. The primary and secondary antibodies used in this study are presented in Table 3. The primary antibodies used were mouse monoclonal antibody to cilia (1:1000, ab24610) and mucus production (1:1000, ab3649) from Abcam (Cambridge, United Kingdom), and rabbit monoclonal antibody to E-cadherin (1:1000, 24E10) from Cell Signaling Technology. Additionally, the primary antibody was used to detect F-actin (1:1000, ab176753, Phalloidin-iFluor 488 Reagent) from Abcam (Cambridge, United Kingdom). Afterward, overnight incubation, the sections were washed with 1xPBS for 3 minutes and then incubated with secondary antibodies at a 1:1000 dilution. The secondary antibodies used were goat polyclonal antibody to mouse IgG (FITC; ab97239) or goat polyclonal antibody to rabbit IgG (IR, Texas red; ab6719), both from Abcam company. This incubation with secondary antibodies was performed for 2 hours in the dark at room temperature. Finally, the samples were washed with 1xPBS and stained with DAPI using Fluroshield Mounting medium with DAPI (ab104139, Abcam).

Neocartilage was stained using anti-collagen type II (COL-II) primary antibody (1:1000, ab34712) by immunohistochemistry staining. The tissue sections were permeable with 0.25% Triton-X in PBS for 30 minutes at room temperature. Subsequently, samples were incubated with 2.5% horse serum for 1 hour at room temperature and incubated with primary antibody for 16 hours at 4°C. Afterward, the sections were washed with 1xPBS, 3 times 1 minute per each wash, and then application of goat anti-rabbit IgG H&L HRP (1:1000, ab205718, Abcam) for 2 hours in the dark at 4 °C and rinsed with 0.1% TBST for 3 times. In the final step, Vector HRP

substrate was added to the tissue slides incubated for 30 minutes, and washed with 1xPBS.

The cross-section of airway formation was observed using an optical microscope (Nikon, Tokyo, Japan) using NIS-Elements BR imaging software (vD4.10.02; Nikon Instruments, NY, USA).

Table 3 The series of primary and secondary antibodies in immunofluorescence staining

Primary antibodies				
Presence	Cells	Detect protein	Name of antibody	Types of antibody
Epithelial differentiation	Cilia	Acetylated alpha tubulin (AC-tubulin)	ab24610: Anti-alpha Tubulin (acetyl K40) antibody [6-11B-1]	Mouse monoclonal
Epithelial function	Mucus production	Mucin 5AC (MUC5AC)	ab3649: Anti-Mucin 5AC antibody [45M1]	Mouse monoclonal
	Tight junction protein	E-cadherin (E-cad)	24E10: Anti- Cadherin-1 (Human)	Rabbit monoclonal
Cartilage formation	Cartilage	collagen type II (CoL-II)	ab34712: Anti-Collagen II antibody	Rabbit polyclonal
Housekeeping	Actin	F-actin	ab176753: Phalloidin-iFluor 488 Reagent	-
Secondary antibodies				
Color	Host species	Name	Target species	
Red	Goat	ab6719: Goat Anti-Rabbit IgG H&L (Texas Red ®)	Rabbit IgG H&L	
Green	Goat	ab97239: Goat polyclonal antibody to mouse IgG (FITC)	Mouse IgG	

3.3.7 Protein quantitation using mass spectrometry

Samples (n = 3) of dTracheal scaffolds, dECM hydrogels, and tissue constructs from the tri-culture system were determined the protein composition by mass spectrometry. All samples were collected and kept in 0.5% (w/v) of sodium dodecyl sulfate (SDS) at -80°C until analysis.

Mass spectrometry (MS) analysis of proteins was performed by the Functional Proteomics Technology Laboratory, National Center for Genetic Engineering and Biotechnology, and the National Science and Technology Development Agency, Thailand. The process was performed according to the protocol described previously [53].

Liquid chromatography-tandem mass spectrometry (LC-MS/MS) analysis was conducted using (hybrid quadrupole Q-TOF Impact II™, Bruker Daltonics, USA). The separation of tryptic peptides was analyzed using the Ultimate3000 Nano/Capillary LC System (Thermo Scientific, UK) in conjunction with a nano-CaptiveSpray™ ion source (Bruker Daltonics).

The raw data files from LC-MS/MS (.mzXML) were subjected to analysis using Maxquant 2.1.4.0 [54]. Subsequently, the data were processed with Andromeda to identify proteins based on the Uniprot *Canis familiaris* database [54].

The search parameters employed were included standard label-free quantitation settings such as using trypsin as the enzyme for protein digestion, considering variable modifications including carbamidomethyl and oxidation of methionine residues, utilizing mono-isotopic mass values, not restricting protein mass, setting peptide mass tolerance at ± 1.2 Da, fragment mass tolerance at ± 0.6 Da, accounting for peptide charge states of 1+, 2+, and 3+, and allowing for 2 missed cleavages. Finally, the log₂ expression levels of the identified proteins were calculated as part of the data analysis process.

3.3.8 Bioinformatic analysis of proteomics data

Tissue constructs from the tri-culture system were analyzed with the MetaboAnalyst [55], which is a robust and all-encompassing platform specifically designed for the in-depth analysis of metabolomics and proteomics data. This

platform used a generic format including sample names and the log₂ expression levels of the identified proteins, to generate statistical analysis information. The module of statistical analysis (one factor) was selected and offered data in expression heatmap (reporting protein expressions in different sample), principle component analysis (PCA), Volcano plot (compare two groups), ANOVA (compare more than two groups), self-organizing map (SOM) and dendrograms. Especially, ANOVA analysis was performed following Tukey's post-hoc test to assess the difference between multiple groups, with a corrected p-value <0.05 is considered significant.

The proteins identified as statistically significant through Volcano plot and ANOVA analysis were annotated with their names and functions using the UniProt ID mapping tool (online resource available at <https://www.uniprot.org/id-mapping>).

The interaction of target proteins between protein-protein, chemical-protein, and between chemical was predicted using the STITCH version 5.0 database, involving enrichment biological process, molecular function, components and the Kyoto encyclopedia of genes and genomes (KEGG) pathway. Data with a corrected p-value <0.05 were deemed statistically significant [56].

To simplify gene ontology (GO) enrichment analysis in biological process, and KEGG pathway were conducted using ShinyGO version 0.74. GO terms with a False Discovery Rate (FDR) of less than 0.05 were considered significantly enriched [57].

3.4 Data Analysis and Statistics

Quantitative data obtained will be analyzed using Microsoft Excel and GraphPad Prism 4.0 Software (GraphPad Software, San Diego, CA). In cases of analysis between three groups, statistical difference will be assessed by One-way ANOVA with Bonferroni post hoc analysis. Bonferroni post hoc analysis was performed with a p-value of < 0.05 to consider statistical significance. All data are presented as mean ± standard deviation of n = 4 samples per group.

CHAPTER IV RESULTS

4.1 The presence of decellularized trachea scaffold (VAD)

After 10 days of decellularization, the trachea tissue displayed a whitish appearance (Fig. 5). Together with H&E staining, the unwashed control trachea exhibited the pseudostratified ciliated epithelial cells, glands, and smooth muscle in the mucosa and submucosa layers. In contrast, decellularized trachea (dTrachea) group showed the absence of cells (Fig. 9A). The cartilage layer of unwashed group displayed intact chondrocytes that were surrounded by an extracellular matrix (Fig. 9A). In Pentachrome staining, the dTrachea group presented a comparable signal of muscle and fibrin (appearing as red) to that the unwashed group (Fig. 9B). Collagen staining (appearing as yellow) was identified in the cartilage layer. In dTrachea group, a depletion of glycosaminoglycan depletion (appearing as purple) was observed within the cartilage layer. The MHC class II presence was clearly distinguished in the submucosa layer in the unwashed control group, while no signal was detected in the cartilage layer (Fig 9C). Remarkably, the cartilage layer in both control and dTrachea groups did not display any presence of MHC class II (Fig 9C). Furthermore, dTrachea groups in mucosa layer uniformly preserved laminin and fibronectin by immunofluorescent staining in Fig. 10A and 10B.

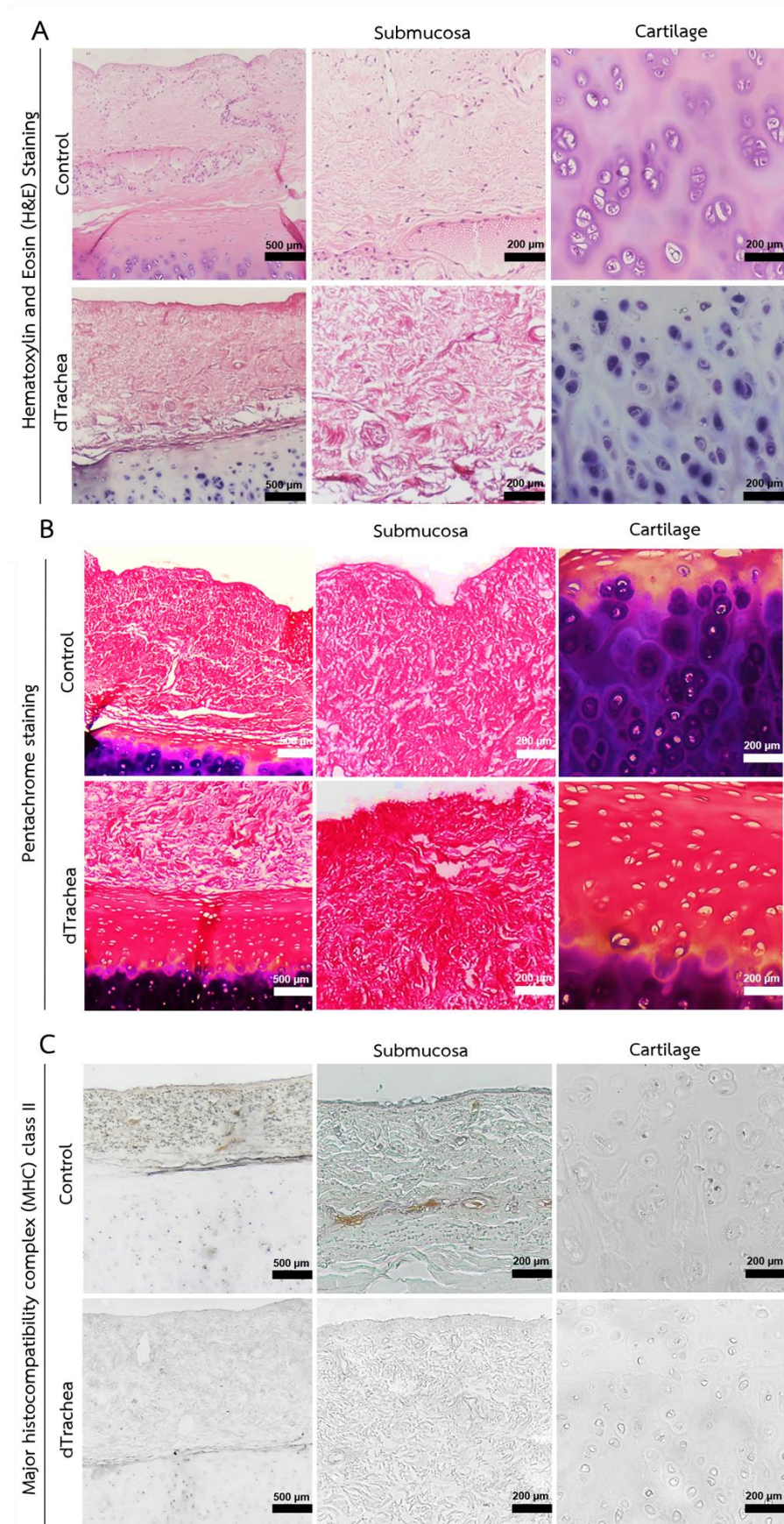


Figure 9 Histological evaluation of decellularized tracheas. **A)** Hematoxylin and eosin (H&E) staining; **B)** Pentachrome staining; **C)** Immunostaining of the MHC-II. Control = Unwashed trachea, dTrachea= Decellularized trachea Scale bar = 500, 200 μm .

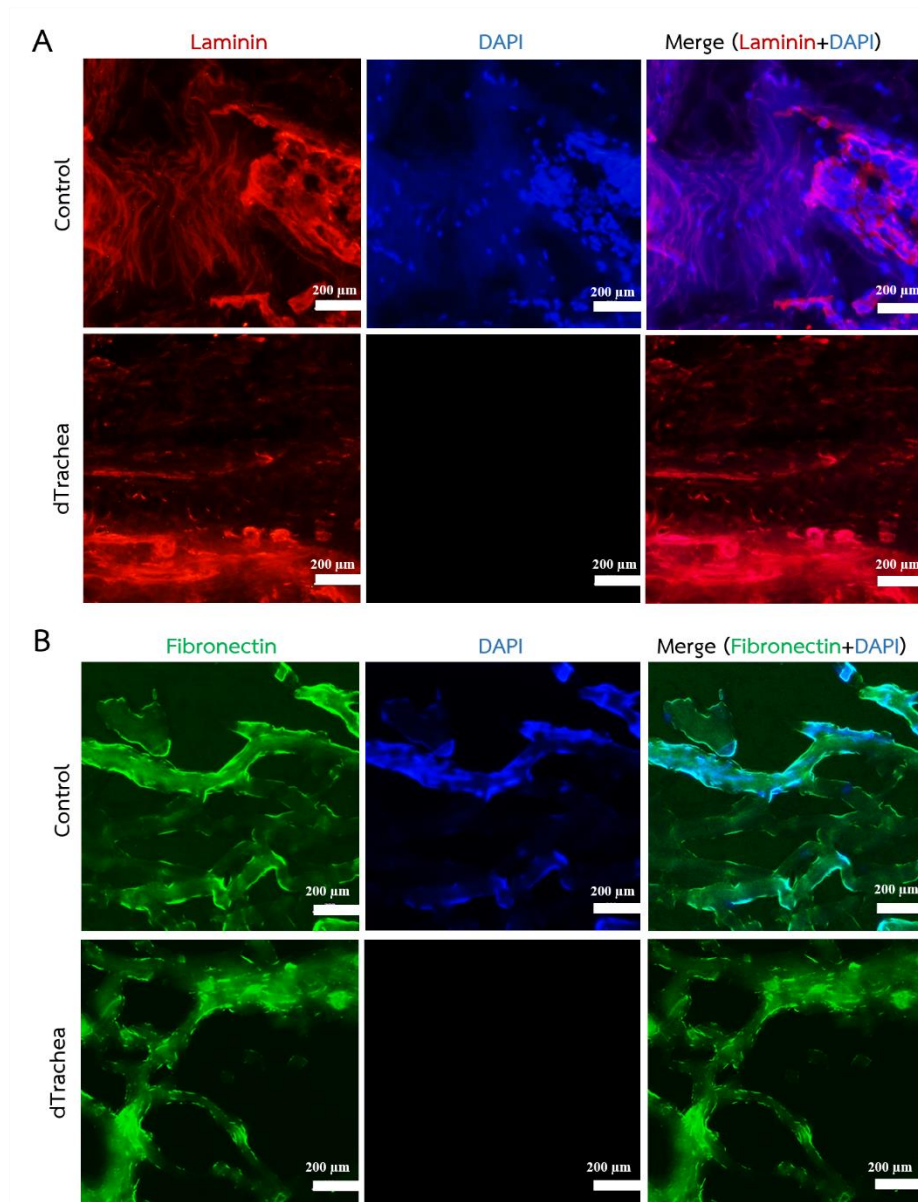




Figure 10 Immunofluorescence detection of laminin and fibronectin in decellularized tracheas. **A)** laminin and **B)** fibronectin in decellularized trachea (dTrachea) compared to the unwashed trachea (Control). Scale bar = 200 μm .

4.2 Biomechanical characteristics of decellularized trachea (dTrachea)

The process of decellularization conserved the mechanical properties of the decellularized canine trachea (**Table 4**). In compressive test, the decellularized trachea demonstrated no significant difference ($P > 0.05$) in Young's modulus ($P = 0.1083$), stress ($P = 0.4246$) and strain ($P = 0.6385$) when compared to unwashed control trachea (**Table 1; Supplementary Table S2**). Additionally, the dTrachea group exhibited the ability to regain its original shape after removal of loads. In terms of tensile testing, there were no significant differences observed between decellularized trachea and control group in terms of tensile strength ($P = 0.8545$), ultimate tensile strength ($P = 0.9554$), and percent elongation ($P = 0.9644$) (**Table 1; Supplementary Table S3**).

Table 4 The mechanical parameters of unwashed trachea and decellularized trachea. Data were expressed as mean \pm standard deviation (n = 4)

Mechanical Test		Unwashed trachea (control)	dTrachea
Compressive Test 	Young's modulus (kPa)	1124.76 \pm 81.42	1030.43 \pm 58.66
	Stress (kPa)	146.78 \pm 28.19	131.86 \pm 20.47
	% Strain	18.36 \pm 7.84	15.91 \pm 6.06
Tensile test 	Tensile strength (kPa)	3920.0 \pm 817.06	3809 \pm 822.54
	Ultimate tensile strength (kPa)	212675.00 \pm 60607.67	210700.00 \pm 30664.75
	% Elongation	43.50 \pm 7.38	43.23 \pm 8.96

4.3 Biochemical qualification of decellularized trachea and dECM solution

The DNA contents of decellularized trachea (2.46 ± 0.33 %DNA/wet weight) and dECM solution (1.16 ± 0.14 %DNA/wet weight) exhibited a significant reduction when compared to unwashed control trachea ($P < 0.0001$), (Fig.11A; Supplementary Table S4). Decellularization did not result in a significant reduction ($P < 0.05$) of ECM components, including glycosaminoglycan (sGAG), collagen, laminin, and fibronectin, in the decellularized trachea. (Fig. 11B-E; Supplementary Table S4). Contextually, the dECM solution revealed a significant decrease in sGAG ($P = 0.0069$), collagen ($P = 0.0018$), and fibronectin ($P = 0.0025$) compared to an unwashed control group. Nevertheless, no significant difference was observed in laminin ($P = 0.761$) between the dECM solution and the unwashed group. (Fig. 11B-E; Supplementary Table S4).

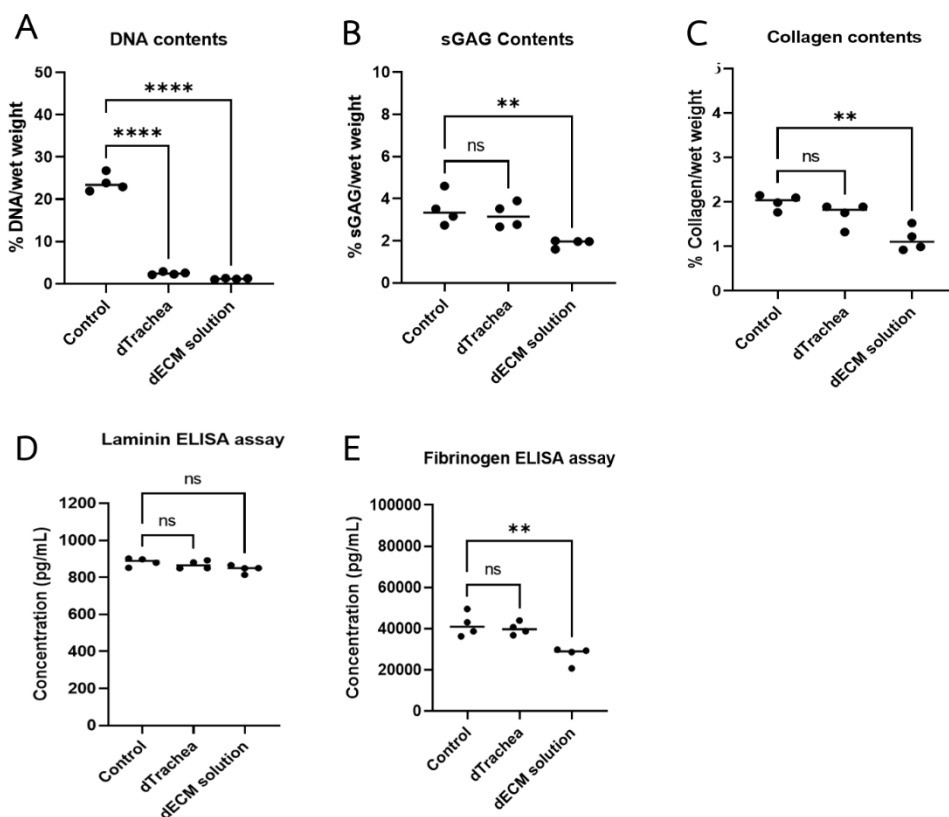


Figure 11 DNA contents and extracellular matrix composition of decellularized trachea. Decellularized tracheal tissues were evaluated for A) DNA contents, B)

sGAG contents, **C**) Collagen contents, **D**) Laminin contents and **E**) Fibronectin contents (n = 4). ns = not-significant, ** = $P < 0.01$, *** = $P < 0.001$ and **** = $P < 0.0001$. Control = Unwashed trachea, dTrachea = decellularized trachea, dECM solution = The Extracellular matrix-derived solution (dECM solution)

4.4 The evaluation of re-epithelization in decellularized trachea

Decellularization effectively eliminated epithelial cells from the trachea. Considering the seeding of newly cultured human bronchial epithelial cells (HBEpCs) on the luminal surface of the decellularized trachea, excellent cell viability was observed after 3 days. (**Fig 12A**). The microarchitecture of the decellularized trachea presented a mesh-like structure and an intricate ECM network. This provided a favorable environment for the attachment of HBEpCs on the mucosa layer of the luminal surface. (**Fig 12B**). The presence of HBEpCs on the decellularized scaffold constructs was examined through DNA quantification (**Fig. 12C**).

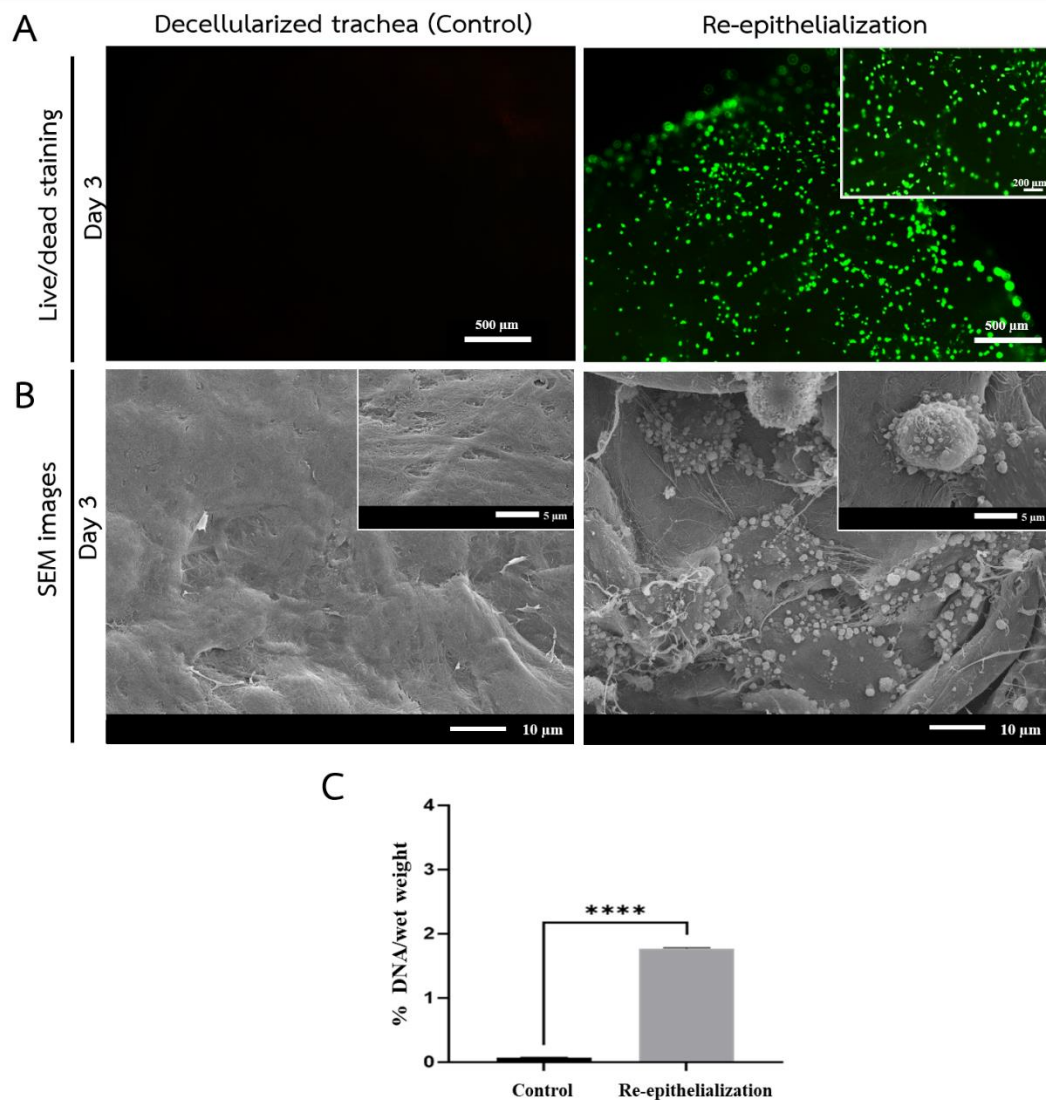


Figure 12 Re-epithelialization of decellularized trachea

A) Primary HBEpC were seeded on decellularized trachea for 3 days. Live cells (green) and dead cells (Red), (Scale bars = 500 and 200 μm); and **B)** DNA contents of the cell-seeded constructs on 3 days. **C)** Scanning electron micrographs of decellularized trachea without and with primary HBEpC for 3 days (Scale bars = 10 and 5 μm). Control = decellularized trachea. Re-epithelialization = HBEpC seeded on decellularized trachea **** = $P < 0.0001$.

4.5 Characterization and gelation process of the dECM solution

SDS-PAGE and Western blot analysis were employed to investigate the extracellular matrix-derived solution (dECM solution) from the extracellular matrix. The protein bands from the digested trachea, approximately 140 kDa in size, exhibited more pronounced signals as the peptic digestion duration increased from 4 hours to 72 hours (**Fig. 13A**). The Western blot analysis revealed the presence of collagen type II, with monomeric and dimeric structures detected at approximately 140 kDa and 270 kDa, respectively (**Fig. 13B**).

Among the different peptic digestion durations, the dECM solution obtained after 72 hours demonstrated the highest absorbance value of 0.7 at 405 nm over a period of 60 minutes. On the other hand, the 4-hour and 12-hour groups presented a clearer solution and exhibited similar absorbance values of approximately 0.4 (**Fig. 13C**). The dECM solutions obtained from peptic digestion for 4 hours and 12 hours experienced a temporary gelation process lasting for 20 minutes, as indicated by a decrease in absorbance. In contrast, the 24-hour, 48-hour, and 72-hour peptic digestion groups consistently formed hydrogels throughout the entire duration of the experiment, which lasted for 60 minutes (**Fig. 13D**).



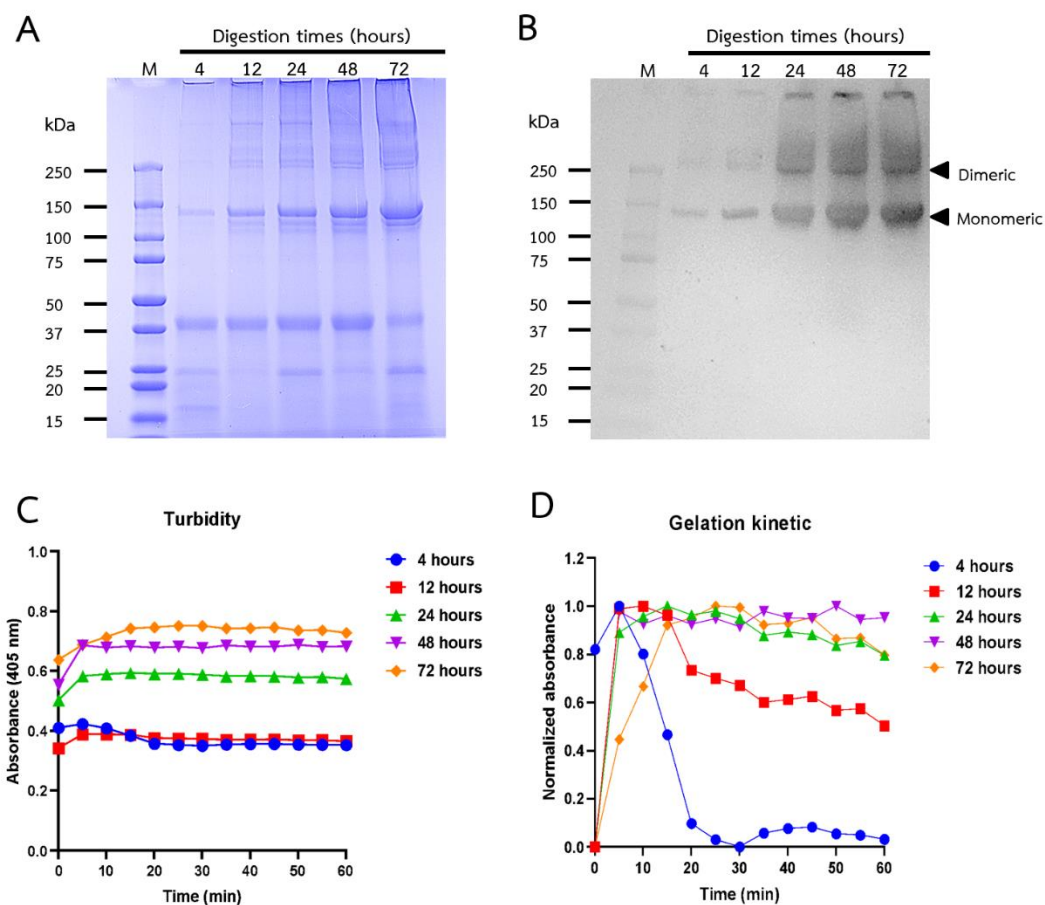


Figure 13 Characterization of extracellular matrix-derived solution (dECM solution) A) Analysis by SDS-PAGE of the decellularized trachea underwent pepsin digestion for 4, 12, 24, 48, and 72 hours. B) Western blot analysis reveals collagen type II in dECM solution. C) Increase in turbidity of dECM solution with different peptic digestion times. D) Examination of gelation kinetics in dECM solution.

4.6 The microarchitectural features of dECM hydrogel

The scanning electron microscope (SEM) image of dECM hydrogels, generated through the peptic digestion of decellularized trachea for 24 hours, exhibited a greater amount of debris when compared to the hydrogels from longer digestion periods (Fig. 14A). Interestingly, the dECM hydrogel from the 72-hour digestion group displayed observable and well-preserved extracellular matrix fibers with a diameter of $0.085 \pm 0.005 \mu\text{m}$. Notably, this diameter was significantly smaller compared to the 24-hour group ($0.168 \pm 0.015 \mu\text{m}$) and the 48-hour group ($0.131 \pm 0.010 \mu\text{m}$). The

interconnectivity of fibers demonstrated an increase when decellularized tissues were subjected to longer peptic digestion times, as shown in **Figure 14B**. Particularly, the 72-hour group exhibited the highest interconnectivity of ECM fibers, with an average of 0.840 ± 0.182 intersection points/ μm^2 (**Fig. 14C**; **Supplementary Table S5**).

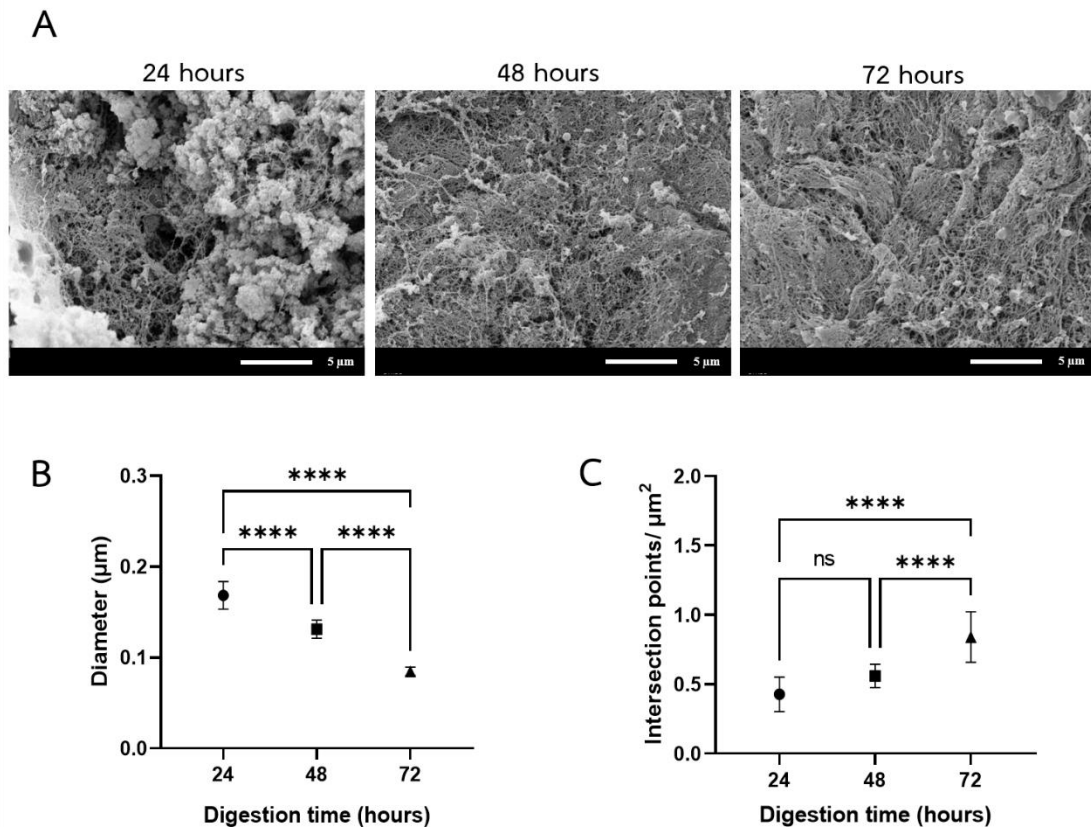


Figure 14 Characterization of extracellular matrix-derived hydrogel (dECM hydrogel) **A**) SEM images of microarchitecture of dECM hydrogels, prepared from peptic digestion of decellularized trachea for 24, 48 and 72 hours (Scale bar = $5 \mu\text{m}$) **B**) Fiber diameters at different peptic digestion times **C**) Interconnectivity of fibers represents by number of intersection points/ μm^2

4.7 Cytocompatibility of dECM hydrogel

To evaluate the impact of dECM hydrogels on hMSCs viability, PrestoBlue™ and LIVE/DEAD® assays were conducted. The viability percentages of hMSCs cultured in the extracted media from all dECM hydrogels for 24 hours exceeded 70% (**Fig.**

15A), indicating the non-cytotoxic nature of the dECM hydrogels towards hMSCs. Furthermore, at 3 days after encapsulation, hMSCs exhibited remarkable cell viability and displayed a uniform distribution within all dECM hydrogels (Fig. 15B).

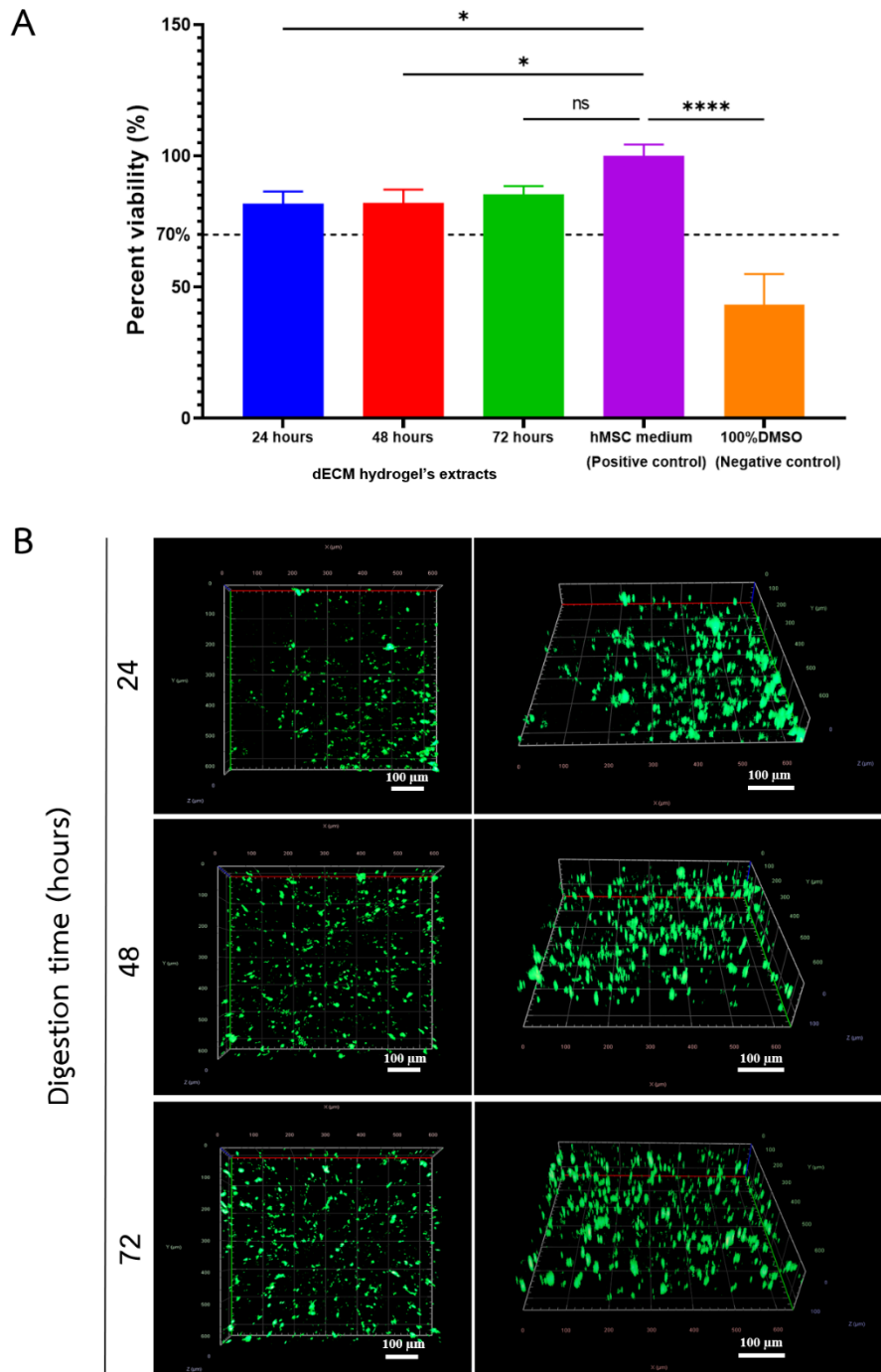


Figure 15 *In vitro* cytotoxicity evaluation of dECM hydrogels

A) Evaluation of the metabolic activity of hMSCs cultured in the dECM

hydrogel's extracts, derived from peptic digestion of decellularized trachea (dTracea) for 24, 48, and 72 hours, was measured by PrestoBlue™ assay. hMSCs medium = positive control and 100% DMSO = negative control. Data are displayed as mean \pm standard deviation (n = 3). **B)** Assessment of hMSCs embedded in the dECM hydrogels at day 3. Scale bars = 100 μ m.

4.8 Viability and tube formation assay of HUVECs

The results indicate that HUVECs successfully formed tube-like structures on Matrigel® within 4 hours, whereas on fibrin gel and dECM hydrogels, the cells were evenly distributed as a monolayer (**Fig. 16A**). After 24 hours, HUVECs exhibited excellent viability on both fibrin gel and dECM hydrogel, while the tube-like structures formed on the Matrigel® group became detached (**Fig. 16B**).



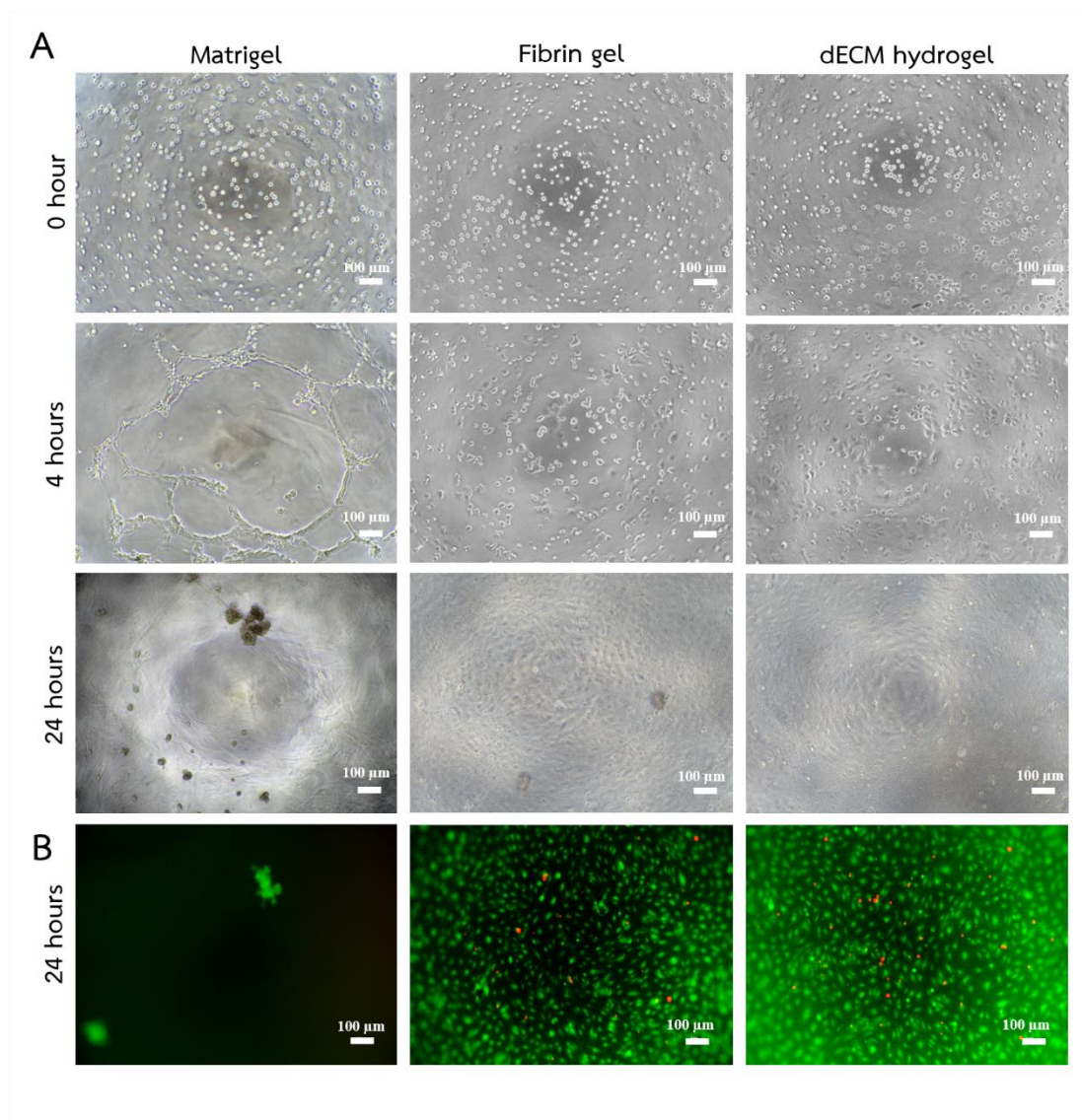


Figure 16 HUVEC viability and tube formation

A) Tubular formation assay of HUVECs on Matrigel®, fibrin gel and dECM hydrogel B) HUVECs at 24 hours observed by LIVE/DEAD® assay. Scale bars = 100 μm

4.9 Histological analysis of chondrogenic differentiation of hMSCs in dTracheal scaffold

During the optimization of the injectable hydrogel, the canine dECM solution was mixed with fibrin, thrombin and gelatin to achieve a homogeneous and easy-to-deliver hydrogel from a syringe.

dECM-fibrin hydrogel exhibited greater cell contraction compared to the fibrin

hydrogel starting from day 3 of observation. This was evident by the presence of small white dots in the culture well plate. In contrast, the size of the fibrin hydrogels decreased in relation to the concentration of cells on day 3. By day 7, both the fibrin hydrogel and the canine dECM fibrin hydrogel appeared as small white dots in each cell concentration (**Fig. S1**). On the other hands, the dECM-fibrin hydrogel mixed with hMSCs was intended to be used in formation of cartilage rings, located on the outer surface of the decellularized tracheal scaffold. The cells/hydrogel mixture did not show any significant contraction or shrinkage within the decellularized scaffold (**Fig. S2**). The absence of contraction or shrinkage of the injected cells/hydrogel mixture indicates that the decellularized scaffold may offer a stable and supportive environment of formation of cartilage rings.

An intriguing observation was made during the study: dTracheal scaffolds, the chondrogenic differentiation of hMSCs was observed in the adventitia layer of the trachea (**Fig. 17A; Fig. S3**). Additionally, punched dTracheal scaffolds showed that hMSCs were cultured within the central lumen of tracheal, and chondrogenic differentiation occurred within the cartilage layer. hMSCs infill through a making-hole for improvement of the cell contract area and cells spread around tracheal cartilage due to porous cartilage structure (**Fig. 17A; Fig. S3**). Particularly, the secretion of sGAG were presented in both dTracheal scaffolds and punched dTracheal scaffolds compared to dTracheal scaffold (control) after 3 weeks (**Fig. 17B; Fig. S3**), indicating cartilage-like tissue formation.

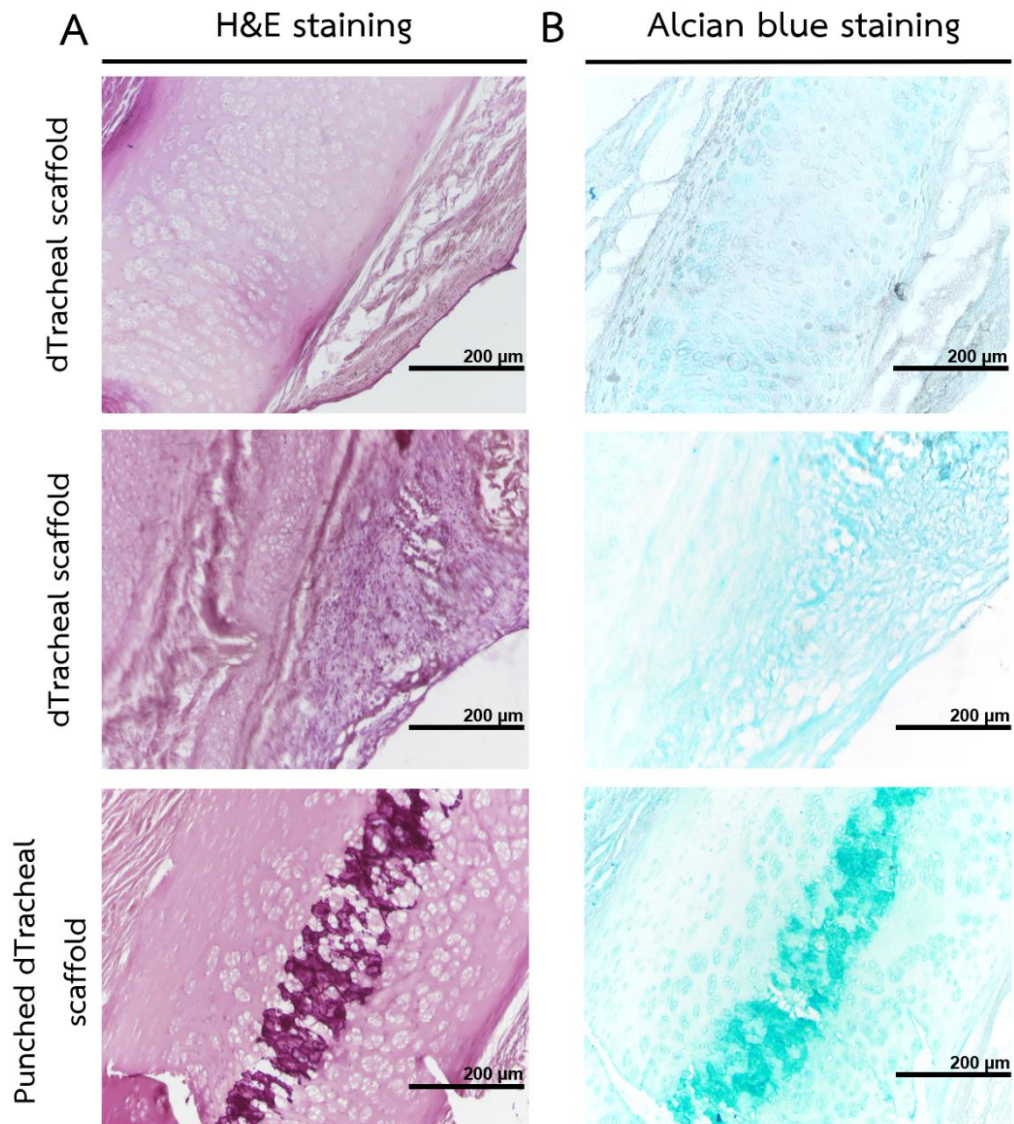


Figure 17 Histological analysis

A) Microstructural of cartilage regeneration from chondrogenic differentiation of hMSCs embedded in an injectable canine dECM-fibrin hydrogel on dTracheal scaffolds by H&E staining. B) Glycosaminoglycan secretion from chondrogenic differentiation of hMSCs by Alcian blue staining. Scale bars = 200 µm

4.10 Fibroblasts support epithelium tissue formation and ciliated epithelial cell differentiation on decellularized tracheal scaffold (dTracheal scaffold)

4.10.1 Histoarchitecture

In H&E staining of co-culturing, fibroblasts prevent epithelium infiltration into the submucosa layer of dTracheal scaffold, showing epithelium maintained a confluent layer on mucosa through 21 days (**Fig. 18A**). Epithelium cultivation alone presented cells infiltrating in the dTracheal's submucosa layer on day 21 compared to day 7 (**Fig 18B**). Fibroblasts cultured alone form a compact monolayer of cells on the mucosa of dTracheal scaffold (**Fig. 18C**). Non-seeded dTracheal scaffold had no cells appearance in both mucosa and submucosa layer of dTracheal scaffold (**Fig. 18D**).

Through the implementation of tri-culturing, the cultivation of epithelium alongside fibroblasts resulted in the formation of a monolayer of cells that displayed a distributed pattern along the mucosa layer of the trachea (**Fig. 19E**). Conversely, the absence of fibroblast support, the epithelium of the trachea lost its monolayer structure, leading to the infiltration of epithelial cells into the submucosa layer (**Fig. 19F**). Non-seeded epithelium cells had no cells appearance in both mucosa and submucosa layer of hMSCs constructs (**Fig. 19G**).

In tri-culture conditions, the differentiation of epithelium cells in 3D culture showed a remarkably elongated columnar phenotype when supported by fibroblasts and/or hMSCs. This enhanced polarization of the epithelium closely mirrored the characteristic features observed in the trachea in its natural environment (**Fig. 19E**).

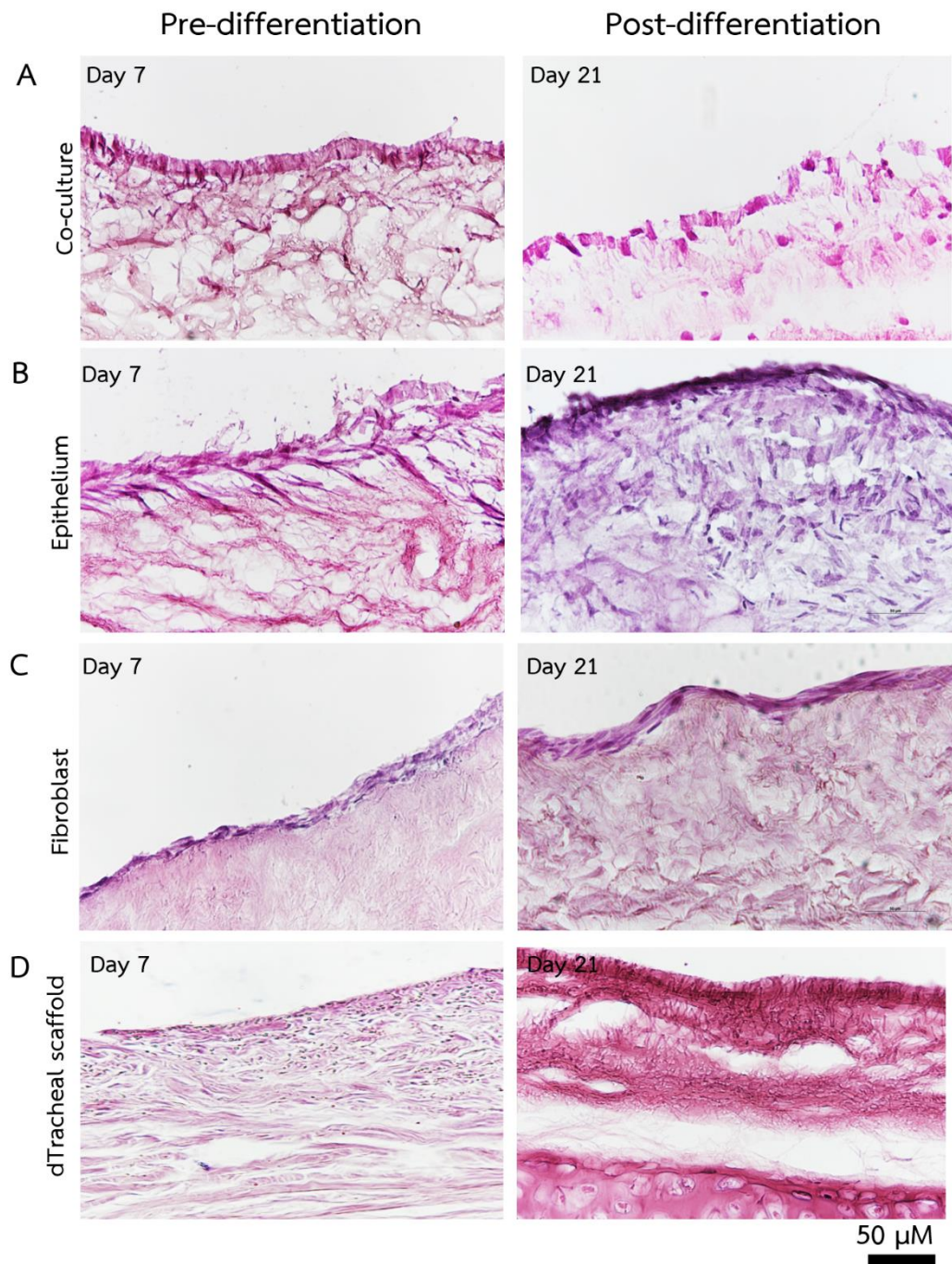


Figure 18 Comparison of co-culture system pre- and post-differentiation stained with H&E staining. The appearance of the mucosa layer showed A) co-culture constructs, B) Epithelium constructs, C) Fibroblasts constructs, and D) dTracheal scaffold. Scale bar: 50 μ m

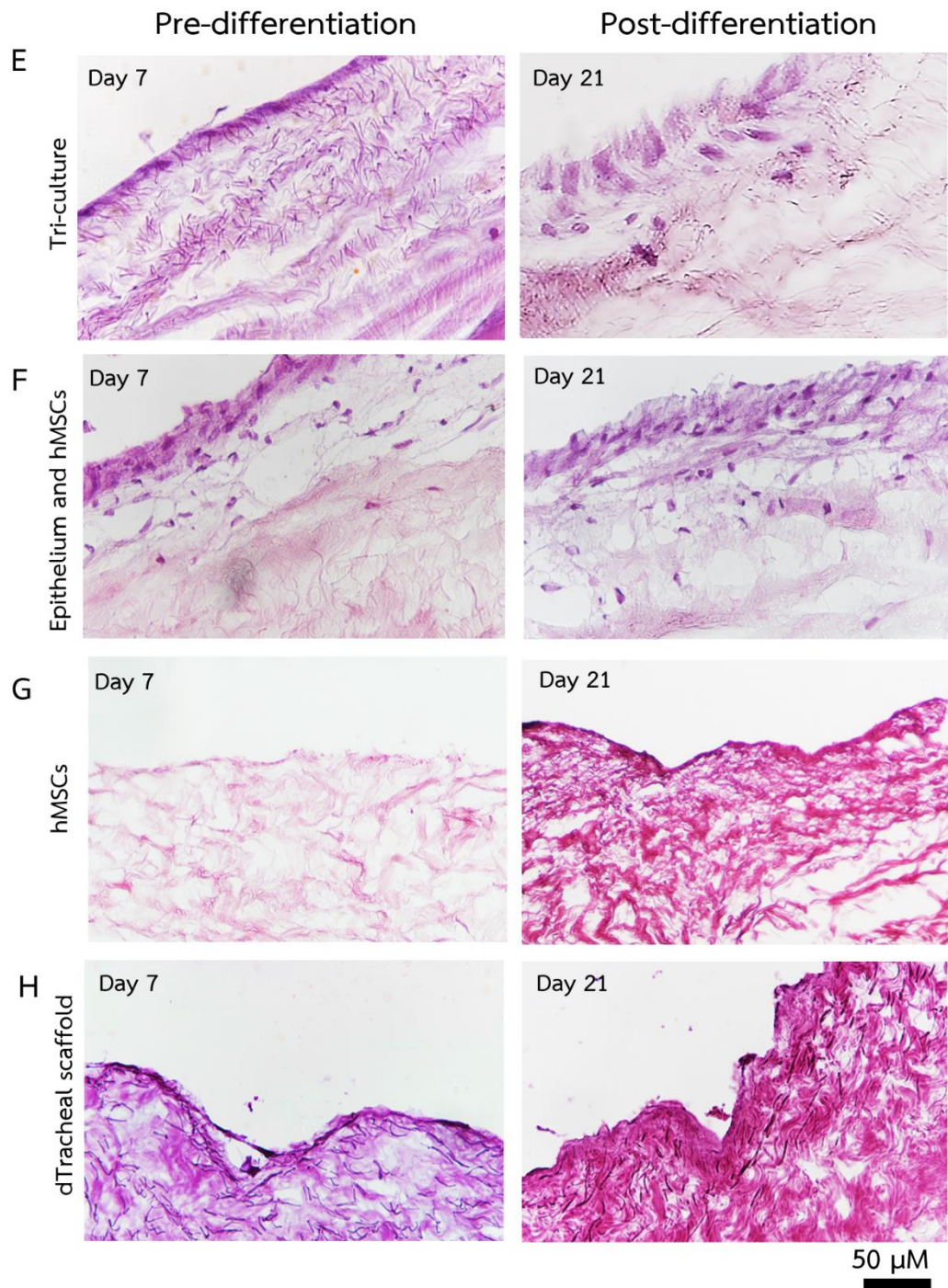


Figure 19 Comparison of tri-culture system pre- and post-differentiation stained with H&E staining. The appearance of the mucosa layer showed E) tri-culture constructs, F) epithelium/hMSCs constructs, G) hMSCs constructs, and H) dTracheal scaffold. Scale bar: 50 μ m

4.10.2 Cartilage formation

Interestingly, human mesenchymal stem cells (hMSCs) demonstrated the ability to differentiate into chondrocytes, resulting in cartilage reorganization within the central part of dTrachea's tracheal cartilage in all conditions of a tri-culture system (Fig. 20) after long-term cultivation. Furthermore, the detection of sGAG in a tri-culture system using Alcian blue staining, proteoglycan (sGAG) secretion was observed in epithelium/fibroblasts/hMSCs (tri-culture) construct, epithelium/hMSCs construct, and hMSCs construct (Fig. 21). sGAG production was identified in dark blue color when compared to the surrounding area, which is donor tracheal cartilage, and also when compared to dTracheal scaffold as a control group. Immunohistochemically staining of tissue reorganization from neocartilage explants was positive for collagen type II (brown) in tri-culture construct and hMSCs construct (Fig. 21).



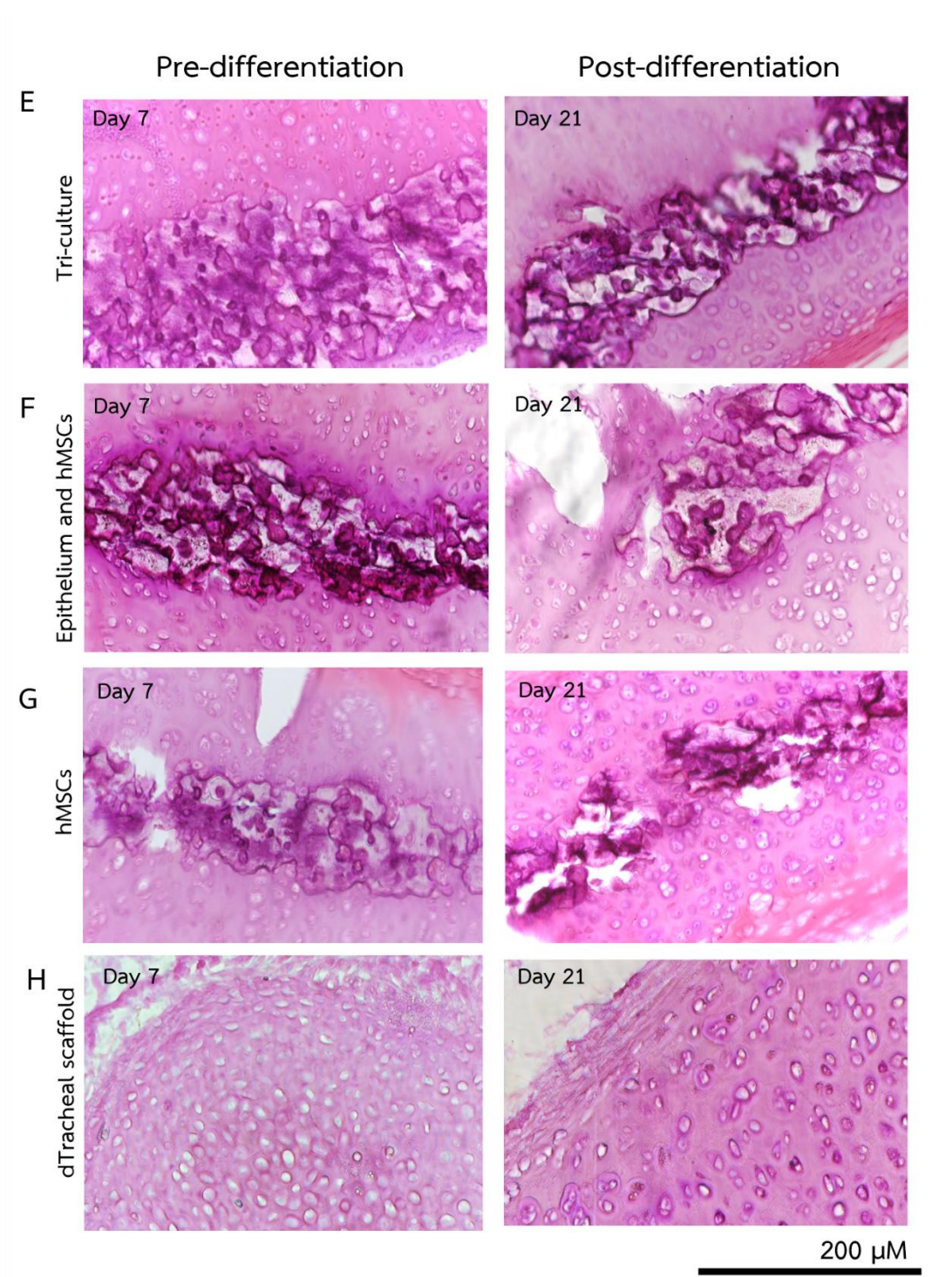


Figure 20 Comparison of tri-culture system pre- and post-differentiation stained with H&E staining. The appearance of the tracheal cartilage showed E) tri-culture constructs, F) epithelium/hMSCs constructs, G) hMSCs constructs, and H) dTracheal scaffold. Scale bar: 200 μ m

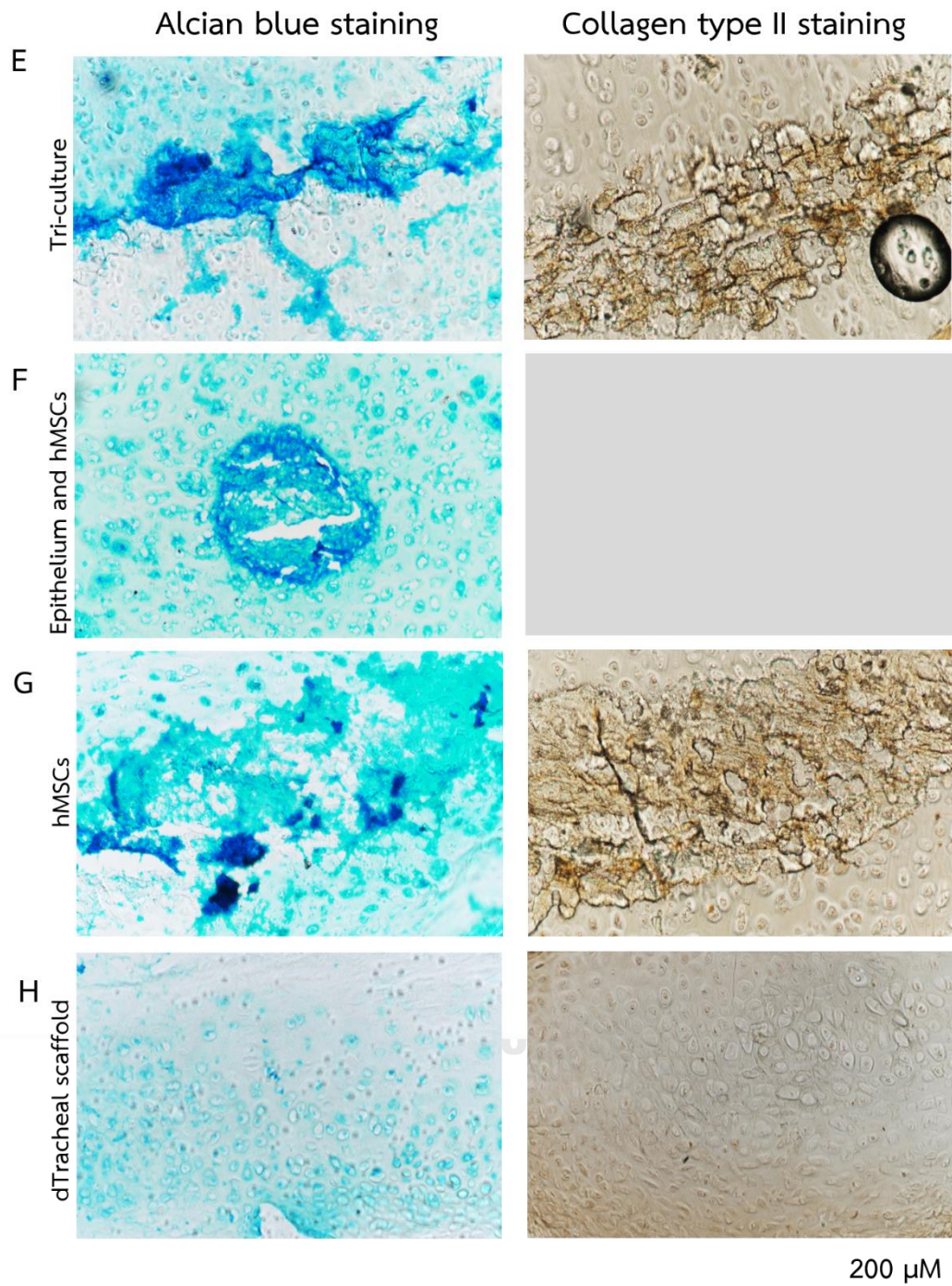


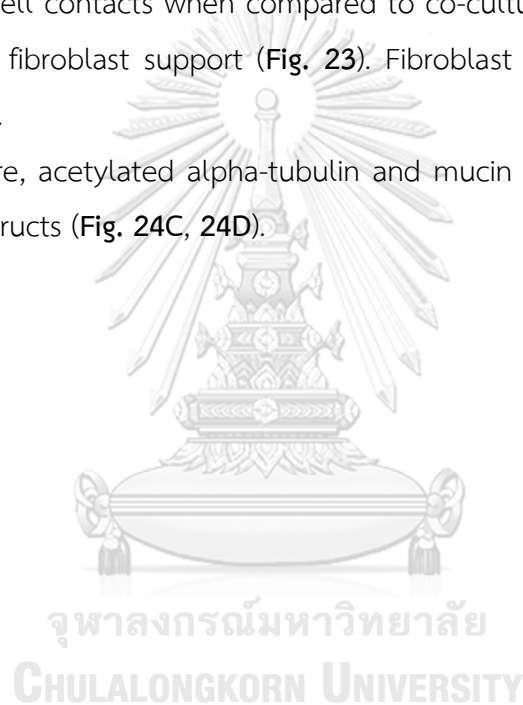
Figure 21 Histological analysis of study in tri-culture system: the appearance of the tracheal cartilage stained with Alcian blue and Immunohistochemistry staining post-differentiation. E) tri-culture constructs, F) epithelium/hMSCs constructs, G) hMSCs constructs, and H) dTracheal scaffold. Scale bar: 200 μ m.

4.10.3 Protein expression proves epithelium differentiation and function by immunofluorescence staining

Actin was stained in all constructs of co- and tri-culture system as an internal control to confirm housekeeping protein expression in pre-and post-differentiation (Fig. 22).

Focusing on the tri-culture construct, E-cadherin was identified as key component of a junctional molecule that is synthesized from epithelial cells. The construct of epithelium/fibroblasts/hMSCs (tri-culture) revealed a distinct morphology of epithelial cell-cell contacts when compared to co-culture, and epithelium/hMSCs construct without fibroblast support (Fig. 23). Fibroblast constructs are severed as control constructs.

Furthermore, acetylated alpha-tubulin and mucin production were detected in tri-culture constructs (Fig. 24C, 24D).



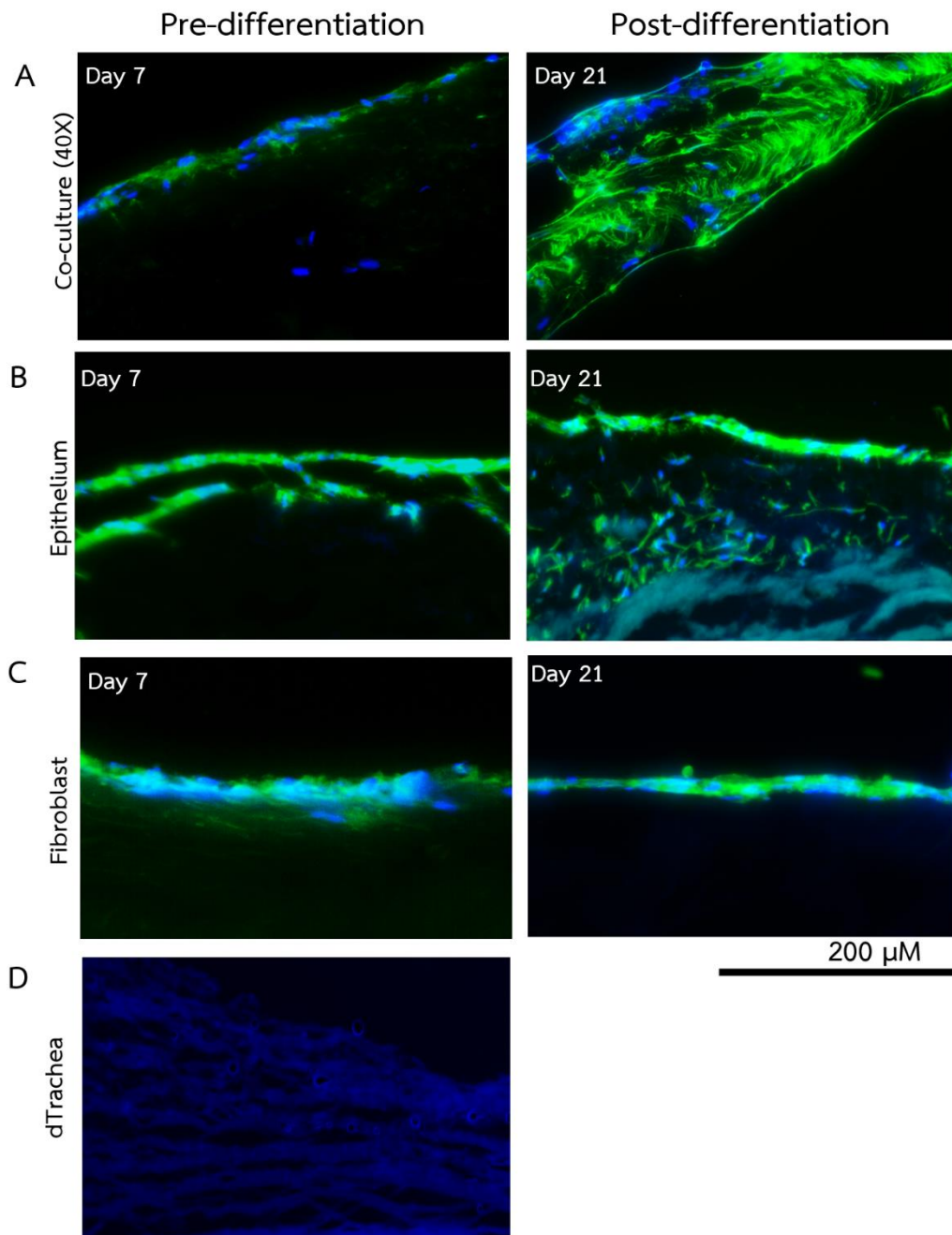


Figure 22 Immunofluorescence staining of co-culture and tri-culture system in pre-and post-differentiation. The appearance of actin positive housekeeping protein (green) and nuclei (blue) stained **A)** co-culture constructs, **B)** epithelium constructs, **C)** fibroblasts constructs, and **D)** dTracheal scaffold, **E)** tri-culture constructs, **F)** epithelium/hMSCs constructs, **G)** hMSCs constructs, and **H)** dTracheal scaffold. Scale bar: 200 μm

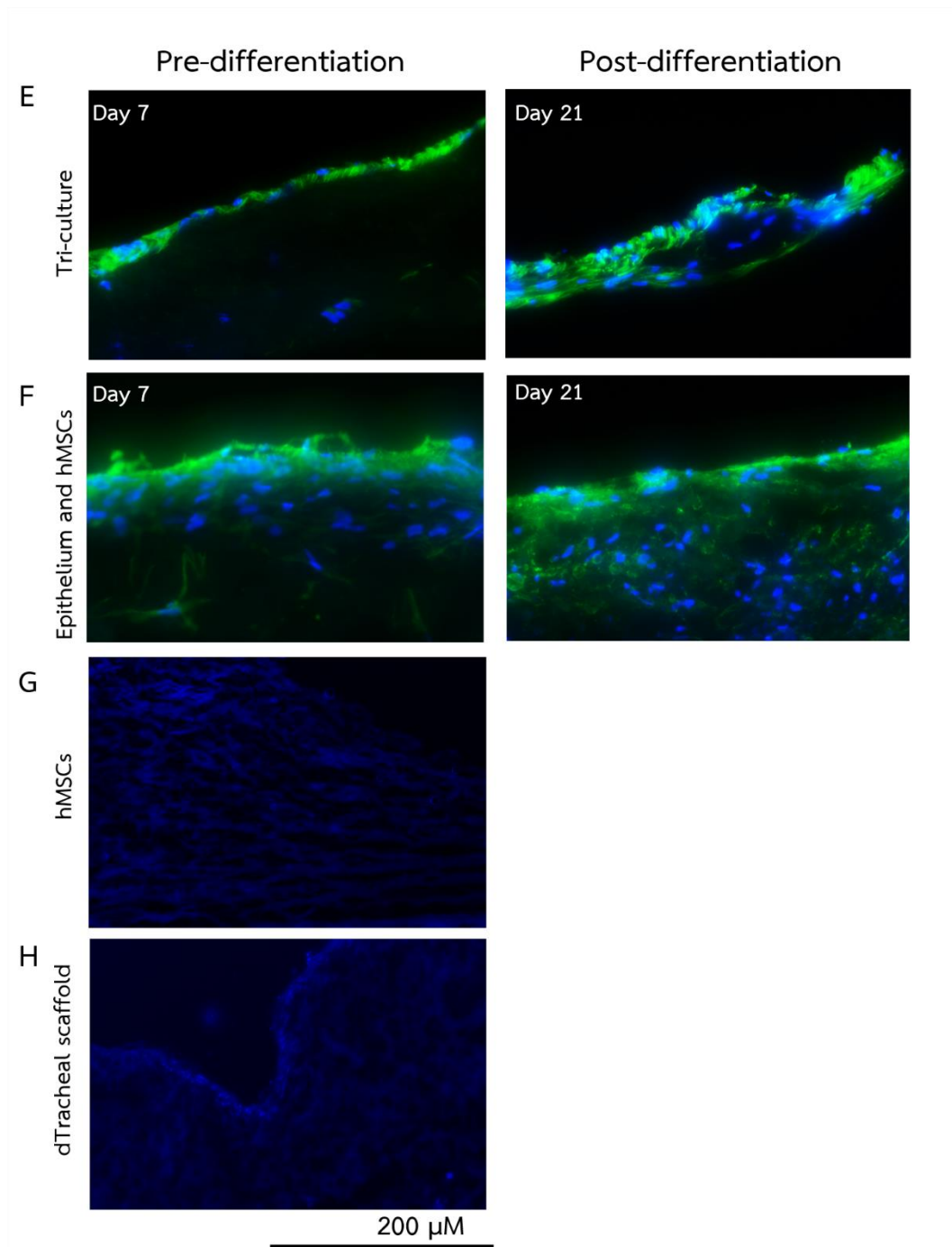


Figure 22 Immunofluorescence staining of co-culture and tri-culture system in pre-and post-differentiation (continuous). The appearance of actin positive housekeeping protein (green) and nuclei (blue) stained **A)** co-culture constructs, **B)** epithelium constructs, **C)** fibroblasts constructs, and **D)** dTracheal scaffold, **E)** tri-culture constructs, **F)** epithelium/hMSCs constructs, and **G)** hMSCs constructs **H)** dTracheal scaffold. Scale bar: 200 μm

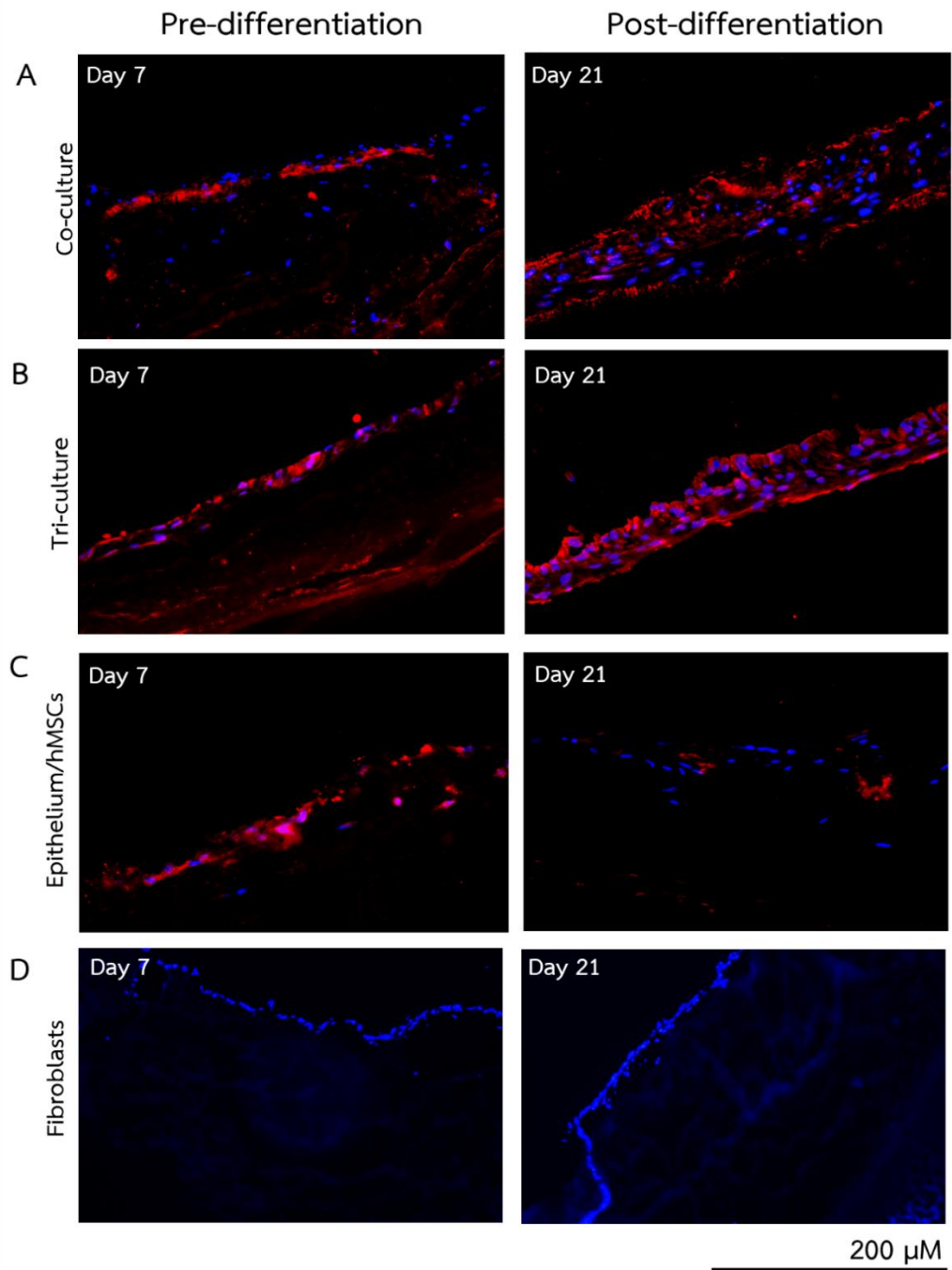


Figure 23 Immunofluorescence staining of E-cadherin in pre-and post-differentiation. The appearance of E-cadherin positive epithelium tight junction (red) and nuclei (blue) stained **A)** co-culture constructs, **B)** tri-culture constructs, **C)** epithelium constructs, and **D)** fibroblasts constructs served as negative control. Scale bar: 200 μ m

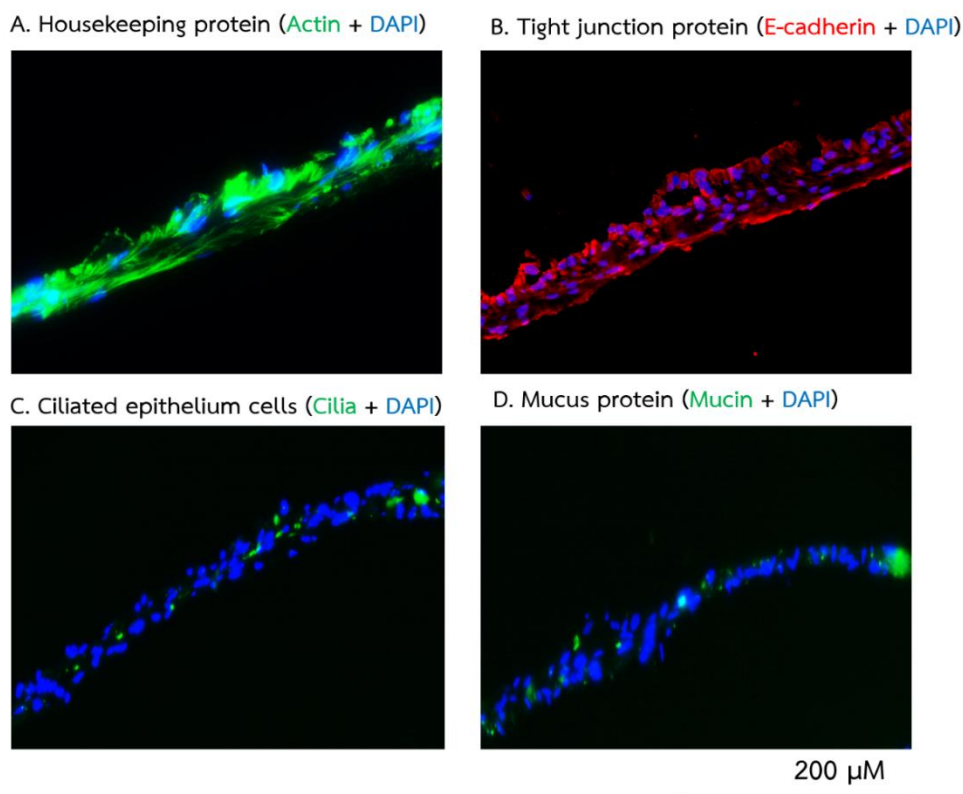


Figure 24 Immunofluorescence staining against A) actin, B) E-cadherin, C) alpha-tubulin and D) mucin on cross sections of tri-culture constructs at 21 days (post-differentiation). Scale bar: 200 μ m.

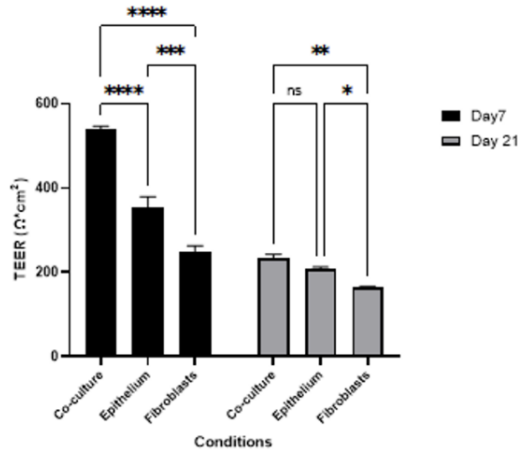
4.11. Evaluation of barrier function มหาวิทยาลัย

For study I, the Trans-Epithelial Electrical Resistance (TEER) values of co-culture increased significantly from $538.72 \pm 7.92 \Omega \cdot \text{cm}^2$ on day 7 compared to epithelium and fibroblasts separated cultured and decreased to $235.20 \pm 7.92 \Omega \cdot \text{cm}^2$ on day 21 (Fig. 25A).

For study II, the TEER values of the tri-culture exhibited a significant increase from $454.72 \pm 7.91 \Omega \cdot \text{cm}^2$ on day 7 compared to the separate cultures of epithelium/hMSCs and hMSCs. However, the TEER values decreased by day 21 to $218.40 \pm 3.17 \Omega \cdot \text{cm}^2$ (Fig. 25B).

On day 7, significant differences were observed between the co-culture and tri-culture groups, with a *p*-value of 0.0106. On the other hand, both groups represented no significant difference (*p*-value = 0.0740) on day 21.

A. Study I: Co-culture system



B. Study II: Tri-culture system

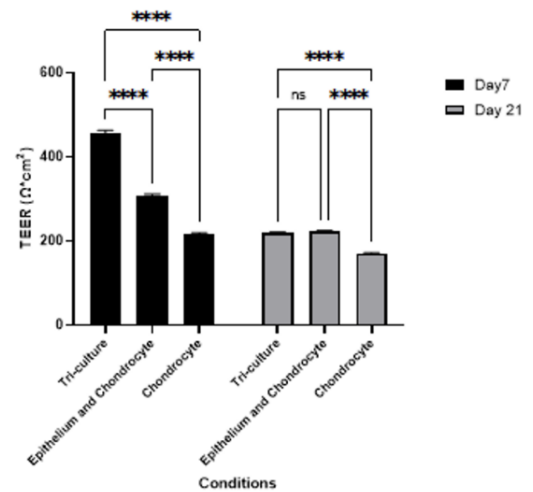


Figure 25 Functional assessment of the epithelial barrier properties for each *in vitro* model. A) TEER values were measured at day 7 and day 21 of co-culture system. B) TEER values of tri-culture system were measured at day 7 and day 21. $n = 3$. Shown are the mean average with standard deviation. $p < 0.05$, ns: not significant.

4.12. Proteomics analysis

4.12.1 Protein composition of dTracheal scaffold and dECM hydrogel

dTracheal scaffold and dECM hydrogel ($n=6$ in each group) (Fig. 26A) were assessed for proteomics profile.

LS-MS/MS analysis identified 7874 proteins and all proteins were selected for statistical differential expression analysis by Metaboanalyst (MetaboAnalyst 5.0). Principal component analysis (PCA) was conducted to reflect the range of variation among samples within the group, revealing distinct distribution of proteins between two groups. The results showed the first component explains 30.8% of the variation and the second component 15.8%, indicating statistical differences due to the majority of protein components (Fig. 26B).

The heatmap analysis showed the enrichment of differential proteins in each

sample (Fig. 26C). In the heatmap, the rows represent protein IDs, while the columns represent samples.

There were 368 significant differential expression proteins identified as shown in the quantitative Volcano plot (Fig. 26D). The red dots represent 295 proteins, indicating a high level of protein content, while the blue dots represent 73 proteins, signifying a low level of protein content (Fig. 26E). Therefore, all 295 proteins were identified and annotated protein name, gene name, gene ontology (biological process), and gene ontology (cellular component) using the Uniplot database.

The results showed significant differences in the main ECM protein components, growth factors and cytokines including collagen type I ($p=3.51 \times 10^{-7}$), collagen type II ($p=4.93 \times 10^{-2}$), collagen type III ($p=3.43 \times 10^{-9}$), collagen type X ($p=5.06 \times 10^{-2}$), collagen type XIV ($p=5.10 \times 10^{-2}$), collagen type XXVIII ($p=5.74 \times 10^{-2}$), mammalian ependymin-related protein1 ($p=4.96 \times 10^{-2}$), osteoglycin ($p=4.93 \times 10^{-2}$), paralemmin 3 ($p=4.93 \times 10^{-2}$), protein wnt ($p=1.13 \times 10^{-2}$), Ras homolog family member j ($p=1.10 \times 10^{-2}$), Rho gdp dissociation inhibitor alpha ($p=1.01 \times 10^{-2}$), Gf-beta family profile domain-containing protein ($p=1.15 \times 10^{-2}$), transmembrane anterior posterior transformation 1 ($p=1.04 \times 10^{-2}$), fibronectin ($p=4.94 \times 10^{-2}$), platelet derived growth factor D ($p=1.12 \times 10^{-2}$), and Insulin like growth factor 2 receptor ($p=5.87 \times 10^{-2}$).

The prediction of key proteins matching with *Canis familiaris* presented that decellularized canine trachea and dECM solution display expressed proteins involvement in biological process such as extracellular structure organization and collagen fibril organization (Fig. 27A). Moreover, KEGG signaling pathways related to cell adhesion (Focal adhesion, ECM-receptor interaction), cell differentiation (PI3K-Akt signaling pathway), and wound healing (Platelet activation) (Fig. 27B).

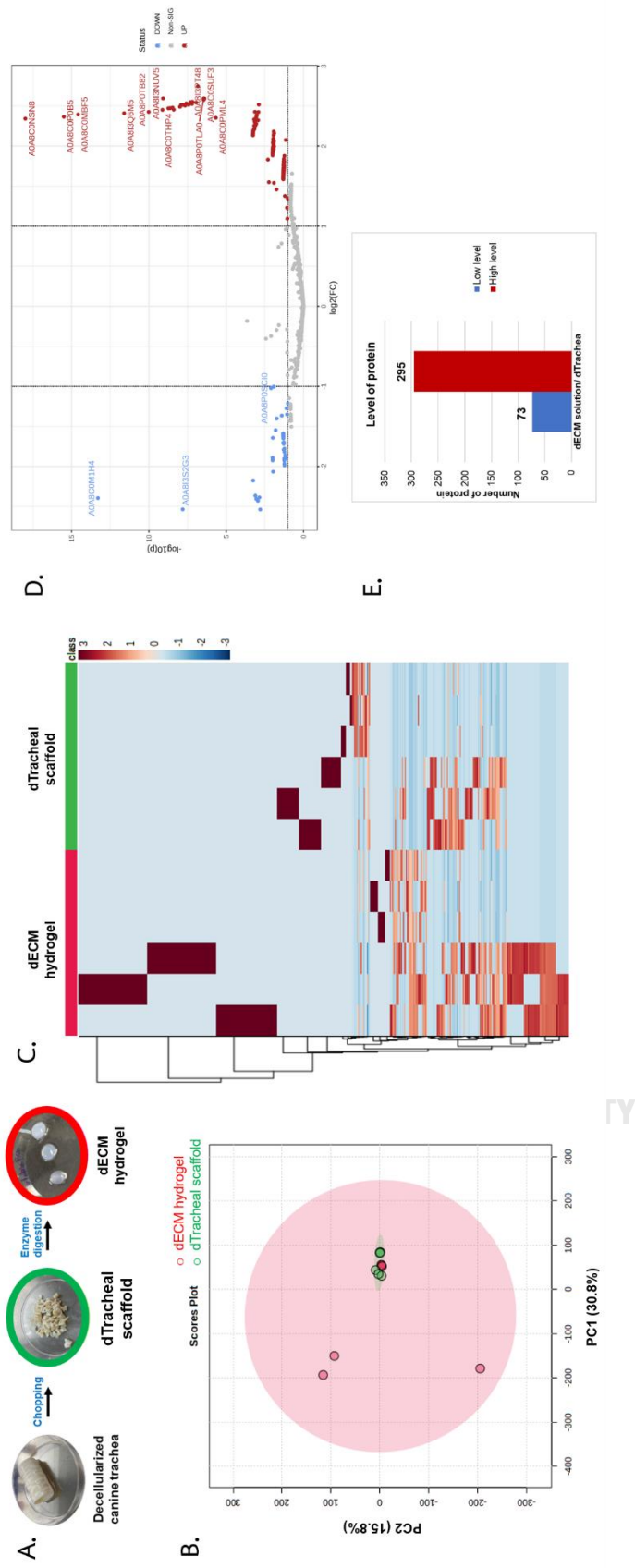


Figure 26 The proteomics dataset analyzed for biological significance of dTracheal scaffold and dECM hydrogel. **A**) Preparation of dTracheal scaffold and dECM hydrogel **B**) Heatmap represented analysis of the differentially expressed proteins in dTracheal scaffold and dECM hydrogel. **C**) The principal component analysis indicated the high aggregation degree of samples in each group (n = 6 in each group). **D,E** Volcano plot showed differentially expressed proteins between dTracheal scaffold and dECM hydrogel (Red dots: High level; Blue dots: low level), which were quantified with histogram.

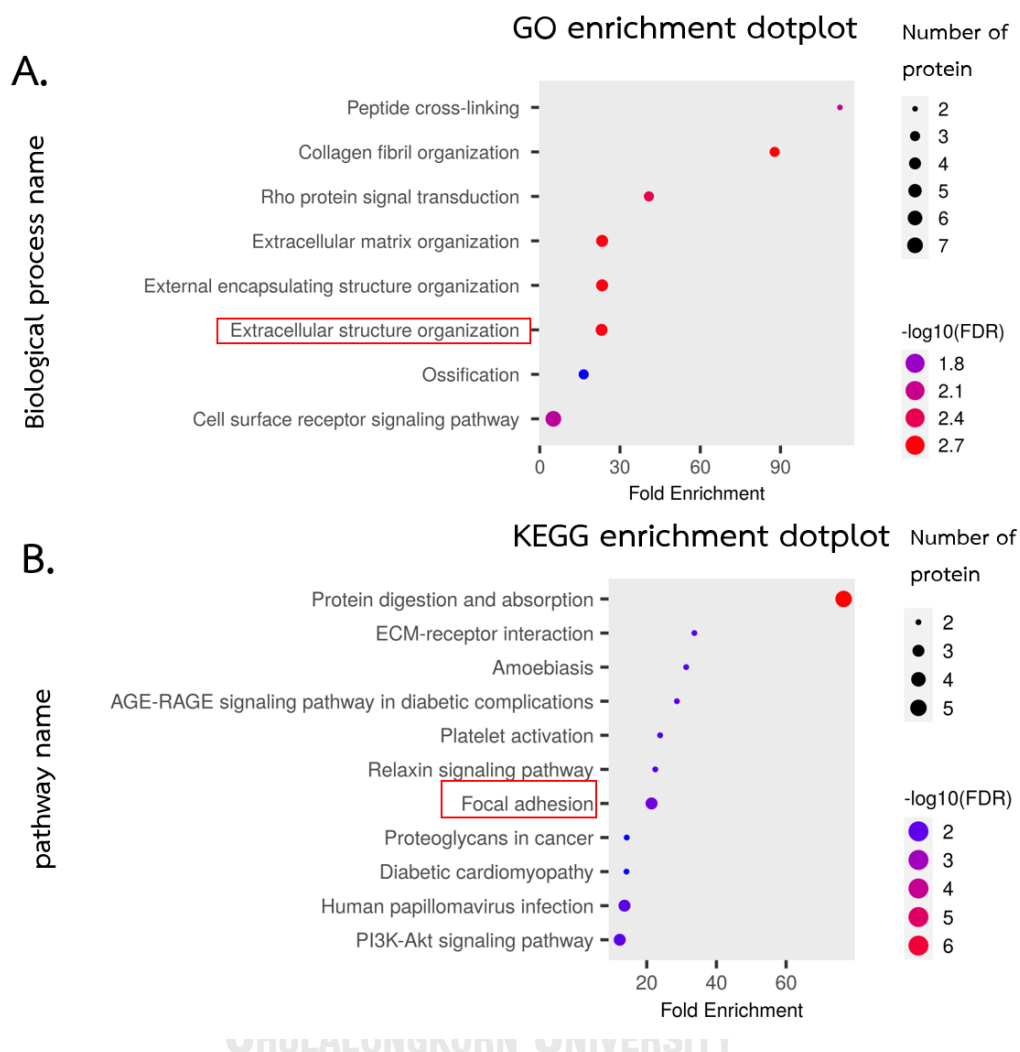


Figure 27 Gene Ontology Enrichment Analysis of dTracheal scaffold and dECM hydrogel by ShinyGO v0.74. **A)** The GO annotation of differentially expressed proteins showed their different biological process roles in the decellularized ECM. **B)** The enrichment analysis of KEGG pathway suggested differentially expressed proteins were annotated in the cell adhesion such as focal adhesion.

4.12.2 Protein profiling of tri-culture construct

Tri-culture (epithelium/fibroblast/hMSCs) constructs (n=3 in each group) (Fig. 28A) were assessed for proteomics profile. dTracheal scaffold and dECM hydrogels

were used to normalize protein components from the construct.

LS-MS/MS analysis identified 7874 proteins and all proteins were selected for statistical differential expression analysis by Metaboanalyst (MetaboAnalyst 5.0). Principal component analysis (PCA) was conducted to reflect the range of variation among samples within the group, revealing distinct distribution of proteins between three groups. The results showed the first component explains 30.8% of the variation and the second component 21.6%, indicating statistical differences due to the majority of protein components (**Fig.28B**).

The heatmap analysis showed the enrichment of differential proteins in each sample (**Fig.28C**). In the heatmap, the rows represent protein IDs, while the columns represent samples.

There were 165 significant differential expression proteins identified as shown in the quantitative ANOVA (**Fig.28D**) The red dots represent 165 proteins, indicating a high level of protein content, while the green dots represent 769 proteins, signifying a low level of protein content. Therefore, all 165 proteins were identified and annotated protein name, gene name, gene ontology (biological process), and gene ontology (cellular component) using the Uniplot database.

The results showed significant differences in the main protein components of epithelium/fibroblasts/hMSCs (tri-culture) construct: Actin as housekeeping protein ($p=7.76 \times 10^{-9}$); Alpha-tubulin ($p=1.67 \times 10^{-12}$) and Beta-tubulin ($p=5.41 \times 10^{-7}$), Keratin 14 ($p=1.14 \times 10^{-12}$) for ciliated epithelium cells; Vimentin ($p=6.67 \times 10^{-6}$) for the fibroblast marker; and Collagen type I ($p=1.48 \times 10^{-12}$), Collagen type VI ($p=2.24 \times 10^{-14}$), and Tenascin-c ($p=2.89 \times 10^{-10}$) for hMSCs differentiate into chondrogenic.

The prediction of key proteins matching with Homo sapiens presented that epithelium/fibroblasts/hMSCs (tri-culture) construct display expressed proteins involvement in biological process such as epithelial differentiation, wound healing, and cell junction organization (**Fig. 29A**). Moreover, KEGG pathways related to cell adhesion (ECM-receptor interaction, focal adhesion), and cell differentiation (PI3K-Akt signaling pathway) (**Fig. 29B**).

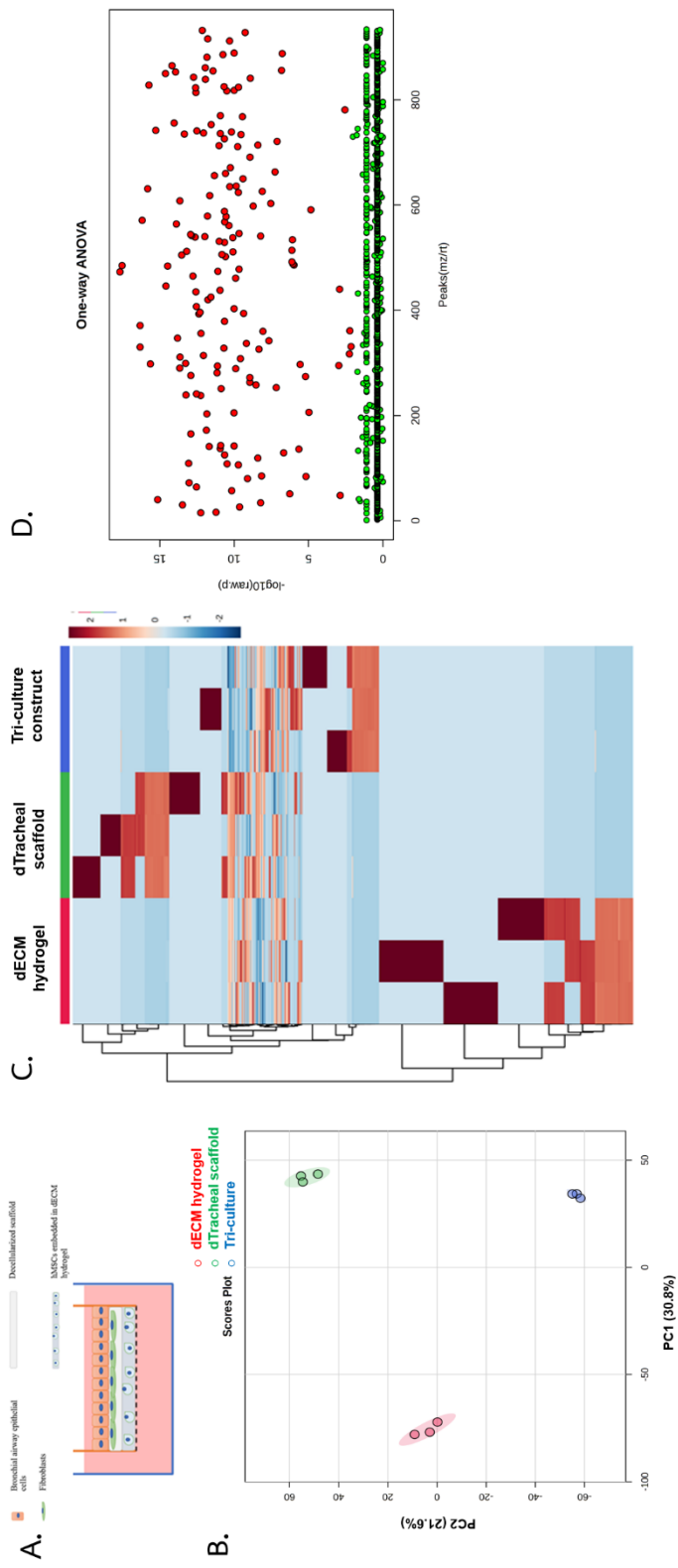


Figure 28 The proteomics dataset analyzed for biological significance of tri-culture. A) Sampling of tri-culture constructs for proteomics analysis. B) Heatmap represented the cluster analysis of the differentially expressed proteins in tri-culture constructs compared to dTracheal scaffold and dECM hydrogel. C) The principal component analysis indicated the high aggregation degree of samples in each group ($n = 3$ in each group). D) ANOVA plot showed differentially expressed proteins between tri-culture constructs, dTracheal scaffold and dECM hydrogel (Red dots: High level; green dots: low level).

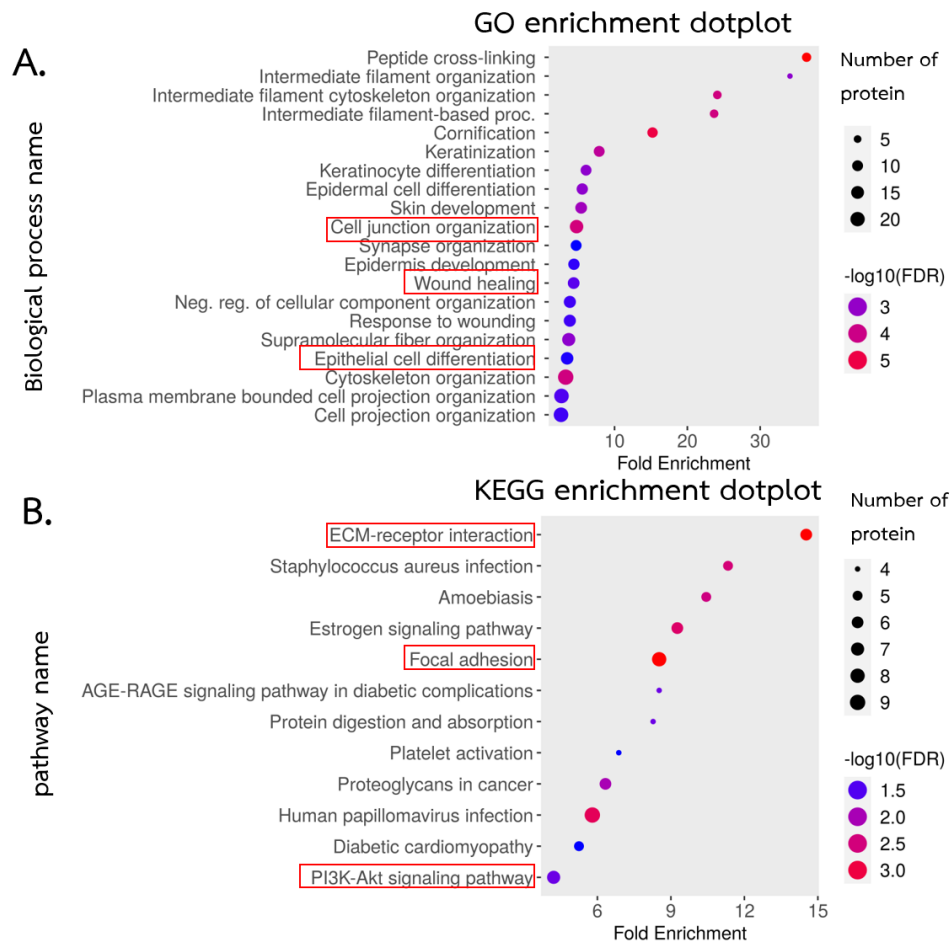


Figure 29 Gene Ontology Enrichment Analysis of tri-culture constructs by ShinyGO v0.77. A) The GO annotation of differentially expressed proteins showed their different biological process roles in the tri-culture construct. B) The enrichment analysis of KEGG pathway suggested the differentially expressed proteins were annotated in the cell adhesion and cell proliferation, such as ECM-receptor interaction, focal adhesion, PI3K-Akt signaling pathway.

CHAPTER V Discussion and conclusion

Tracheal tissue engineering exhibits the potential for the regeneration of compromised tracheal segments through the combination of respiratory epithelial cells within a tubular scaffold matrix. The fabrication of hollow structures suitable for cellular culture poses inherent challenges, necessitating the development of constructs with the structural integrity to resist collapse or necessitate sutures while concurrently affording an optimal milieu for cellular adhesion and proliferation. The decision to utilize all six canine tracheas in the decellularization process was based on their excellent representation of mechanical properties and dimensional features, making them a valuable model to translate into clinical studies.

In the present study, the decellularized canine trachea exhibited a preservation of its structural integrity, as evidenced by comparable biomechanical properties when compared to the non-treated trachea. Furthermore, it provided an artificial microenvironment conducive to the adhesion of epithelial cells. The process involved the preparation of decellularized trachea (dTrachea) through a vacuum-based procedure along with detergents and nuclease enzymes [6, 8] for the removal of cellular constituents such as proteins, lipids, and nucleic acids, known as significant triggers for immune responses and potential complications associated with organ rejection [5]. Histological evaluation via H&E staining and DNA quantification (**Fig. 2a and 4a**) revealed an absence of cells within the mucosa and submucosa layers of the dTrachea. However, residual traces of cellular components appeared within the cavities (lacunae) at the cartilage layer (**Fig. 2a**). Remarkably, the vacuum-assisted decellularization process involves freeze and thaw steps (thermal changes) that can lead to cell necrosis and apoptosis. After the decellularization process, this may be described in the presence of residual cells within decellularized tissues. The remaining cells do not trigger an immune response, as apoptosis-assisted

decellularization [58, 59]. Herein, we lack an evaluation of cell death such as cell apoptosis and necrosis in decellularized tissue samples to confirm the presence of remaining cells by flow cytometry analysis.

The decellularization process of the vacuum-assisted technique demonstrated effectively eliminated MHC class II molecules; in addition, dTrachea showed no statistical differences in key the extracellular matrix (ECM) components, including sGAG, collagen, laminin, and fibronectin, compared to the unwashed control group. These ECM elements play multifaceted roles in tissue development, encompassing the provision of physical support for cells, serving as a barrier between different tissue types, facilitating intercellular communication and guidance during development, storing essential growth factors and cytokines vital for cellular viability and proliferation, aiding in nutrient transport within tissue compartments, and regulating the gene expression profiles associated with specific cell types or functions [49, 60-64].

Excessive removal of the extracellular matrix (ECM) affected cell attachment, as evidenced by a reduction in epithelial cell attachment observed in a decellularized lung tissue with a low glycosaminoglycan (GAG) content [65]. In our study, primary human bronchial epithelial cells (HBEpCs) were evenly distributed on the mucosa layer and exhibited robust attachment to the ECM networks of the dTrachea. The re-epithelialization of the decellularized trachea is a critical stage in cell-based tracheal reconstruction, playing a vital role in restoring the normal structure and function of the airway tissue [66]. Moreover, it enhances the tracheal strength and flexibility, rendering it more suitable for implantation in patients with compromised airways [67].

The dTrachea has not been seeded with epithelial cells and has been documented as a viable platform for facilitating the infiltration of epithelial cells from healthy portions of the trachea [68]. These unseeded dTracheas have also

shown promise in promoting the healing process and mitigating inflammatory responses [68, 69]. Furthermore, their porous structure makes them suitable candidates for potential drug or therapeutic agent delivery systems, as they enable controlled release over time [61].

According to dTracheas lack native cellular components, rendering them unable to undergo self-repair or regeneration ability. Consequently, we introduced HBEpCs to the inner lining of the dTrachea, a strategy with potential benefits for tracheal tissue reconstruction and the promotion of long-term tissue regeneration. The newly introduced HBEpCs not only adhered to the dTrachea but also migrated into its submucosal layers, showcasing their capacity to re-establish a functional mucosal lining during tracheal reconstruction. In contrast, unseeded dTrachea was more susceptible to degradation over time [31, 69]. Outstandingly, our study demonstrated that the ECM-rich dTrachea exhibited no toxicity and provided suitable attachment sites for epithelial cells. Furthermore, epithelial cells are exposed to growth factors such as epidermal growth factor (EGF) and fibroblast growth factor (FGF), leading to the ability to differentiate into ciliated pseudostratified columnar epithelial cells [70, 71].

The complex tissue architecture of the trachea poses a one major challenge for replicating biofabrication technologies. Nevertheless, decellularized trachea emerges as a promising avenue for reinstating tracheal structure without triggering an immune response because it eliminates DNA content and major histocompatibility complex (MHC). Herein, the suitable structural framework and biochemical environment offered by the decellularized trachea will facilitate the proper function of the trachea. The fundamental hypothesis behind utilizing decellularized trachea (dTrachea) as a scaffold in the present study revolves around the notion that the diverse biochemical cues secreted by the native cells of tracheal tissue will create a microenvironment conducive to the development of newly seeded cells for

regenerative medicine of trachea. To conclude part I: preparation of dTrachea, the dTrachea revealed that the quality of decellularized ECM preserves four aspects after the decellularization process, including removing the cellular components, eliminating genetic material, preserving protein contents, and retaining mechanical properties. Moreover, the dTrachea supports epithelial lining.

The secondary purpose of the dECM hydrogel is to serve as a vehicle for encapsulating human mesenchymal stem cells (hMSCs) and subsequently guiding their differentiation into chondrocytes. The ECM hydrogel employed in this study is a collagen-based self-assembling matrix supplemented with other proteins. This matrix was neutralized to a physiological pH of 7.4 and allowed to form a hydrogel at a temperature of 37°C [50]. The dECM comprised a mixture of tissues from various tracheal components, including mucosa, submucosa, cartilage, and adventitia, which were previously inhabited by different cell types, including chondrocytes. Consequently, it is imperative to conduct further research to thoroughly investigate the biological microenvironment provided by this ECM-rich hydrogel and assess its capacity to facilitate the chondrogenic differentiation of hMSCs.

Furthermore, we conducted experiments to assess the vascularization potential of endothelial cells on the dECM hydrogel. While the ECM hydrogel served as a suitable biological matrix for human umbilical vein endothelial cell (HUVEC) attachment, it did not induce the formation of tube-like structures by HUVECs. However, our findings demonstrated that the dECM hydrogel supported the viability of HUVECs for a longer duration compared to Matrigel®. In contrast, HUVECs cultured on Matrigel® disintegrated and detached within 24 hours, whereas they exhibited healthy spreading on both the ECM hydrogel and a commercially available fibrin gel derived from bovine plasma. The composition of the dECM hydrogel in this study may have contained biochemical profiles more akin to the fibrin gel than Matrigel®, which is composed of extracellular matrix proteins from mouse sarcoma. In summary, our study indicates that the dECM hydrogel holds promise for

encapsulating hMSCs and potentially promoting the formation of cartilage rings. However, a significant challenge remains in devising strategies to facilitate vascularization within the trachea.

Moreover, decellularized trachea provide a natural scaffold as a biodegradable product. Herein, the benefit of chondrocyte growth is needed to support a biodegradable scaffold to maintain the original tubular structure and facilitate tissue reformation. Because tracheal cartilage is compact and tubular, dECM hydrogel would be helpful as a cell carrier for cell supporter during cultivation *in vitro*. Several methods have been applied to complete cartilage regeneration of the trachea, such as fragmented cartilage into micro-sized pieces [72], sliced cartilage into sheets [73], pulverized decellularized porcine articular cartilage into a powdered form [74], and created porosity of trachea by a laser micropore technique [23]. These approaches effectively addressed certain drawbacks; in contrast, they share a limitation in compromising the inherent integrity of the initial tubular structure, and the surrounding matrix microenvironment.

In our study, we employed punched dTracheal scaffolds, along with embedding human mesenchymal stem cells (hMSCs) at a concentration of 1×10^6 cells/mL within the dECM hydrogel to support cartilage formation during a three-week cultivation period. The rough surface of dTracheal scaffold encourages the entrapment of fibrin protein and cell adhesion is improved by the chemical grafting of adhesion peptides such as Arg-Gly-Asp to material surfaces [75]. After 7 days, canine dECM fibrin hydrogel still appears surrounding dTracheal scaffold. Thus, dTracheal scaffold prevents hydrogel contraction from cell-cell interaction (**Fig. S2**). The absence of contraction or shrinkage of the injected cells/hydrogel mixture indicates that the decellularized scaffold may offer a stable and supportive environment of formation of cartilage rings. This approach resulted in promising outcomes, as confirmed by histological assessments such as H&E staining and Alcian blue staining, which revealed cell reorganization and the secretion of sulfated glycosaminoglycans (sGAG) in the middle part of the lacunae within the decellularized scaffold (**Fig. 10**). These findings highlight the potential of our method for cartilage regeneration in the trachea and contribute to the growing body of

knowledge in the field of tracheal tissue engineering.

To delve into the diverse applications of decellularized trachea within the realm of airway regenerative medicine, this study harnessed tracheal extracellular matrix (ECM) to fashion two distinct types of cell carriers for three unique cell types: epithelial cells, human mesenchymal stem cells (hMSCs), and human umbilical vein endothelial cells (HUVECs). Looking ahead, the decellularized trachea is poised to become a valuable instrument for investigating the differentiation of ciliated cells that line the tracheal lumen and for examining the growth and maturation of the crucial cartilage rings. Nevertheless, human umbilical vein endothelial cells (HUVECs) did not form tube-like structures, typically indicative of vascularization. In this study, HUVECs demonstrated robust viability and effectively spread across the surface of the decellularized trachea ECM (dECM) hydrogel. However, the dECM hydrogel properties could optimize the stiffness and cell-matrix interaction (hydrophobic) properties in the future.

This underscores the potential of utilizing decellularized trachea as a dual cell-carrier system, promoting re-epithelization and cell encapsulation for tracheal reconstruction. The development of dual cell-carrier systems may herald more effective approaches to creating biomaterials for tracheal tissue reconstruction. Our research findings provide valuable insights that contribute to the ongoing advancements in tracheal tissue engineering, bringing us closer to the prospect of clinical applications that can benefit patients who need tracheal repair and regeneration.

To explore the versatility of the dTrachea in the field of airway regenerative medicine, tracheal extracellular matrix (ECM) was employed to generate two distinct cell carriers, which are decellularized scaffold and dECM hydrogel with two specific cell types: epithelial cells and human mesenchymal stem cells (hMSCs). In addition to investigating the capacity of an intact dTrachea to support cell attachment, we also prepared dTrachea in a liquid form, referred to as dECM solution, and induced it to form a hydrogel known as dECM hydrogel. This resulting ECM-rich hydrogel is intended for the encapsulation of hMSCs, which have the potential to differentiate

into chondrocytes typically found in the cartilage rings of the trachea.

Numerous studies have made efforts to develop tracheal substitutes for trachea replacement. However, no standard protocol applies in clinical applications due to the challenges of mimicking trachea structure and function. Decellularized trachea represents an exciting option in the native format and provides mimic microenvironments. In tracheal tissue engineering, many cells are applied to decellularized tracheal scaffold in clinical such as epithelium cells and chondrocyte [37], epithelium cells and bone marrow cells [76], and hemopoietic stem cells and endothelial progenitors [66]. Nonetheless, decellularized tracheal scaffolds used for tracheal replacement had reliable evidence of delayed epithelialization, unsuccessful functional respiratory epithelium, and granulation tissue after implantation, leading to bacteria invasion, and tracheal stenosis [77]. Remarkably, no cells are currently completed satisfactorily due to the technique for recellularization, and inducing cell differentiation required optimization.

The finding indicated that dTracheal scaffolds and dECM hydrogel as a cell carrier coupled fibroblasts supporting investigated ciliated cell differentiation and neocartilage tissue formation *in vitro* 3D model.

Histological staining with Hematoxylin and Eosin (H&E) revealed a diffuse distribution of epithelial cells with and without fibroblasts supporting the mucosa layer of the luminal surface in the short-term culture (day 7). In contrast, epithelial cells were infiltrated into the trachea scaffold in a culture without fibroblasts supporting in the long-term culture (day 21). This might be the reason why epithelium disfunction in long-term implantation. In addition, according to Ravindra A. et al., 2021, epithelium cultured without fibroblasts was poorly grown and undifferentiated into ciliated epithelium on the dTracheal scaffold [78].

In the co-culture and tri-culture constructs with fibroblasts supporting, epithelial cells were present on the mucosa layer of the luminal surface in the long-term culture. Surprisingly, changes in cell morphologies in the co-culture and tri-culture resulted in pseudostratified columnar epithelial morphology similar to native trachea after cell culture in air-liquid interface by 21 days. A protein marker for epithelial differentiation and function was evaluated with immunofluorescent

staining. Ciliated epithelium differentiation was confirmed as positive in protein expression of actin, e-cadherin, acetylated alpha-tubulin, and mucin on the tri-culture construct at 21 days. This study is the first to demonstrate that fibroblasts affect ciliated epithelium formation and differentiation on the mucosa layer of the decellularized tracheal scaffold. Herein, fibroblasts are recognized for their role in modulating the composition of the basement membrane, which enhances the precision of cellular adhesion [79]. Recently, in 3D model culture, human bronchial epithelium cells with fibroblasts presented ciliated epithelium cells on decellularized porcine small intestinal submucosa [60].

Interestingly, hMSCs differentiate into chondrocyte (neocartilage) was found in tri-culture system; epithelium/fibroblasts/hMSCs (Tri-culture) construct, epithelium/hMSCs construct, and hMSCs construct. Alcian blue and immunohistochemistry staining indicated sGAG secretion and collagen type II production, respectively. dTracheal scaffold combined with dECM hydrogel as a cell carrier from decellularized tissue offers the *in vivo* microenvironment, encompassing essential elements like ECM components, growth factors, and structural support [80].

TEER (Transepithelial Electrical Resistance) measurement is used to assess epithelial barrier function, where a high TEER value indicates a better epithelial barrier. Typically, TEER measurement is used to evaluate airway *in vitro* 2D culture model for airway disease or infection. It was found that TEER measurement was higher on day 7 in co-culture and tri-culture constructs more than on day 21, related to the monolayer and squamous morphology of epithelium cells, which confirms cell morphology in H&E staining of pre-differentiation (pre-phase 5:) (**Fig. 11**). The finding is consistent with higher TEER values in 3D airway models with squamous epithelial cells reported by Yamaya et al., 1992 [81]. There is no description of *in vivo* TEER measurements of human bronchial epithelium in the available literature. The TEER values of ALI cultivated 3D models were quite similar to measurements of bronchial rabbit epithelium *in vivo*, showing values around $266 \pm 97 \Omega \cdot \text{cm}^2$ [82], and human bronchial epithelium cells with fibroblasts on decellularized porcine small intestinal submucosa presented TEER value of $224.76 \pm 99.88 \Omega \cdot \text{cm}^2$ in 3D model culture [83].

Characterization focused on proteomics profiling of the tri-culture system aimed to identify valuable protein components involved in ciliated epithelium differentiation, fibroblast support, and chondrogenic differentiation and to investigate the impact of fibroblasts on ciliated epithelium differentiation.

Protein composition in both dTracheal scaffold and dECM hydrogel was confirmed by proteomics analysis. This finding indicated the potential as cell carrier support for newly seeded cells by providing microenvironment, which are ECM components, growth factor, and cytokine. There is enrichment in biological process, function, component, and KEGG pathway, specifically collagen, Ras homolog family member j, and platelet-derived growth factor D and Insulin-like growth factor 2 receptor that may help to regulate cell adhesion and cell proliferation (Ras signaling pathway/Rap1 signaling pathway).

Transcriptomics analysis revealed that the tri-culture epithelium/fibroblasts/hMSCs construct produced alpha-tubulin, beta-tubulin, and cytokeratins (a.k.a. keratins) type I and type II, all expressed during ciliated epithelium differentiation. Alpha- and beta-tubulin (Tubulin beta 3 class III) polymerize into microtubules and are used as markers of ciliated epithelium cells, along with an ability to clear mucus from the airway [84]. Importantly, the β III-tubulin (TUBB3) is a highly specific marker for multiciliated airway epithelial cells [14]. Keratin type I, and type II are intermediate filament forming protein expression in epithelium cells [85], especially keratin 5 and 14 are positive basal cells of airway epithelium [86]. We found that the composition of the fibroblast protein marker was significantly different from the epithelium/hMSCs construct without fibroblasts, with more vimentin expression.

Vimentin is a general standard marker highly expressed in fibroblasts, and has an effect on cell migration through adhesion-associated signal transduction, and ECM remodeling [87]. The migration of fibroblasts plays a role in collagen remodeling by physical reorganization [88], and maintains tissue health in many organs [89]. Thus, the stiffness of collagen fibrils plays vital mechanical property roles in epithelium cell differentiation [90]. This indicated the ability of fibroblasts to support ciliated epithelium differentiation. Vimentin's significance extends to wound healing, contributing to all four phases: hemostasis, inflammatory, proliferative, and

remodeling [91]. Wound healing, a meticulously regulated process aimed at restoring tissue homeostasis post-injury, involves vimentin in various capacities. In the hemostasis phase, vimentin supports platelet adhesion and clot formation. During the inflammatory phase, it enhances macrophage activities and promotes the production of anti-inflammatory cytokines. In the last two stages of wound healing, vimentin plays a pivotal role by amplifying diverse fibroblast-related activities crucial for the restoration of tissue function.

As expected, collagen type VI, and tenascin-c components in chondrogenic differentiation were found in the epithelium/fibroblasts/hMSCs (tri-culture) construct and the epithelium/hMSCs construct. Actually, ECM molecules are produced during the early stage of chondrogenic differentiation including proteoglycans (sGAG), fibronectin, dermatopontin, cartilage oligomeric protein, type I collagen, type VI collagen, and tenascin-c [92]. Collagen type VI has profound impact over pericellular matrix composition and biomechanical behavior surrounding hMSCs undergoing chondrogenesis [93]. In stage I of pre-cartilage condensation, fibronectin synthesis is stimulated by transforming growth factor- β (TGF β) for stabilization of the mesenchymal-endothelial junction. At this stage, hMSCs stop proliferation and express tenascin-C and other adhesion protein [94]. Consequently, these three proteins indicated that pre-cartilage condensation occurred in tri-culture constructs. KEGG analysis reveals signaling pathways relating to cell adhesion (ECM-receptor interaction, Focal adhesion) and differentiation (PI3K-Akt signaling pathway), which may play a role in tissue reorganization through ECM components and recellularization.

The limitation of this study is the evaluation of gene expression levels to confirm ciliated epithelium differentiation and cartilage formation for molecular experiments using qRT-PCR.

Collectively, it was believed that dTracheal scaffold mimic microenvironment is crucial for functional tissue regeneration and recellularization of three types of cells: epithelium cells, fibroblasts, and hMSCs present the greatest construct to promote airway tissue reformation as the native trachea. In the present study, we propose a novel that revealed the effect of fibroblast support epithelium

differentiation on the dTracheal scaffold and found cartilage formation in tracheal cartilage from a 3D tri-culture construct. This study provides an insightful understanding of structure associated with biological function of trachea, and also shows an essential tool for tracheal reconstruction in the future. The present study has initiated to floor the way for a new therapeutic option to resolve the shortcomings of current treatment options, potentially improving patient outcomes.

Further research on the tri-culture condition is needed to establish scale-up in patch trachea scaffold and long-segment tracheal scaffold in a bioreactor, followed by pre-clinical studies. Additionally, the cartilage formation and induction of vascularization would be optimized to create the perfect grafts for tracheal reconstruction in clinical applications. For example, firstly, the dECM hydrogel combined the use of platelet-rich plasma (PRP) or freeze-dried noncoagulating platelet-derived factor concentrate coatings, which help to improve cartilage maturation, revascularization, and wound healing, resulting in a would size decreased and shortening times. Second, a fluid flow chamber is used to stimulate the cilia formation. Third, mechanical force mimics native trachea movement during cultivation, which could enhance faster airway tissue reformation.

Ethical Consideration

Canine tracheas for decellularization were harvested under sterile condition from canine cadaver, donated for anatomy class of the Faculty of Veterinary science, Chulalongkorn University, Thailand. Animal surgery and husbandry were performed by the Thailand guidelines on the use of experimental animals (ANIMALS FOR SCIENTIFIC PURPOSES ACT, B.E. 2558 (A.D. 2015). This study was approved by the Institutional Animal Care and Use Committee (IACUC) of Chulalongkorn University (no. 2231001).

This study used primary human bronchial epithelial cells, primary human lung fibroblast cells, and primary human mesenchymal stem cells from bone marrow from Promocell company, Germany, *in vitro* studies.



Funding

This work was supported by Ratchadapiseksompotch Fund, Chulalongkorn University [grant number CU_GR_62_76_31_06]; PMUC 2566 [grant number C10F640050]; a research assistant from the Graduate school, Chulalongkorn University [grant number GCUGE1725622004D].



Supplementary data



จุฬาลงกรณ์มหาวิทยาลัย
CHULALONGKORN UNIVERSITY

Table S1 Dimension of canine tracheal samples

Group	Length (mm)	P-value	Diameter (mm)	P-value	Thickness (mm)	P-value
Unwashed (Control)	25.29 ±4.67	1.000 ^{ns}	17.17 ±2.17	1.000 ^{ns}	1.70 ±0.63	1.000 ^{ns}
dTrachea	25.13 ±4.40		16.25 ±3.02		1.63 ±0.38	

NS = no significant difference, *P<0.05

Table S2 The compressive parameters of unwashed trachea and decellularized trachea

	Unwashed (Control)	dTrachea	P-value	95% confidence interval
1. Young's modulus (kPa)	1094.60	1023.04	0.1092 ^{ns}	-271.84 to 28.44
	1185.66	1102.34		
	1023.38	959.25		
	1195.38	1035.92		
	1124.76	1030.43 ±58.66		
Mean ± SD	±81.42			
2. Stress (kPa)	164.34	128.60	0.4246 ^{ns}	-57.54 to 27.70
	160.81	144.24		
	157.27	104.37		
	104.72	150.22		
	146.78 ±28.19	131.86 ±20.47		
Mean ± SD				
3. % Strain	9.89	25.00	0.6385 ^{ns}	-14.57 to 9.673
	24.97	12.92		
	25.08	12.85		
	13.49	12.88		
	18.36 ±7.84	15.91 ±6.06		
Mean ± SD				

NS = no significant difference, *P<0.05

Table S3 The tensile parameters of unwashed trachea and decellularized trachea

	Unwashed (Control)	dTrachea	P- value	95% confidence interval
1. Tensile strength (kPa)	4490.00	3040.00	0.8545	-1529.0 to 1307.0
	4680.00	4689.00		
	2926.00	4327.00		
	3585.00	3180.00		
Mean ± SD	3920.0 ±817.06	3809 ±822.54		
2. Ultimate tensile strength (kPa)	280700.00	173800.00	0.9555	-85077.0 to 81127.0
	230000.00	247500.00		
	135000.00	218000.00		
	205000.00	203500.00		
Mean ± SD	212675.00 ±60607.67	210700.00 ±30664.75		
3. % Elongation	42.68	44.60	0.9644	-14.47 to 13.93
	53.60	50.60		
	41.80	47.40		
	35.90	30.30		
Mean ± SD	43.50 ±7.38	43.23 ±8.96		

NS = no significant difference, *P<0.05

Table S4 Biochemistry testing of unwashed, decellularized trachea and dECM solution

ECM components	Control (Unwashed)	dTrachea	dECM solution	P-value		95% confidence interval	
				Control vs. dTrachea	Control vs. dECM solution	Control vs. dTrachea	Control vs. dECM solution
1. % DNA content/ wet weight	22.93	2.89	1.26	<0.0001*	<0.0001*	19.10 to 23.72	20.40 to 25.02
	26.76	2.27	1.10				
	23.86	2.54	1.30				
Mean ± SD	21.94	2.15	1.00				
	23.87 ±2.08	2.46 ±0.33	1.16 ±0.14				
2. % sGAG content/ wet weight	2.74	3.89	1.96	0.0076*	0.0069*	-0.8198 to 1.395	0.5156 to 2.730
	3.16	2.66	1.96				
	4.59	3.52	1.59				
Mean ± SD	3.50	2.77	1.99				
	3.50 ±0.79	3.21 ±0.59	1.88 ±0.19				
3. %Collagen content/ wet weight	1.76	1.89	1.52	0.0027*	0.0018*	-0.1762 to 0.7442	0.3753 to 1.296
	1.98	1.32	1.22				
	2.09	1.75	0.99				
Mean ± SD	2.15	1.89	0.92				
	2.00 ±0.17	1.71 ±0.27	1.16 ±0.27				
4. Laminin (pg/mL)	851.88	892.50	849.12	0.1004*	0.0761*	-27.48 to 57.18	-4.035 to 80.63
	902.50	880.62	865.63				
	879.38	849.37	813.65				
Mean ± SD	898.13	850.00	850.30				
	882.97 ±23.03	868.12 ±21.84	844.68 ±22.01				

*P<0.05

Table S4 Biochemistry testing of unwashed, decellularized trachea and dECM solution (continuous)

ECM components	Control (Unwashed)	dTrachea	dECM solution	P-value	P-value		95% confidence interval	
					Control vs. dTrachea	Control vs. dECM solution	Control vs. dTrachea	Control vs. dECM solution
5. Fibronectin (pg/mL)	38708.3 43083.3 36291.7 49541.7	43916.7 36791.7 40682.8 38731.5	20735.75 28623.8 29283.2 29758.9	0.0024*	>0.9999*	0.0025*	-6704 to 10456 6226 to 23386	
Mean ± SD	41906.25 ±5814.80	40030.68 ±3038.93	27100.41 ±4268.56					

*P<0.05

Table S5 Quantitative analysis of fiber diameter and intersection points

Parameters	dECM solution collected at 24 hours	dECM solution collected at 48 hours	dECM solution collected at 72 hours	P-value	P-value			95% confidence interval		
					dECM solution 24 hours vs. 48 hours	dECM solution 24 hours vs. 72 hours	dECM solution 48 hours vs. 72 hours	dECM solution 24 hours vs. 48 hours	dECM solution 24 hours vs. 72 hours	dECM solution 48 hours vs. 72 hours
1. Fiber diameter (μm)	0.175 0.169 0.189 0.153 0.153 0.189 0.189 0.169 0.153 0.153 0.175 0.153	0.129 0.147 0.147 0.129 0.122 0.129 0.129 0.122 0.122 0.147 0.122 0.129	0.081 0.081 0.090 0.081 0.081 0.081 0.090 0.081 0.081 0.090 0.090 0.090	<0.0001*	<0.0001*	<0.0001*	<0.0001*	0.02598 to 0.04835	0.07240 to 0.09477	0.03523 to 0.05760
Mean \pm SD	0.168 \pm 0.015	0.131 \pm 0.010	0.085 \pm 0.005							

*P<0.05

Parameters	dECM solution collected at 24 hours	dECM solution collected at 48 hours	dECM solution collected at 72 hours	P-value	P-value			95% confidence interval		
					dECM solution 24 hours vs. 48 hours	dECM solution 24 hours vs. 72 hours	dECM solution 48 hours vs. 72 hours	dECM solution 24 hours vs. 48 hours	dECM solution 24 hours vs. 72 hours	dECM solution 48 hours vs. 72 hours
2. Intersection points (area per point 6.25 μm^2)	0.320	0.480	0.960	<0.0001*	<0.0001*	<0.0001*	-0.2736 to 0.006922	-0.5536 to -0.2731	-0.4203 to -0.1397	
	0.480	0.480	0.800							
	0.480	0.640	0.960							
	0.640	0.480	1.120							
	0.320	0.640	0.960							
	0.480	0.640	0.960							
	0.320	0.480	0.640							
	0.640	0.640	0.800							
	0.320	0.480	0.800							
	0.480	0.640	0.640							
0.320	0.480	0.480								
0.320	0.640	0.960								
Mean \pm SD	0.427 \pm0.125	0.560 \pm0.084	0.840 \pm0.182							

*P<0.05

1. Gel contraction

dECM solution from peptic digestion 72 hours after neutralization was combined with fibrin solution (Kang et al. 2016) in a ratio of 1:1 to develop injectable canine dECM-fibrin solution and keep at -20°C until further use. As the main components of hydrogel contained fibrin and collagen that cells might affect hydrogel contraction, an examination of hydrogel contraction was performed to assess the properties of cells embedded in a hydrogel ($200\ \mu\text{l}$). Numerous concentrations of hMSCs (1×10^5 , 2×10^5 , 5×10^5 , 1×10^6 , and 2×10^6) were observed on day 3 and day 7 ($n=4$) (Fig. S1). Gelation of canine dECM-fibrin solution occurred by mixing with thrombin at a concentration of 20 IU/ml, using a ratio of 2 parts canine dECM-fibrin solution to 1 part thrombin.

Results

Canine dECM fibrin hydrogel exhibited greater cell contraction compared to the fibrin hydrogel starting from day 3 of observation. This was evident by the presence of small white dots in the culture well plate. In contrast, the size of the fibrin hydrogels decreased in relation to the concentration of cells on day 3. By day 7, both the fibrin hydrogel and the canine dECM fibrin hydrogel appeared as small white dots in each cell concentration (Fig. S1).

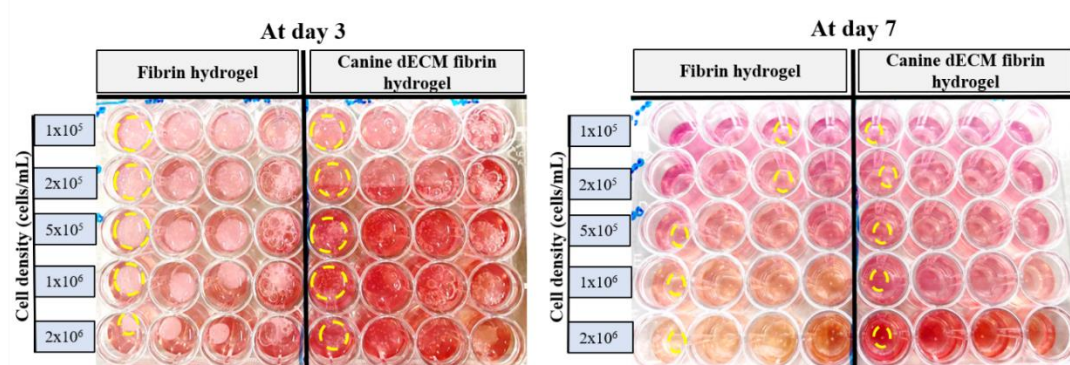


Figure S1 Hydrogel contraction

The hydrogel contraction of both Fibrin hydrogel (Kang et al. 2016) and canine dECM fibrin hydrogel were evaluated using different concentrations of hMSCs (1×10^5 , 2×10^5 , 5×10^5 , 1×10^6 , and 2×10^6) at day 3 and day 7 ($n=4$).

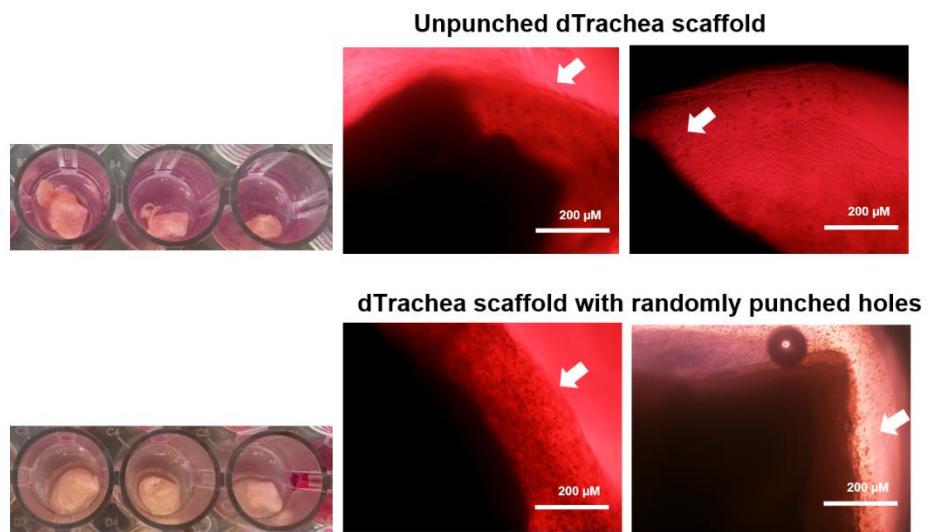


Figure S2 Test injectability of hydrogel on an outer surface of the decellularized tracheal scaffold (dTracheal scaffold). The dECM-fibrin hydrogel was present around dTracheal or *ex vivo* cell culture. The white arrow indicates cell/hydrogel mixture around the dTracheal scaffold up to 7 days.

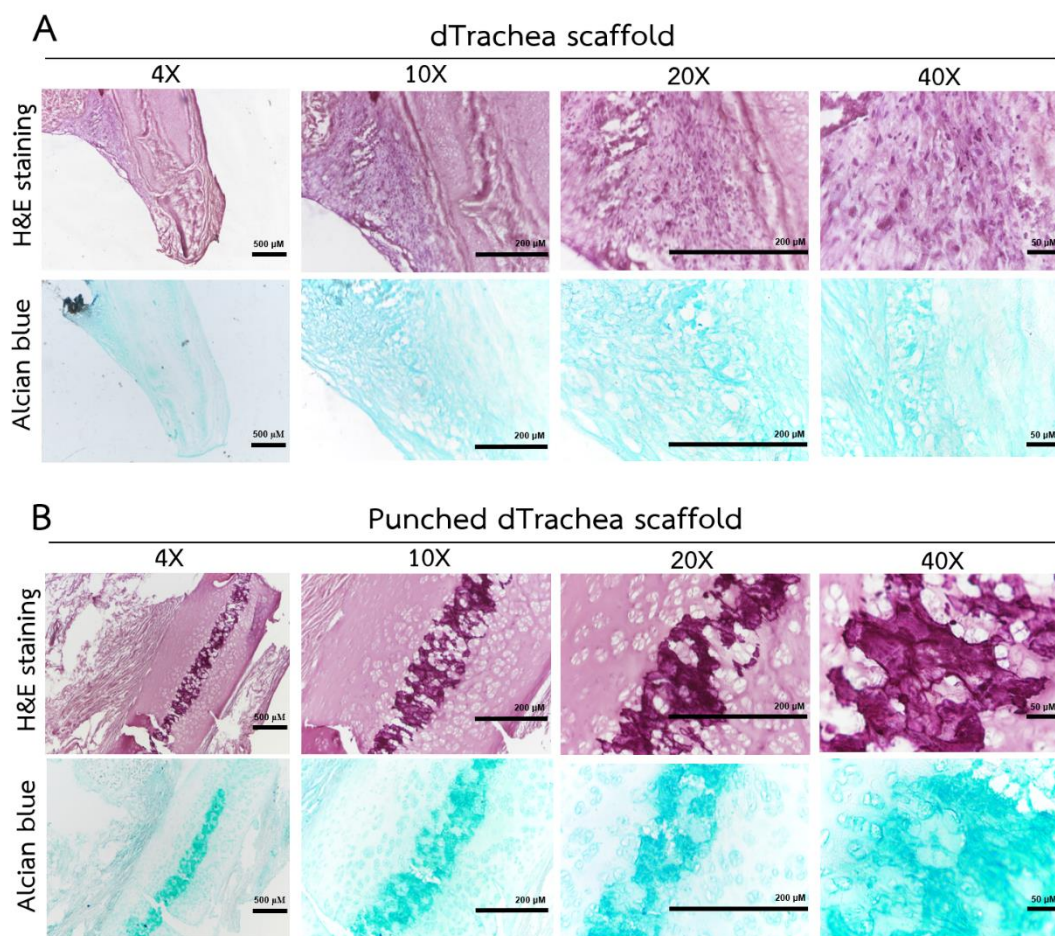


Figure S3 Histological analysis

H&E staining of cartilage regeneration and alcian blue staining of sGAG secretion from chondrogenic differentiation of hMSCs embedded in an injectable canine dECM-fibrin hydrogel on **A)** dTracheal scaffolds and **B)** punched dTracheal scaffolds.

Scale bars = 200 μ m

Table S6 TEER value of TEER measurement in 3D culture

Parameters of study I: co-culture	Co-culture (Epithelium/ Fibroblasts)	Epithelium	Fibroblasts	P-value	P-value		
					Co-culture vs. Epithelium	Co-culture vs. Fibroblasts	Epithelium vs. Fibroblasts
1. TEER value (Ω^*cm), Day 7 (Mean \pm SD)	538.70 \pm 7.92	352.80 \pm 26.93	250.88 \pm 12.67	<0.0001***	<0.0001****	<0.0001****	0.0007***
2. TEER value (Ω^*cm), Day 21 (Mean \pm SD)	235.20 \pm 7.92	0.560 \pm 3.17	164.64 \pm 1.58	<0.0001****	0.2882 ^{ns}	0.0050**	0.0419*
Parameters of study I: tri-culture	Tri-culture (Epithelium/ Fibroblasts/ hMSCs)	Epithelium/ hMSCs	hMSCs	P-value	P-value		
					Tri-culture vs. Epithelium/ hMSCs	Tri-culture vs. hMSCs	Epithelium/ hMSCs vs. hMSCs
3. TEER value (Ω^*cm), Day 7 (Mean \pm SD)	454.70 \pm 7.91	306.88 \pm 4.75	216.16 \pm 3.16	<0.0001****	<0.0001****	<0.0001****	<0.0001****
4. TEER value (Ω^*cm), Day 21 (Mean \pm SD)	218.40 \pm 3.16	222.88 \pm 1.58	170.24 \pm 1.58	<0.0001****	0.9999 ^{ns}	<0.0001****	<0.0001****

2. Proteomics analysis

2.1 Protein profiling of epithelium/hMSCs construct

Epithelium/hMSCs constructs (n=3 in each group) (**Fig.S4A**) were assessed for proteomics profile. dTracheal scaffold and dECM hydrogels were used to normalize protein components from the construct.

LS-MS/MS analysis identified 7874 proteins and all proteins were selected for statistical differential expression analysis by Metaboanalyst (MetaboAnalyst 5.0). The heatmap analysis showed the enrichment of differential proteins in each sample (**Fig.S4B**). In the heatmap, the rows represent protein IDs, while the columns represent samples.

Principal component analysis (PCA) was conducted to reflect the range of variation among samples within the group, revealing distinct distribution of proteins between three groups. The results showed the first component explains 31.7% of the variation and the second component 19.4%, indicating statistical differences due to the majority of protein components (**Fig.S4C**).

There were 131 significant differential expression proteins identified as shown in the quantitative ANOVA (**Fig.S4D**). The red dots represent 131 proteins, indicating a high level of protein content, while the green dots represent 719 proteins, signifying a low level of protein content. Therefore, all 131 proteins were identified and annotated protein name, gene name, gene ontology (biological process), and gene ontology (cellular component) using the Uniplot database.

The results showed significant differences in the main protein components of epithelium/hMSCs construct: Actin as housekeeping protein ($p=2.78 \times 10^{-7}$); Formin like 2 ($p=1.9 \times 10^{-8}$), FERM domain containing 1 ($p=4.11 \times 10^{-15}$), Desmoplakin ($p=2.72 \times 10^{-6}$) for cytoskeleton component; Keratin 14 ($p=1.14 \times 10^{-12}$) for epithelium. Collagen type I for for hMSCs differentiate into chondrogenic (Supplement data in .CSV file).

The prediction of STITCH analysis matching with Homo sapiens presented that epithelium/hMSCs construct display expressed proteins involvement in several biological processes such as localization, transport, cell activation, movement of cell or subcellular component and regulation of signaling. Function enrichment analysis presented differentially expressed proteins related to protein binding, cytoskeletal

protein binding and actin binding. Meanwhile, components enrichment analysis showed extracellular exosome, extracellular region part, and membrane-bounded vesicle. In addition, some signaling pathways related to cell adhesion (Adherens junction, regulation of actin cytoskeleton, Focal adhesion), and cell proliferation (MAPK signaling pathway).

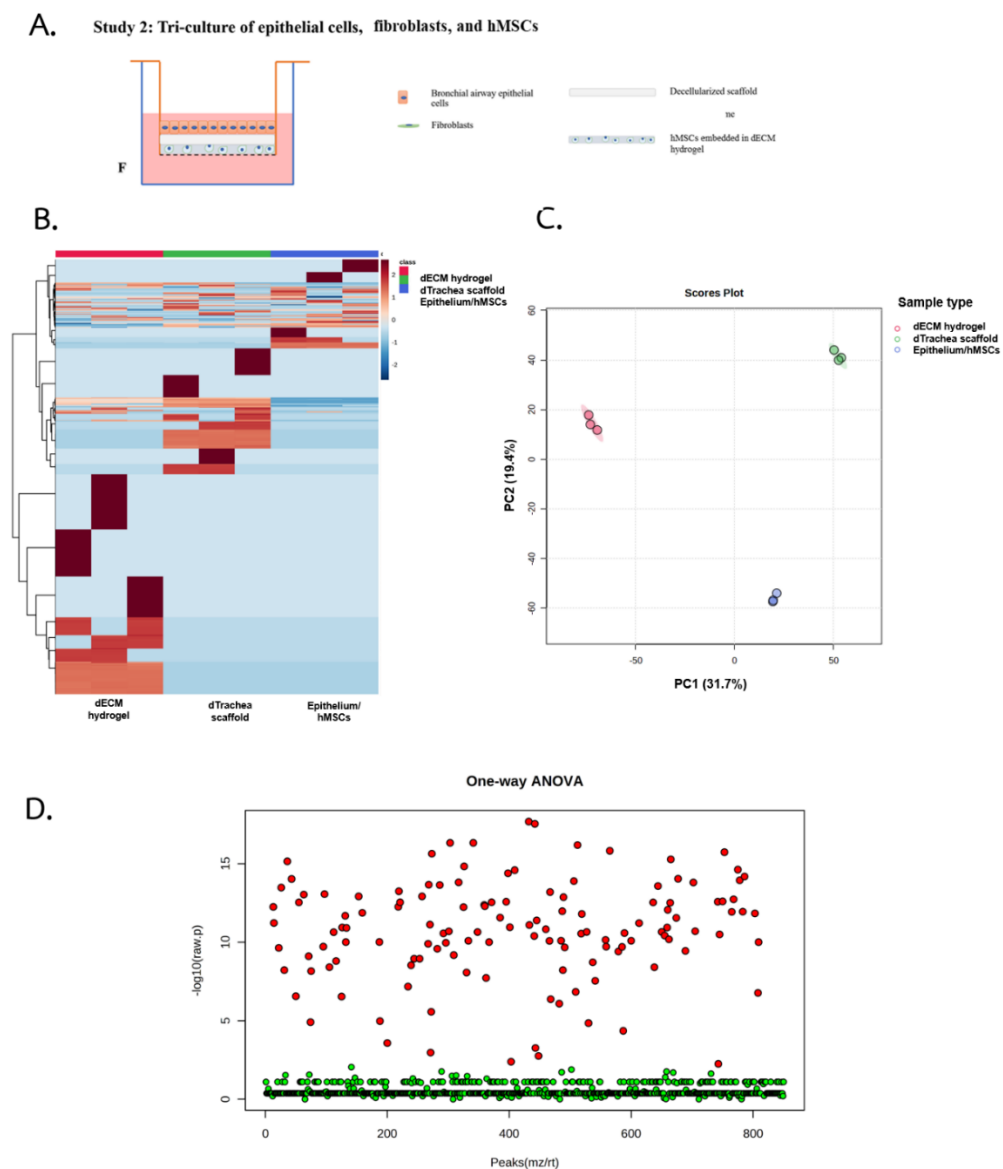


Figure S4. The proteomics dataset analyzed for biological significance of Epithelium/hMSCs constructs. A) Sampling of Epithelium/hMSCs constructs for proteomics analysis. B) Heatmap represented the cluster analysis of the differentially

expressed proteins in Epithelium/hMSCs constructs compared to dTracheal scaffold and dECM hydrogel. **C)** The principal component analysis indicated the high aggregation degree of samples in each group (n = 3 in each group). **D)** ANOVA plot showed differentially expressed proteins between Epithelium/hMSCs constructs, dTracheal scaffold and dECM hydrogel (Red dots: High level; green dots: low level).

2.2 Protein profiling of hMSCs construct

hMSCs constructs (n=3 in each group) were assessed for proteomics profile. dTracheal scaffold and dECM hydrogels were used to normalize protein components from the construct.

LS-MS/MS analysis identified 7874 proteins and all proteins were selected for statistical differential expression analysis by Metaboanalyst (MetaboAnalyst 5.0). The heatmap analysis showed the enrichment of differential proteins in each sample (**Fig.S5**). In the heatmap, the rows represent protein IDs, while the columns represent samples.

Principal component analysis (PCA) was conducted to reflect the range of variation among samples within the group, revealing distinct distribution of proteins between three groups. The results showed the first component explains 32.7% of the variation and the second component 19.3%, indicating statistical differences due to the majority of protein components (**Fig.S5B**).

There were 132 significant differential expression proteins identified as shown in the quantitative ANOVA (**Fig.S5C**) The red dots represent 132 proteins, indicating a high level of protein content, while the green dots represent 693 proteins, signifying a low level of protein content. Therefore, all 132 proteins were identified and annotated protein name, gene name, gene ontology (biological process), and gene ontology (cellular component) using the Uniplot database.

The results showed significant differences in the main protein components of epithelium/hMSCs construct: Actin as housekeeping protein ($p=2.95 \times 10^{-7}$); and Collagen type I ($p=1.48 \times 10^{-12}$) for hMSCs differentiate into chondrogenic (Supplement data in .CSV file).

The prediction of STITCH analysis matching with Homo sapiens presented

that hMSCs construct display expressed proteins involvement in cell migration, tissue development, collagen biosynthetic process, extracellular matrix component. Moreover, KEGG signaling pathways related to cell adhesion (focal adhesion), differentiation (PI3K-Akt signaling pathway).

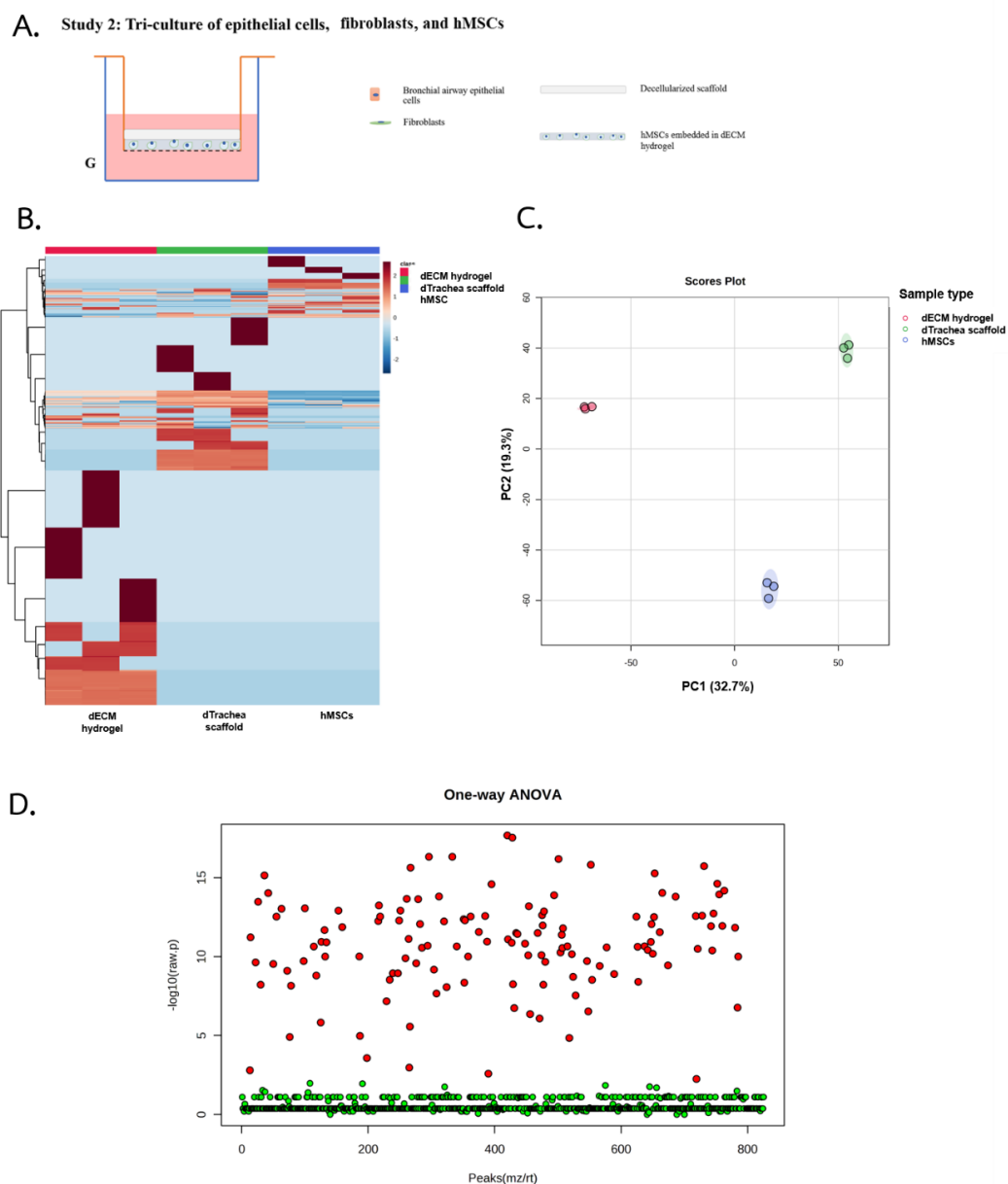


Figure S5. The proteomics dataset analyzed for biological significance of hMSCs constructs. A) Sampling of hMSCs constructs for proteomics analysis. B) Heatmap represented the cluster analysis of the differentially expressed proteins in hMSCs

constructs compared to dTracheal scaffold and dECM hydrogel. **C)** The principal component analysis indicated the high aggregation degree of samples in each group (n = 3 in each group). **D)** ANOVA plot showed differentially expressed proteins between hMSCs constructs, dTracheal scaffold and dECM hydrogel (Red dots: High level; green dots: low level).



Supplementary data (preliminary data)



จุฬาลงกรณ์มหาวิทยาลัย
CHULALONGKORN UNIVERSITY

Objectives

Primary objective

To develop dECM scaffolds functional tracheal tissue substitutes *in vitro*

Secondary objective

To compare decellularized tissue outcomes of trachea between detergent enzymatic decellularization (DED) and vacuum-assisted decellularization (VAD)

Research questions

Primary question

Can the dECM scaffold support tracheal tissue formation *in vitro*?

Secondary question

Can the detergent enzymatic decellularization (DED) and vacuum-assisted decellularization (VAD) methods provide similar biochemical outcomes?

Hypothesis

Decellularized trachea obtained from DED and VAD methods show different tissue biochemical outcomes.

Part I: Preparation of decellularized tracheal scaffold

Materials and methods

1. Chemicals and reagents

Phosphate buffered saline powder, Sodium deoxycholate, DNase I (750KU), Triton X-100 were purchased from Sigma-Aldrich (St. Louis, MO). Antibiotic/antimycotic solution (100X) and Ambion® RNase I (100 U/μL) were purchased from Gibco and Invitrogen (Thermo Fisher Scientific Inc., PA, USA), respectively. Proteinase K and Papain were purchased from Worthington biochemical corporation (Lakewood, NJ).

2. Harvesting canine trachea tissue

Six canine tracheas were obtained in sterile environment from canine donors kindly supported from the Faculty of veterinary science, Chulalongkorn university, Thailand. The uses of cadaveric samples, which do not apply to the Institutional Animal Care and Use Committee (IACUC) approval. Donor tracheas were immediately rinsed in 40 ml of phosphate buffered saline (PBS) containing 1% antibiotic/antimycotic solution and surrounding tissue was dissected away. Each trachea was divided into three segments evenly along the transverse plane (**Fig. Sp1**). Each segment contains 5-6 cartilage rings. The first and second segments of trachea were performed by detergent-enzymatic decellularization (DED) and vacuum-assisted decellularization VAD methods, respectively. The last segment served as unwashed trachea (control).

3. Decellularization of tracheal tissue

Tracheal tissues were conducted by two methods; detergent-enzymatic decellularization (DED) method and vacuum-assisted decellularization (VAD) method. DED method consists of multiple washing cycles of the tissue with detergent and enzymes. VAD method removes cells from pre-frozen tissue under vacuum conditions. Briefly, tracheas were sterilized with 70 % ethanol overnight on a rotating shaker at 4 °C and washed in distilled water type II for 72 hours at 4 °C to remove

ethanol.

For DED method, tracheas were washed in distilled water type II for 72 hours, transferred to 4% sodium deoxycholate for 4 hours and incubated with 2 kU/ml DNase I and 4 U/ml RNase I in PBS for 3 hours. The process was repeated 7 times on a rotating shaker at 4 °C. All solutions were supplemented with 1% antibiotic-antimycotic. The resulting tracheas were stored at 4 °C in PBS containing 1% antibiotic-antimycotic until use.

For VAD method, tracheas were frozen at -80 °C for 24 hours, thawed at room temperature and rinsed with PBS. All steps in VAD were taken place in a vacuum chamber in conjunction with detergent and enzymatic treatment. All solutions will be supplemented with 1% antibiotic-antimycotic. The trachea was incubated in a detergent solution containing 0.25% sodium deoxycholate and 0.25% Triton X-100 in PBS and then placed inside the vacuum chamber for 24 hours at 37°C on a rocker. Afterward, the tracheas were rinsed twice in distilled water type II for 2 hours and incubated for another 44 hours in distilled water type II at 4 °C. At enzymatic treatment, the tissues were incubated in an enzymatic solution containing 2 kU/ml DNase I and 4 U/ml RNase I at 37 °C for 24 hours and washed with distilled water type II at 4 °C for 24 hours. This enzymatic treatment step was performed again. Finally, tracheas were washed with distilled water type II for 48 hours and stored at 4 °C in PBS containing 1% antibiotic-antimycotic until use.

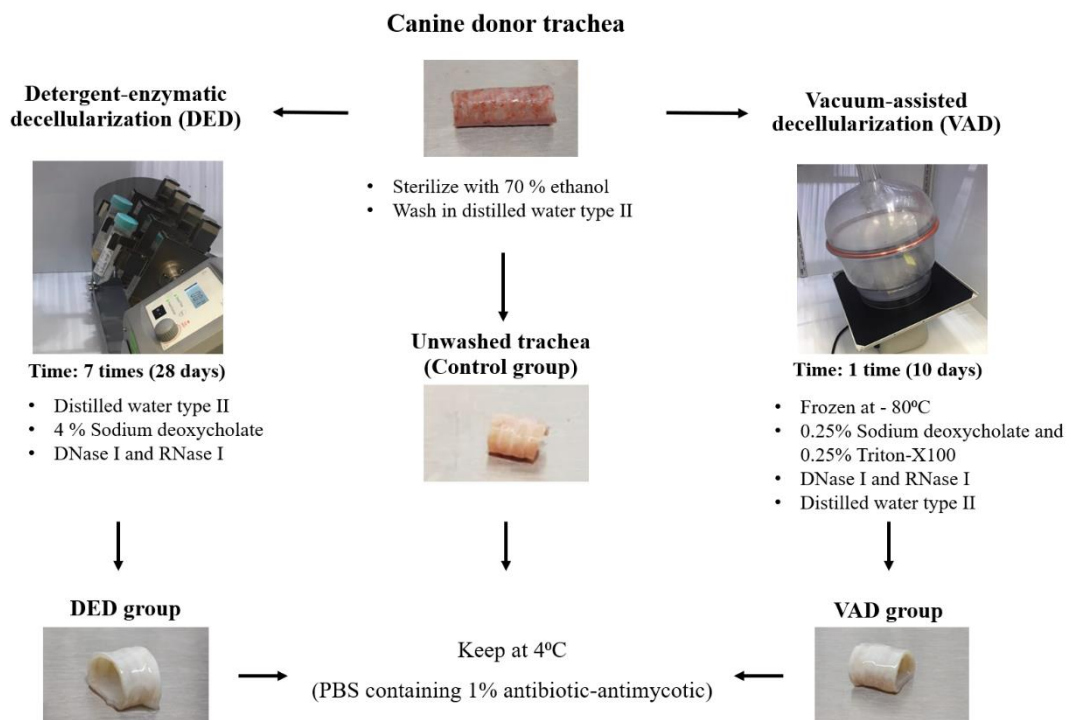


Fig. Sp1. Schematic of tracheal decellularization Canine tracheas were treated by detergent-enzymatic decellularization (DED) and vacuum-assisted decellularization (VAD) methods. The resulting decellularized tracheas were kept in 4 °C in aseptic condition until use.

4. Histology and immunohistochemistry

Histological analyses were performed on the unwashed trachea (control) and decellularized trachea (dTrachea) in both methods after decellularization process. The samples were fixed with 4% paraformaldehyde in PBS, embedded in paraffin and sectioned to 3 μm thickness. The sections were stained with hematoxylin and eosin (H&E) to assess cell nuclei and general tissue histoarchitecture. The glycosaminoglycans (sGAG) extracellular matrix components were determined using Alcian blue staining to confirm the proteoglycan content. The extracellular matrix components (i.e. collagen, elastin, muscle, mucin and fibrin) were examined using Movat Pentachrome stain kit (Modified Russell-Movat).

The presence of a major histocompatibility complex (MHC) marker was

evaluated using immunohistochemistry. The MHC class II marker was labeling by monoclonal mouse anti-human HLA-DP, DQ, DR antibody [CR3/43] at 1:100 dilution (M0775, Dako). Horse anti-mouse IgG antibody (H+L) biotinylated at 1:200 dilution (BA-2000-1.5, Vector Laboratories) was used as secondary antibody. Then, sections were incubated with ImmPACT DAB substrate kit (Vector Laboratories) according to the manufacturer's instructions and finally counterstained with hematoxylin.

All sections were observed under an optical microscope (Nikon, Tokyo, Japan) using a NIS-Elements BR imaging software (vD4.10.02; Nikon Instruments, NY, USA). The characteristics of the decellularized tracheal scaffolds for DED and VAD were evaluated by images compared with the control untreated trachea (native trachea). Three images were in the same sample and compared with the tissue and cell compositions in the same region of the control sample.

5. Biomechanical assessment

Decellularized trachea (dTrachea) and unwashed trachea (control) was analyzed for mechanical properties: compression test ($n = 4$) and tensile tests ($n = 4$) using the Universal testing machine (Hounsfield-H10KM, USA). Length and wall thickness of unwashed and dTrachea were recorded (Supplementary Table Sp4). Decellularized trachea was compressed at a speed of 5 mm/min in the anterior-posterior direction until the diameter decreases to 50% of the starting diameter (**Fig. Sp4**). Young's Modulus was calculated as the slope of the straight-line portion of a stress and strain curve using ASTM C 165 compressive properties software (Tinius Olsen, Kongsberg, Norway). For tensile testing, two fixtures were placed inside the lumen of trachea. Each sample underwent tensile testing at a rate of 50 mm/min. The tensile strength, ultimate tensile strength and % elongation were calculated using ASTM D 882 Simplified Tensile & Break software (Tinius Olsen, Kongsberg, Norway).

6. Biochemical assay

Decellularized tissues were digested in 1 ml of proteinase K buffer (1 mg/ml Proteinase K and 0.88 mg/ml papain), incubated at 60 °C overnight and centrifuged

at 6,000 rpm at 4 °C for 20 minutes. The supernatant was transferred to new tubes to quantify DNA and Sulfated glycosaminoglycan (sGAG) contents. The DNA content was measured using the Quant-iT PicoGreen® dsDNA Assay Kit (Life Technologies, Grand Island, NY). Sulfated glycosaminoglycan (sGAG) content was determined by DMMB dye-binding assay [1]. DNA and sGAG contents were normalized to tissue wet weight (n=4).

7. Re-epithelization and cytocompatibility

7.1 Cell culture and cell seeding

Primary human bronchial epithelial cells (HBEpC, Promocell GmbH, Heidelberg, Germany) was expanded in airway epithelial cell growth medium (Promocell GmbH, Heidelberg, Germany) and maintained in 5% CO₂ at 37 °C, with medium change every 2 days. The 1x10⁶ HBEpC in 200 µl of growth medium were seeded directly on the lumina side of decellularized trachea disks 5 mm in diameter. The constructs were kept in a 96-well plate (NUNC, Fisher Scientific GTF, Sweden), 5% CO₂ at 37 °C overnight to allow cell absorption. Then, the growth medium was changed every 48 hours for 3 and 7 days. Non-seeded decellularized trachea serve as a control group.

7.2 Cytocompatibility

Following ISO standard 10993-5:2009, decellularized trachea was assessed using cytotoxicity by LIVE/DEAD® Viability/Cytotoxicity Kit (Thermo Fisher Scientific). Briefly, constructs at day 3 and 7 and were incubated in 200 µl of PBS containing 2 µM Calcein AM and 4 µM Ethidium homodimer-1 (EthD-1) for 45 minutes at 37 °C, 5% CO₂. The constructs were washed two times with PBS and visualized under fluorescent microscope. Subsequently, all constructs were collected to analyze DNA content by Quant-iT PicoGreen® dsDNA Assay.

8. Micromorphological assessment

The constructs were fixed with 2.5% glutaraldehyde in 1xPBS at 4 °C overnight, washed with 1xPBS for 3 times, 10 minutes each at room temperature and

rinsed with distilled water. The constructs were dehydrated through a graded ethanol series from 30% to 100% ethanol, and evaporated using a critical point dryer (Leica EM CPD300). The dry constructs were sputter-coated with Gold (Au) (BALZERS SCD 040), and visualized by a scanning electron microscope (SEM) and energy dispersive x-ray spectrometer at 5000X and 3000X magnification (JSM-IT500HR, JEOL Group Companies, Japan).

Results (preliminary data)

1. Appearance of decellularized trachea

The canine tracheal tissues subjected to either the DED or VAD methods displayed a white appearance and demonstrated similar levels of preservation when compared to the unwashed trachea (control) (**Fig. Sp1**). The tracheal tissues obtained through the DED method exhibited a decrease in stiffness as the number of washing cycles increased. However, it is noteworthy that the cartilage rings maintained their original shape after washing using both the DED and VAD methods. The tissues obtained through the DED method were softer in comparison, while those obtained through the VAD method preserved shapes that resembled the unwashed native tissues (control group).

To assess the effectiveness of both the DED and VAD methods in decellularizing the trachea, histological staining techniques such as H&E (Hematoxylin and Eosin), Alcian blue, and Pentachrome staining were employed to detect the presence of cells and extracellular matrix (ECM) components in the decellularized trachea and to compare them with the unwashed native trachea (control group). In the treated groups both DED and VAD methods did not detect the presence of nucleated epithelial cells on the lumen side, whereas the control tissue was observed the presence of nucleated cells in H&E staining (**Fig. Sp1A**).

In the unwashed group, a blue color indicative of glycosaminoglycans (GAGs) staining was detected around chondrocytes and in the lumen. However, in the DED

and VAD decellularized groups, a lighter blue signal was observed. (Fig. Sp2B).

The DED method resulted in the removal of a significant portion of cells and ECM located on the lumen side, in comparison to both unwashed and the VED groups. Particularly, the VED method retained elements such as collagen, fibrous network, mucosa and submucosa (Fig. Sp3C). Immunohistochemistry staining for MHC-II was not observed in the decellularized trachea. (Fig. Sp3D).

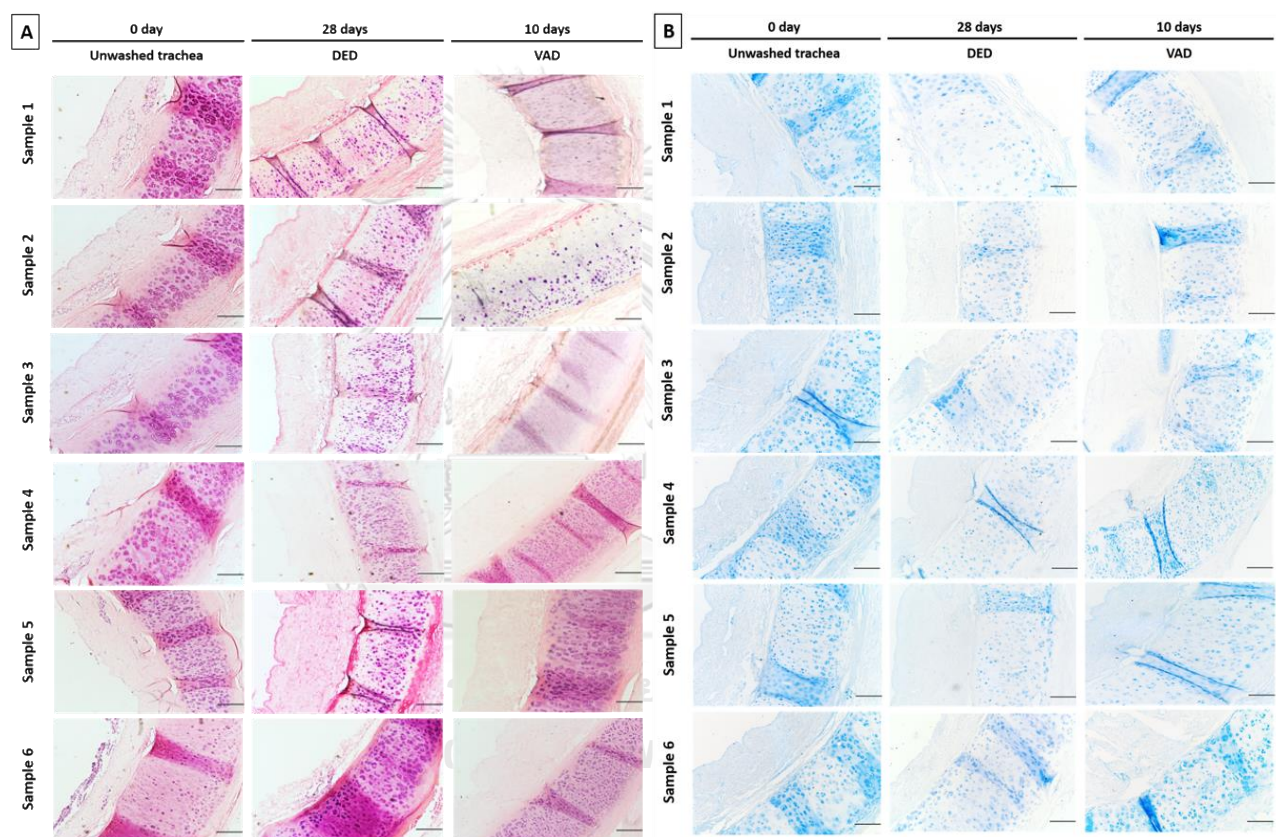


Fig. Sp2 Histological and Immunohistochemical analysis

Canine trachea decellularized using DED and VAD methods were stained by Hematoxylin and eosin (H&E) staining (A), Alcian blue (B), Pentachrome (C) and Scale bars = 500 μ m. (D) Immunostaining of MHC-II. Scale bars = 100 μ m. DED = detergent-enzymatic decellularization method, VAD = vacuum assisted decellularization method.

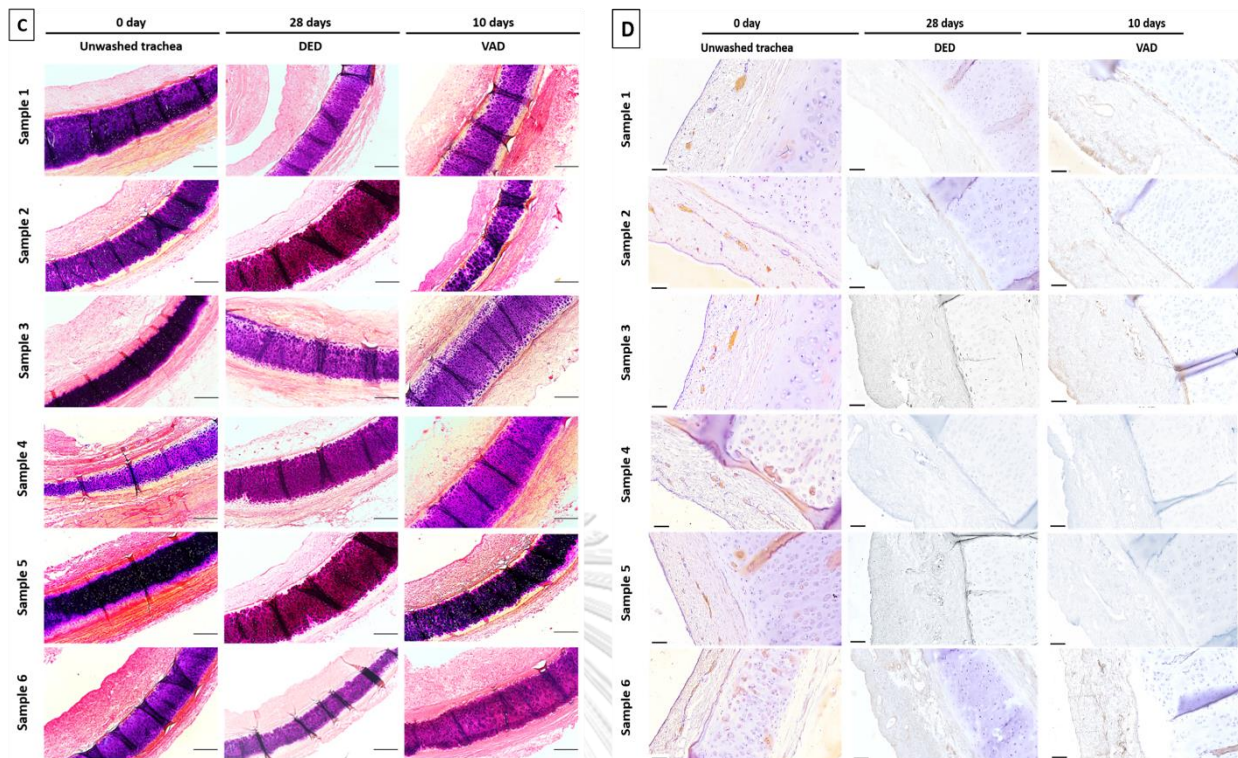


Fig. Sp3 Histological and Immunohistochemical analysis

Canine trachea decellularized using DED and VAD methods were stained by Hematoxylin and eosin (H&E) staining (A), Alcian blue (B), Pentachrome (C) and Scale bars = 500 μm . (D) Immunostaining of MHC-II. Scale bars = 100 μm . DED = detergent-enzymatic decellularization method, VAD = vacuum assisted decellularization method.

2. Biomechanical properties of decellularized trachea

The process of decellularization conserved the mechanical properties of the decellularized canine trachea. Both the DED and VAD methods of decellularization effectively maintained the mechanical properties of the canine trachea. There were no significant differences observed in Young's modulus, stress, and strain between the decellularized tracheas using the DED and VAD methods when compared to the unwashed control trachea. (Fig. Sp4A, Table. Sp2). The decellularized trachea demonstrated tensile strength within the range of 2 MPa to 4 MPa, which was

comparable to the control group (Fig. Sp4B, Table Sp3). Moreover, there were no significant differences observed in the ultimate tensile strength and percentage of elongation between the unwashed trachea and the decellularized groups. (Fig. Sp4B, Table Sp3).

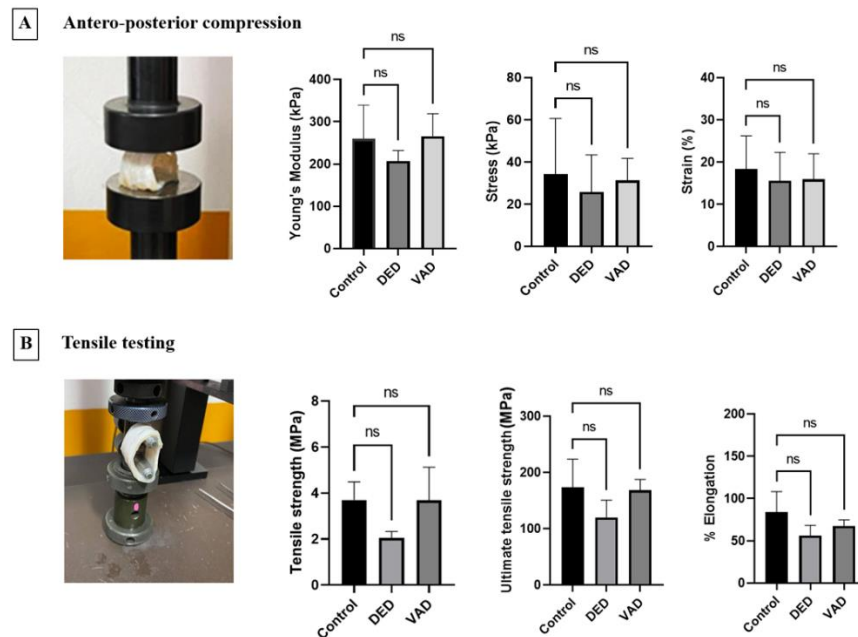


Fig. Sp4 The mechanical properties of decellularized trachea

(A) Young's modulus, stress and strain of decellularized trachea (n=4) obtained from antero-posterior compression; (B) Tensile strength, ultimate tensile strength and % elongation were obtained from tensile testing. DED = detergent-enzymatic decellularization method on day 28, VAD = vacuum assisted decellularization method on day 10, Control = unwashed trachea, ns = not significant

Table Sp1 Dimension of canine tracheal samples

Group	Length (mm)	P-value	Diameter (mm)	P-value	Thickness (mm)	P-value
Unwashed (Control)	25.29 ±4.67	1.000 ^{ns}	17.17 ±2.17	1.000 ^{ns}	1.70 ±0.63	1.000 ^{ns}
dTrachea	25.13 ±4.40		16.25 ±3.02		1.63 ±0.38	

NS = no significant difference, *P<0.05

Table. Sp2 The compressive parameters of native trachea and decellularized trachea from DED and VAD methods. Data were expressed as mean \pm standard deviation (n = 4).

Characteristics	Unwashed (Control)	dTrachea DED	dTrachea VAD	P-value Control VS DED	P-value Control VS VAD
1. Young's modulus (kPa)	218.92	235.18	264.61	0.4442 ^{ns}	>0.9999 ^{ns}
	377.13	183.66	300.47		
	204.68	221.45	191.25		
	239.08	187.83	307.18		
Mean \pm SD	259.95 \pm 79.39	207.03 \pm 25.27	265.88 \pm 53.15		
2. Stress (kPa)	12.87	50.11	45.72	>0.9999 ^{ns}	>0.9999 ^{ns}
	72.16	26.67	28.85		
	31.45	16.95	20.87		
	20.94	9.63	30.04		
Mean \pm SD	34.36 \pm 26.33	25.84 \pm 17.62	31.37 \pm 10.40		
3. % Strain	9.89	25.09	25.00	>0.9999 ^{ns}	>0.9999 ^{ns}
	24.97	15.57	12.92		
	25.08	11.28	12.85		
	13.49	10.36	12.88		
Mean \pm SD	18.36 \pm 7.84	15.58 \pm 6.74	15.91 \pm 6.06		

ns = no significant difference, *P<0.05

Table. Sp3 The tensile parameters of native trachea and decellularized trachea from DED and VAD methods. Data were expressed as mean \pm standard deviation (n = 4).

Characteristics	Unwashed (Control)	dTrachea DED	dTrachea VAD	P-value Control VS DED	P-value Control VS VAD
1. Tensile strength (MPa)	4.49	1.87	2.04	0.0752 ^{ns}	>0.9999 ^{ns}
	3.68	2.37	4.69		
	2.93	3.38	4.33		
	1.59	1.90	5.18		
Mean \pm SD	3.17 \pm 1.23	2.38 \pm 0.70	4.06 \pm 1.39		
2. Ultimate tensile strength (MPa)	80.70	149.60	173.80	0.1273 ^{ns}	>0.9999 ^{ns}
	230.00	192.20	447.50		
	135.00	202.40	284.00		
	155.00	88.80	403.50		
Mean \pm SD	150.18 \pm 61.79	158.25 \pm 51.64	327.20 \pm 123.41		
3. % Elongation	38.68	69.40	74.60	0.0812 ^{ns}	0.3833 ^{ns}
	93.60	53.70	67.60		
	101.80	45.62	80.40		
	55.90	88.00	60.30		
Mean \pm SD	72.50 \pm 30.13	64.18 \pm 18.70	70.73 \pm 8.70		

ns = no significant difference, *P<0.05

3. Biochemical examination of decellularized trachea

DNA and sulphated glycosaminoglycans (sGAGs) contents were quantified. The DNA content of six specimens was significantly decreased compared to control unwashed trachea ($P < 0.0001$) (Fig. Sp5A; Table Sp4). DED method did not show significant difference in DNA content compared to VAD method in sample 1 to 5 ($P = 1$), while DNA content of sample 6 showed higher DNA content in DED method compared to VAD method ($P = 0.0153$). The DED method was able to reduce sGAG content of sample 1, 4 and 5 compared to the native trachea tissue (Fig. Sp5B; Table Sp5). However, all samples treated by the VAD method did not exhibit significant differences in sGAG contents compared to the untreated control group.

Based on sGAG content, the decellularized tracheas were categorized into three groups: Group 1, DED/low sGAG (from the DED method, samples 1, 4, and 5); Group 2, DED/high sGAG (from the DED method, samples 2 and 6); and Group 3, VAD/high sGAG (from the VAD method, samples 1, 2, 3, 4, 5, and 6). Importantly, quantitative sGAG contents from Table Sp5 confirmed that dTrachea DED had a reliable low sGAG component in samples 1, 4, and 5, while dTrachea VAD had no significant difference compared to the control group after the decellularization process.

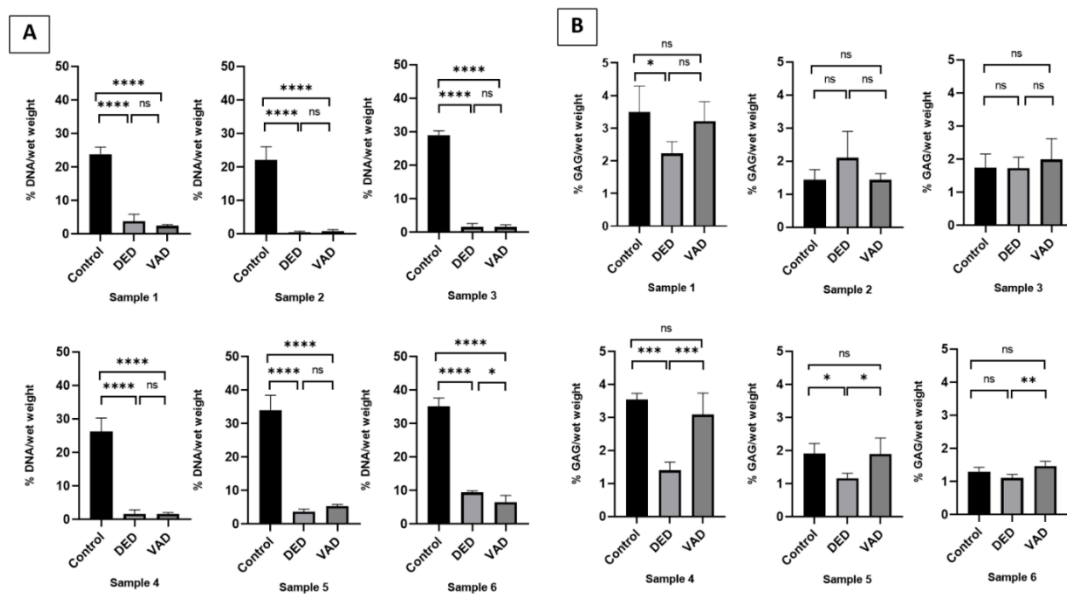


Fig. Sp5 DNA contents and extracellular matrix composition of decellularized trachea. Decellularized trachea ($n = 4$) were analyzed for (A) DNA and (B) sGAG contents. ns = not significant, ** = $P < 0.01$, *** = $P < 0.001$ and **** = $P < 0.0001$. DED = detergent-enzymatic decellularization method day 28, VAD = vacuum-assisted decellularization method day 10. Control = unwashed trachea

Table Sp4 Biochemistry testing of unwashed and decellularized trachea. Data were expressed as mean \pm standard deviation (n = 4).

DNA content (% DNA content/ wet weight)	Unwashed (Control)	dTrachea DED	dTrachea VAD	P-value		
				Control vs dTrachea DED	Control vs dTrachea VAD	DED vs VAD
Sample 1	22.93	1.31	2.89	<0.0001 ^{****}	<0.0001 ^{****}	0.8289 ^{ns}
	26.76	3.17	2.27			
	23.86	4.91	2.54			
	21.94	6.02	2.15			
Mean \pmSD	23.87 \pm2.08	3.85 \pm2.06	2.46 \pm0.33			
Sample 2	27.25	0.26	1.57	<0.0001 ^{****}	<0.0001 ^{****}	>0.9999 ^{ns}
	19.15	0.27	0.80			
	18.75	0.85	0.70			
	23.18	0.70	0.51			
Mean \pmSD	22.08 \pm3.98	0.52 \pm0.30	0.90 \pm0.47			
Sample 3	27.92	2.79	0.99	<0.0001 ^{****}	<0.0001 ^{****}	>0.9999 ^{ns}
	29.13	1.77	1.26			
	30.80	0.36	1.78			
	28.15	1.64	2.44			
Mean \pmSD	29.00 \pm1.31	1.64 \pm1.00	1.62 \pm0.64			
Sample 4	31.77	2.27	1.2	<0.0001 ^{****}	<0.0001 ^{****}	>0.9999 ^{ns}
	26.51	3.05	2.10			
	22.36	1.21	1.84			
	24.39	0.37	1.79			
Mean \pmSD	26.26 \pm4.05	1.73 \pm1.18	1.73 \pm0.38			

ns = no significant difference, ** = $P < 0.01$, *** = $P < 0.001$ and **** = $P < 0.0001$.

Table Sp4 Biochemistry testing of unwashed and decellularized trachea. Data were expressed as mean \pm standard deviation (n = 4).
(continuous)

DNA content (% DNA content/ wet weight)	Unwashed (Control)	dTrachea DED	dTrachea VAD	P-value		
				Control vs dTrachea DED	Control vs dTrachea VAD	DED vs VAD
	33.02	4.37	5.95	<0.0001 ^{****}	<0.0001 ^{****}	>0.9999 ^{ns}
	37.08	4.13	4.78			
	37.77	3.56	5.51			
Mean \pm SD	34.02 \pm 4.40	3.70 \pm 0.72	5.35 \pm 0.50			
Sample 6	37.34	9.13	3.74	<0.0001 ^{****}	<0.0001 ^{****}	0.0153 [*]
	35.72	9.26	8.91			
	31.15	10.14	7.30			
	36.28	9.41	6.24			
Mean \pm SD	35.12 \pm 2.73	9.49 \pm 0.45	6.55 \pm 2.17			

ns = no significant difference, ** = $P < 0.01$, *** = $P < 0.001$ and **** = $P < 0.0001$.

Table Sp5 Biochemistry testing of unwashed and decellularized trachea. Data were expressed as mean \pm standard deviation (n = 4).

ECM components (% sGAG content/ wet weight)	Unwashed (Control)	dTrachea DED	dTrachea VAD	P-value		
				Control vs dTrachea DED	Control vs dTrachea VAD	DED vs VAD
Sample 1	2.74	2.67	3.90	0.0473*	>0.9999 ^{ns}	0.1410 ^{ns}
	3.16	2.25	2.66			
	4.59	1.81	3.52			
	3.50	2.14	2.77			
Mean \pm SD	3.50 \pm 0.79	2.22 \pm 0.35	3.21 \pm 0.60			
Sample 2	1.04	1.40	1.59	0.2908 ^{ns}	>0.9999 ^{ns}	0.2981 ^{ns}
	1.54	1.39	1.16			
	1.35	2.83	1.48			
	1.79	2.75	1.50			
Mean \pm SD	1.43 \pm 0.32	2.09 \pm 0.81	1.43 \pm 0.19			
Sample 3	1.76	2.11	1.22	>0.9999 ^{ns}	>0.9999 ^{ns}	>0.9999 ^{ns}
	1.67	1.68	1.75			
	2.27	1.32	2.67			
	1.26	1.79	2.29			
Mean \pm SD	1.74 \pm 0.41	1.73 \pm 0.33	1.98 \pm 0.63			
Sample 4	3.31	1.23	2.43	0.0001 ^{***}	0.4530 ^{ns}	0.0009 ^{***}
	3.62	1.66	3.07			
	3.52	1.56	2.85			
	3.73	1.15	3.98			
Mean \pm SD	3.55 \pm 0.18	1.40 \pm 0.25	3.08 \pm 0.65			

ns = no significant difference, ** = P < 0.01, *** = P < 0.001 and **** = P < 0.0001.

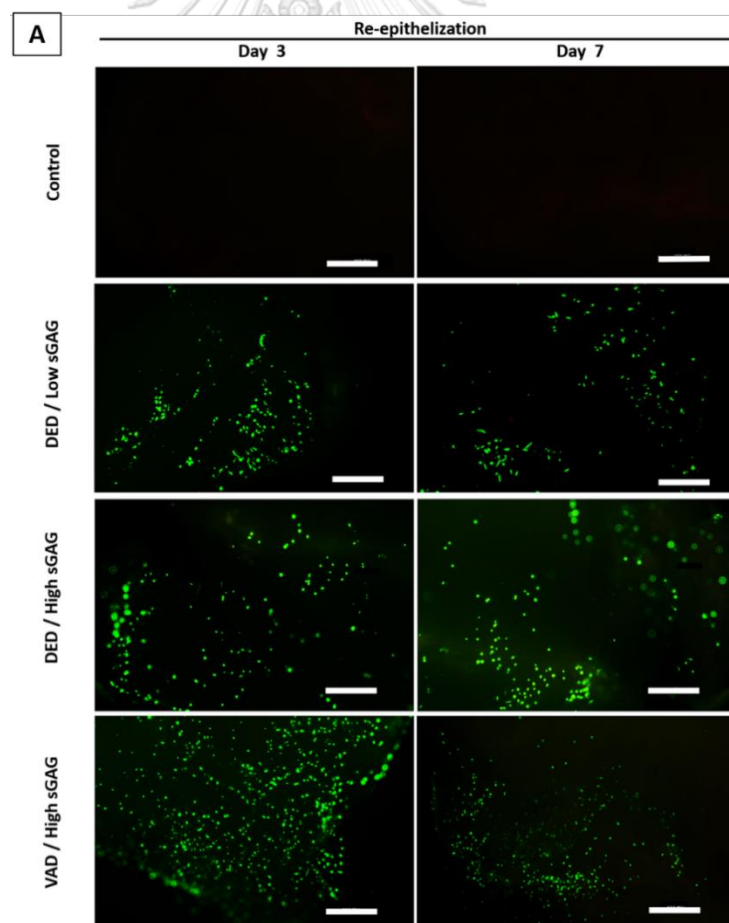
Table Sp5 Biochemistry testing of unwashed and decellularized trachea. Data were expressed as mean \pm standard deviation (n = 4).
(continuous)

ECM components (% sGAG content/ wet weight)	Unwashed (Control)	dTrachea DED	dTrachea VAD	P-value		
				Control vs dTrachea DED	Control vs dTrachea VAD	DED vs VAD
Sample 5	1.58	0.95	2.10	0.0393*	>0.9999 ^{ns}	0.0426*
	2.01	1.27	1.49			
	1.73	1.25	2.48			
	2.27	1.19	1.51			
Mean \pm SD	1.90 \pm 0.31	1.17 \pm 0.15	1.90 \pm 0.48			
Sample 6	1.37	1.11	1.51	0.1626 ^{ns}	0.2829 ^{ns}	0.0082**
	1.39	0.97	1.50			
	1.12	1.22	1.59			
	1.32	1.12	1.26			
Mean \pm SD	1.30 \pm 0.12	1.11 \pm 0.10	1.47 \pm 0.14			

ns = no significant difference, ** = $P < 0.01$, *** = $P < 0.001$ and **** = $P < 0.0001$.

4. The assessment of re-epithelization in the decellularized trachea

The HBEPc were seeded on the luminal surface of the decellularized trachea prepared by DED and VAD methods. By day 3 of culture, HBEPc were attached on low and high sGAG scaffolds. Interestingly, the high sGAG groups obtained from DED and VAD methods showed higher cell attachment than the low sGAG group (Fig. Sp6A), corresponding to DNA content result analysis (Fig. Sp6B; Table Sp6). When culture was extended to 7 days, HBEPc were detected on decellularized scaffolds. The high/sGAG VAD scaffold showed the highest DNA content on day 7 (Fig. 5B). For DED method, the high/sGAG scaffold exhibited higher DNA content than the low/sGAG scaffold on day 3. However, these 2 groups did not show a significant increased DNA content on day 7.



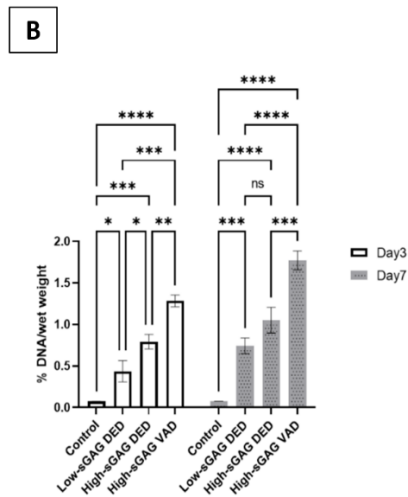


Fig. Sp6 Cytotoxicity of decellularized canine donor trachea demonstrates biocompatibility (A) Primary HBEpC cells were cultured on luminal surface of decellularized trachea for 3 and 7 days. Live cells (green) and dead cells (Red), scale bars = 500 μ m; (B) DNA content of the constructs on day 3 and 7 days. ** = $P < 0.01$, *** = $P < 0.001$ and **** = $P < 0.0001$. DED = detergent-enzymatic decellularization method, VAD = vacuum-assisted decellularization method, and Control = cell-free decellularized trachea.

Table Sp6 DNA qualification of unwashed and re-epithelization on decellularized trachea. Data were expressed as mean \pm standard deviation (n = 2).

DNA content (% DNA content/ wet weight)	Day 3	P-value					
		Control vs DED/Low sGAG	Control vs DED/High sGAG	Control vs VAD/High sGAG	DED/Low sGAG vs DED/High sGAG	DED/Low sGAG vs DED/High sGAG	DED/High sGAG vs DED/High sGAG
Unwashed (Control) (Mean \pm SD)	0.0731 \pm 0.0010	0.0229*	0.0003***	<0.0001****	0.0256*	0.0001***	0.0041**
DED/Low sGAG (Mean \pm SD)	0.4364 \pm 0.1285						
DED/High sGAG (Mean \pm SD)	0.7919 \pm 0.0871						
VAD/High sGAG (Mean \pm SD)	1.2836 \pm 0.0707						
DNA content (% DNA content/ wet weight)	Day7	P-value					
		Control vs DED/Low sGAG	Control vs DED/High sGAG	Control vs VAD/High sGAG	DED/Low sGAG vs DED/High sGAG	DED/Low sGAG vs DED/High sGAG	DED/High sGAG vs DED/High sGAG
Unwashed (Control) (Mean \pm SD)	0.0730 \pm 0.0011	0.0005***	<0.0001****	<0.0001****	0.0501 ^{ns}	<0.0001****	0.0003*
DED/Low sGAG (Mean \pm SD)	0.7429 \pm 0.0948						
DED/High sGAG (Mean \pm SD)	1.0518 \pm 0.1538						
VAD/High sGAG (Mean \pm SD)	1.7707 \pm 0.1127						

ns = no significant difference, ** = $P < 0.01$, *** = $P < 0.001$ and **** = $P < 0.0001$.

5. Micromorphological evaluation

HBEpC were seeded on decellularized trachea and visualized by scanning electron microscopy (SEM). The DED scaffold showed smooth surface and did not expose fibrous network compared to the VAD scaffold. HBEpC were able to attach on mesh-like network on the luminal surface of decellularized scaffolds. The high sGAG/VAD groups exhibited cell attachment more than other groups on both day 3

and day 7 (Fig. Sp7).

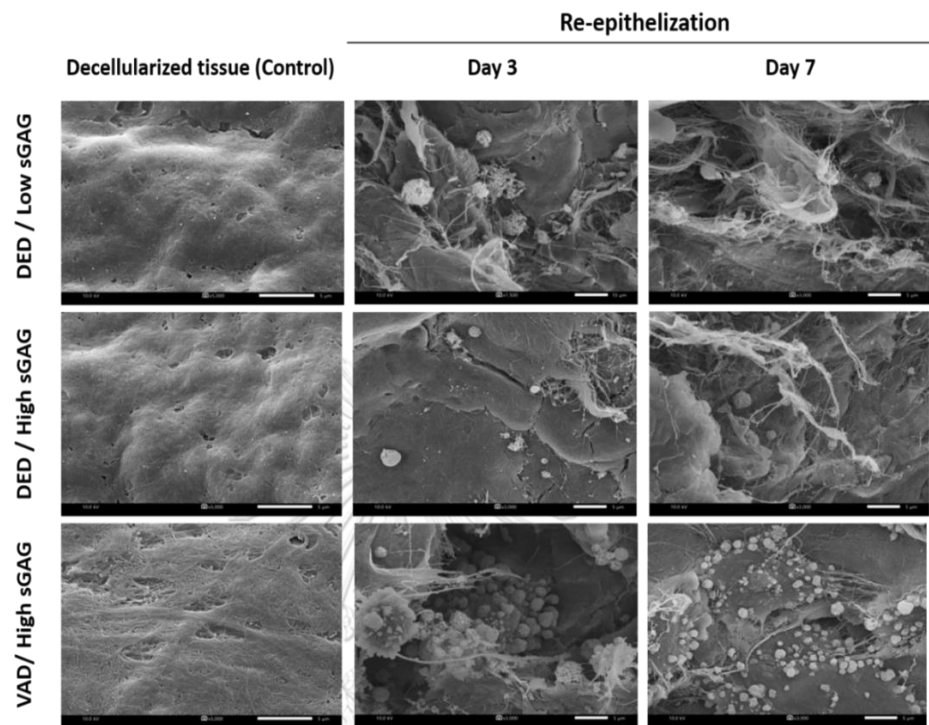


Fig. Sp7 Scanning electron micrographs of HBEPc seeded on decellularized trachea. HBEPc were seeded on decellularized trachea and cultured for 3 and 7 days. DED = detergent-enzymatic decellularization method, VAD = vacuum-assisted decellularization method, and control = cell-free decellularized scaffold (Scale bars = 5 and 10 μm)

Discussion

This study aimed to generate decellularized canine trachea that can be utilized as a scaffold to fabricate an in vitro tissue-engineered human trachea. One of the essential outcomes in trachea decellularization is the maintenance of the dense matrix of cartilaginous tissue while preserving a structurally intact and biocompatible ECM scaffold [2]. The VAD method significantly reduced the DNA content less than 10% of DNA/wet weight from the fresh canine trachea tissue similar to DED methods, while VAD reduced processing time by 18 days when compared to DED. This outcome is in line with the earlier literature [3, 4], where the VAD method could rapidly produce decellularized tracheal scaffolds, and the freezing step allowed for the banking of donor tracheas as a clinically relevant strategy. For the DED method, the repeated detergent exposure is important to disrupt the chondrocyte membranes and remove major histocompatibility complex antigens [5]. The optimization of DED method depends on the cycle of decellularization, size and it is species-specific [5, 6]. Furthermore, H&E staining showed that DED and VAD methods had a clear epithelial cell component on mucosa and submucosa of trachea while the compact structure of cartilage makes it difficult for the removal of chondrocytes. Previous studies have reported decellularization methods significantly reduced DNA content. In addition, no decellularization protocol has completely removed all cells from trachea fresh tissues [7]. Both VAD and DED approaches were able to produce intact decellularized trachea while removing MHC class II antigens, as well as cells and cell debris since DNA content less than 10% of DNA/wet weight. As a reminder, MHC class II and double-stranded DNA can induce immune responses after implantation to the host, resulting in implant rejection [8]. The Alcian blue and Safranin-O staining correlated with biochemical quantification of sGAG content. The DED method effectively removed sGAG from trachea better than the VAD. The Pentachrome findings showed that the ECM components of decellularized trachea

with both methods were decreased compared to native trachea. Hence, the decellularization approach cannot remove all cells/DNA from ECM without physically damaging the tissues.

Decellularized trachea shared similar biomechanical properties with native trachea, which is an important aim for a successful tissue-engineered trachea scaffold. The biomechanical properties of trachea are derived from the trachea cartilage layer rather than other layers like the epithelial mucosa [9]. Hence, supporting the trachea cartilage must be considered. Here, we comprehensively tested the biomechanical properties of both VAD and DED decellularized scaffolds. All decellularized trachea returned to their original state after mechanical forces were removed, which indicated that the trachea dECM for each group was highly elastic. Interestingly, sGAG are the essential components of the tracheal cartilage and provided its mechanical strength to resist compressive forces [5]. Tensile properties (tensile strength, ultimate tensile strength and % elongation) of both decellularized trachea methods were not significantly different from native trachea. These indicated that the decellularized trachea of both methods had good radial support capacity and elasticity. Therefore, a decellularized trachea matrix might have no detrimental effect on trachea collapse after implantation. Nevertheless, this study demonstrated a feasible approach for producing robust biomechanical properties from canine dECM trachea.

The potential to regenerate a transplantable respiratory mucosal layer with mucociliary function would be a major step forward in the field of airway regenerative medicine. The approach to regenerate respiratory mucosa needs to consider the ECM microenvironment [10]. Previous studies have shown the proteomic data indicated that collagen I, collagen IV, laminin, vitronectin, and fibronectin play critical roles in modifying epithelial cell behavior. [11-13]. Sulfates glycosaminoglycans (sGAG) are native components of the ECM that regulate many

cellular processes, such as adhesion, proliferation, migration, differentiation, survival, and death [14]. The preservation of sGAG in the decellularized trachea is important for scaffold biocompatibility. While cells are in contact with a scaffold, many cell behaviors can occur, and a mechanosensing process takes place between cells and the scaffolds through integrins and cytoskeleton [15]. As airway epithelial cells represent a key functional aspect of the bioengineered trachea [16, 17]. Here, we demonstrated scaffold biocompatibility using primary human bronchial epithelial cells (HBEpC) in high and low sGAG. The uniqueness of this study exists in the fact that high sGAG content in DED and VAD scaffolds influenced cell adhesion on a scaffold more than low sGAG in DED scaffold. Moreover, SEM analysis indicated that more HBEpC attached to VAD scaffold corresponds with DNA content removal. A related study demonstrated sGAG have robust effect on matrix-associated growth factor binding and lung cell metabolism in ECM gel from decellularized lungs [18]. Hence, ECM components, especially sGAG are an essential component for cell-matrix interactions. Further research might focus on the functional role of sGAG in intact decellularized scaffolds.

The DED method is likely the most conventional method for tissue or organ decellularization while the VAD method seems to help support the chemical and enzymatic methods. The finding of the present study suggests that vacuum-assisted decellularization (VAD) of canine trachea can be maintained ECM components, biomechanical properties and biocompatibility for epithelial cells compared to the detergent enzymatic decellularization (DED). Importantly, canine trachea derived from decellularized VAD scaffolds demonstrate the ability to retain sGAG and preserve the structural integrity of the tracheal lumen after the decellularization process.

The VAD method offers several advantages, including rapidity, cost reduction, and high efficiency, making it a valuable approach for developing tissue-engineered

trachea scaffolds in canines. Hence, the VAD method has the potential to be a powerful tool in the field of tracheal tissue engineering. The future direction from preliminary data will be to use the VAD method for further study of the development of decellularized tracheal scaffold and hydrogel.

References (Supplementary data; preliminary data)

- [1] S. Yodmuang, S.L. McNamara, A.B. Nover, B.B. Mandal, M. Agarwal, T.-A.N. Kelly, P.-h.G. Chao, C. Hung, D.L. Kaplan, G. Vunjak-Novakovic, Silk microfiber-reinforced silk hydrogel composites for functional cartilage tissue repair, *Acta Biomater* 11 (2015) 27-36.
- [2] U. Mendibil, R. Ruiz-Hernandez, S. Retegi-Carrion, N. Garcia-Urquia, B. Olalde-Graells, A. Abarategi, Tissue-specific decellularization methods: rationale and strategies to achieve regenerative compounds, *Int J Mol Sci* 21(15) (2020) 5447.
- [3] B. Ozpolat, O.A. Gurpinar, E.S. Ayva, S. Gazyagci, M. Niyaz, The effect of basic fibroblast growth factor and adipose tissue-derived mesenchymal stem cells on wound healing, epithelization and angiogenesis in a tracheal resection and end-to-end anastomosis rat model, *Turk J Thorac Cardiovasc Surg* (2013).
- [4] M. Abdul-Al, G.K. Kyeremeh, M. Saeinasab, S. Heidari Keshel, F. Sefat, Stem cell niche microenvironment: review, *Bioengineering (Basel)* 8(8) (2021) 108.
- [5] D. Zhu, Z. Jiang, N. Li, X. Wang, L. Ren, Y. Ye, Y. Pan, G. Yang, Insights into the use of genetically modified decellularized biomaterials for tissue engineering and regenerative medicine, *Adv Drug Deliv Rev* 188 (2022) 114413.
- [6] U. Mendibil, R. Ruiz-Hernandez, S. Retegi-Carrion, N. Garcia-Urquia, B. Olalde-Graells, A. Abarategi, Tissue-specific decellularization methods: rationale and strategies to achieve regenerative compounds, *Int J Mol Sci* 21(15) (2020) 5447.
- [7] M. Brown, J. Li, C. Moraes, M. Tabrizian, N.Y. Li-Jessen, Decellularized extracellular matrix: New promising and challenging biomaterials for regenerative medicine, *Biomaterials* 289 (2022) 121786.
- [8] K. Ohata, H.C. Ott, Human-scale lung regeneration based on decellularized matrix scaffolds as a biologic platform, *Surg Today* 50(7) (2020) 633-643.

- [9] A. Badileanu, C. Mora-Navarro, A.M. Gracioso Martins, M.E. Garcia, D. Sze, E.W. Ozpinar, L. Gaffney, J.R. Enders, R.C. Branski, D.O. Freytes, Fast automated approach for the derivation of acellular extracellular matrix scaffolds from porcine soft tissues, *ACS Biomater Sci Eng* 6(7) (2020) 4200-4213.
- [10] C. Ye, J. Chen, Y. Qu, H. Qi, Q. Wang, Z. Yang, A. Wu, F. Wang, P. Li, Naringin in the repair of knee cartilage injury via the TGF- β /ALK5/Smad2/3 signal transduction pathway combined with an acellular dermal matrix, *JOT* 32 (2022) 1-11.
- [11] F. Sensi, E. D'angelo, A. Biccari, A. Marangio, G. Battisti, S. Crotti, M. Fassan, C. Laterza, M. Giomo, N. Elvassore, Establishment of a human 3D pancreatic adenocarcinoma model based on a patient-derived extracellular matrix scaffold, *Transl Res* 253 (2022) 57-67.
- [12] A. Biehl, A.M.G. Martins, Z.G. Davis, D. Sze, L. Collins, C. Mora-Navarro, M.B. Fisher, D.O. Freytes, Towards a standardized multi-tissue decellularization protocol for the derivation of extracellular matrix materials, *Biomater Sci* 11 (2023) 641-654.
- [13] A. Frey, L.P. Lunding, J.C. Ehlers, M. Weckmann, U.M. Zissler, M. Wegmann, More than just a barrier: the immune functions of the airway epithelium in asthma pathogenesis, *Front Immunol* 11 (2020) 761.
- [32] G.C. Hansson, Mucus and mucins in diseases of the intestinal and respiratory tracts, *J Intern Med* 285(5) (2019) 479-490.
- [33] H. Zhang, W. Fu, Z. Xu, Re-epithelialization: a key element in tracheal tissue engineering, *Regen Med* 10(8) (2015) 1005-1023.
- [34] D.J. Minnich, D.J. Mathisen, Anatomy of the trachea, carina, and bronchi, *Thorac Surg Clin* 17(4) (2007) 571-585.
- [35] A.A. Mete, İlknur Hatice, Functional anatomy and physiology of airway, in: R.H. Erbay (Ed.), *Tracheal Intubation*, IntechOpen2018.
- [36] M.J. Elliott, P. De Coppi, S. Speggin, D. Roebuck, C.R. Butler, E. Samuel, C. Crowley, C. McLaren, A. Fierens, D. Vondrys, Stem-cell-based, tissue engineered tracheal replacement in a child: a 2-year follow-up study, *Lancet* 380(9846) (2012) 994-1000.

REFERENCES



จุฬาลงกรณ์มหาวิทยาลัย
CHULALONGKORN UNIVERSITY



จุฬาลงกรณ์มหาวิทยาลัย
CHULALONGKORN UNIVERSITY

VITA

NAME Pensuda Sompunga

DATE OF BIRTH 2 November 1990

PLACE OF BIRTH Sisaket

INSTITUTIONS ATTENDED MASTER OF SCIENCE (BIOTECHNOLOGY)
School of Biotechnology, Institute of Agricultural
Technology (IAT), Suranaree University of Technology,
THAILAND.

BACHELOR OF SCIENCE (BIOMEDICAL SCIENCE)
Faculty of Science from Rangsit University, THAILAND.

HOME ADDRESS 120/1 Moo.7, Pho Sub-District, Muang District, Sisaket,
THAILAND 33000.

PUBLICATION Sompunga P, Pruksametanan N, Rangnoi K,
Choowongkomon K, Yamabhai M (2019) Generation of
human and rabbit recombinant antibodies for the
detection of Zearalenone by phage display antibody
technology. *Talanta* 201:397–405.

AWARD RECEIVED BRONZE MEDAL AWARD
45th International Exhibition of Inventions of Geneva, at
Geneva, Switzerland.
Yamabhai M., Rangnoi K., and Sompunga, P.
Title: Mycotoxin test kits using recombinant antibodies.

1. Ainsworth D, Hackett R. Chapter 7-Disorders of the respiratory system. J Equine Internal Medicine . Saint Louis: WB Saunders 2004.
2. Etienne H, Fabre D, Caro AG et al. Tracheal replacement. J European Respiratory Journal. 2018; 51.
3. Delaere P, Van Raemdonck D. Tracheal replacement. J Journal of thoracic disease. 2016; 8: S186.
4. Dolcimascolo A, Calabrese G, Conoci S, Parenti R. Innovative biomaterials for tissue engineering. In Biomaterial-supported Tissue Reconstruction or Regeneration. IntechOpen 2019.
5. Mendibil U, Ruiz-Hernandez R, Retegi-Carrion S et al. Tissue-specific decellularization methods: Rationale and strategies to achieve regenerative compounds. Int J Mol Sci 2020; 21: 5447.
6. Lange P, Greco K, Partington L et al. Pilot study of a novel vacuum-assisted method for decellularization of tracheae for clinical tissue engineering applications. J tissue engineering and regenerative medicine. 2017; 11: 800-811.
7. Wang Z, Sun F, Lu Y et al. Rapid Preparation Method for Preparing Tracheal Decellularized Scaffolds: Vacuum Assistance and Optimization of DNase I. J ACS omega. 2021; 6: 10637-10644.
8. Butler CR, Hynds RE, Crowley C et al. Vacuum-assisted decellularization: an accelerated protocol to generate tissue-engineered human tracheal scaffolds. J Biomaterials 2017; 124: 95-105.
9. Lee JS-j, Park J, Shin D-A et al. Characterization of the biomechanical properties of canine trachea using a customized 3D-printed apparatus. J Auris Nasus Larynx 2019; 46: 407-416.
10. Furlow PW, Mathisen D. Surgical anatomy of the trachea. J Annals of cardiothoracic surgery. 2018; 7: 255.
11. Dhasmana A, Singh A, Rawal S. Biomedical grafts for tracheal tissue repairing and regeneration “Tracheal tissue engineering: an overview”. J Tissue Eng Regen Med. 2020; 14: 653-672.
12. Thornton DJ, Rousseau K, McGuckin MA. Structure and function of the

- polymeric mucins in airways mucus. *J Annu. Rev. Physiol.* 2008; 70: 459-486.
13. Ma J, Rubin BK, Voynow JA. Mucins, mucus, and goblet cells. *J Chest.* 2018; 154: 169-176.
 14. Zepp JA, Morrissey EE. Cellular crosstalk in the development and regeneration of the respiratory system. *J Nature reviews Molecular cell biology.* 2019; 20: 551-566.
 15. Zhang H, Fu W, Xu Z. Re-epithelialization: a key element in tracheal tissue engineering. *J Regenerative medicine.* 2015; 10: 1005-1023.
 16. Turakhia A, Little BP, Henry TS. Tracheal narrowing and tracheomalacia. *J Chest Imaging.* 2019; 313.
 17. Mattioli F, Marchioni A, Andreani A et al. Post-intubation tracheal stenosis in COVID-19 patients. *J European Archives of Oto-Rhino-Laryngology.* 2021; 278: 847-848.
 18. Fiacchini G, Tricò D, Ribechini A et al. Evaluation of the incidence and potential mechanisms of tracheal complications in patients with COVID-19. *J JAMA Otolaryngology–Head Neck Surgery.* 2021; 147: 70-76.
 19. Martinod E, Seguin A, Radu DM et al. Airway transplantation: a challenge for regenerative medicine. *J European journal of medical research.* 2013; 18: 1-5.
 20. Damiano G, Palumbo VD, Fazzotta S et al. Current Strategies for Tracheal Replacement: A Review. *J Life.* 2021; 11: 618.
 21. Chiang T, Pepper V, Best C et al. Clinical translation of tissue engineered trachea grafts. *J Annals of Otolology, Rhinology Laryngology.* 2016; 125: 873-885.
 22. Hamilton NJ, Hynds RE, Gowers KH et al. Using a three-dimensional collagen matrix to deliver respiratory progenitor cells to decellularized trachea in vivo. *J Tissue Engineering Part C: Methods.* 2019; 25: 93-102.
 23. Zhang Y, Xu Y, Liu Y et al. Porous decellularized trachea scaffold prepared by a laser micropore technique. *J Mech Behav Biomed Mater.* 2019; 90: 96-103.
 24. Herberhold C, Franz B, Breipohl W. Chemical preserved human trachea as prosthesis in covering tracheal defects--first experiences (author's transl). *J Laryngologie, Rhinologie, Otologie* 1980; 59: 453-457.
 25. Greaney AM, Niklason LE. The history of engineered tracheal replacements:

- interpreting the past and guiding the future. *J Tissue Engineering Part B: Reviews*. 2020.
26. Bogan SL, Teoh GZ, Birchall MA. Tissue engineered airways: a prospects article. *J. Cell. Biochem*. 2016; 117: 1497-1505.
 27. Zang M, Zhang Q, Chang El et al. Decellularized tracheal matrix scaffold for tissue engineering. *J Plastic reconstructive surgery*. 2012; 130: 532-540.
 28. Baiguera S, Jungebluth P, Burns A et al. Tissue engineered human tracheas for in vivo implantation. *J Biomaterials*. 2010; 31: 8931-8938.
 29. Haag J, Baiguera S, Jungebluth P et al. Biomechanical and angiogenic properties of tissue-engineered rat trachea using genipin cross-linked decellularized tissue. *J Biomaterials*. 2012; 33: 780-789.
 30. Jungebluth P, Go T, Asnaghi A et al. Structural and morphologic evaluation of a novel detergent-enzymatic tissue-engineered tracheal tubular matrix. *J thoracic cardiovascular surgery*. 2009; 138: 586-593.
 31. Sun F, Jiang Y, Xu Y et al. Genipin cross-linked decellularized tracheal tubular matrix for tracheal tissue engineering applications. *J Scientific reports*. 2016; 6: 1-12.
 32. McCrary MW, Vaughn NE, Hlavac N et al. Novel sodium deoxycholate-based chemical decellularization method for peripheral nerve. *J Tissue Engineering Part C: Methods*. 2020; 26: 23-36.
 33. Wang Z, Sun F, Lu Y et al. Rapid preparation of decellularized trachea as a 3D scaffold for organ engineering. *J The International Journal of Artificial Organs*. 2021; 44: 55-64.
 34. Sun F, Lu Y, Wang Z et al. Directly construct microvascularization of tissue engineering trachea in orthotopic transplantation. *J Materials Science Engineering: C* 2021; 112201.
 35. Doolin EJ, Strande LF, Sheng X, Hewitt CW. Engineering a composite neotrachea with surgical adhesives. *J pediatric surgery*. 2002; 37: 1034-1037.
 36. Kojima K, Bonassar LJ, Roy AK et al. A composite tissue-engineered trachea using sheep nasal chondrocyte and epithelial cells. *J The FASEB journal* 2003; 17: 823-828.

37. Macchiarini P, Jungebluth P, Go T et al. Clinical transplantation of a tissue-engineered airway. *J The Lancet* 2008; 372: 2023-2030.
38. Kobayashi K, Nomoto Y, Suzuki T et al. Effect of fibroblasts on tracheal epithelial regeneration in vitro. *J Tissue Engineering Part B: Reviews*. 2006; 12: 2619-2628.
39. Nomoto Y, Kobayashi K, Tada Y et al. Effect of fibroblasts on epithelial regeneration on the surface of a bioengineered trachea. *J Annals of Otolology, Rhinology Laryngology* 2008; 117: 59-64.
40. Hirsch T, Rothoeft T, Teig N et al. Regeneration of the entire human epidermis using transgenic stem cells. *J Nature*. 2017; 551: 327-332.
41. Danahay H, Pessotti AD, Coote J et al. Notch2 is required for inflammatory cytokine-driven goblet cell metaplasia in the lung. *J Cell reports* 2015; 10: 239-252.
42. Tas S, Bölükbas D, Alsafadi H et al. Decellularized extracellular matrix hydrogels for human airway organoid culture. In. *Eur Respiratory Soc* 2021.
43. Ullah I, Busch JF, Rabien A et al. Adult Tissue Extracellular Matrix Determines Tissue Specification of Human iPSC-Derived Embryonic Stage Mesodermal Precursor Cells. *J Advanced Science* 2020; 7: 1901198.
44. Pattar SS, Fatehi Hassanabad A, Fedak PW. Acellular extracellular matrix bioscaffolds for cardiac repair and regeneration. *J Frontiers in cell developmental biology*. 2019; 7: 63.
45. Zhang W, Du A, Liu S et al. Research progress in decellularized extracellular matrix-derived hydrogels. *J Regenerative Therapy* 2021; 18: 88-96.
46. Tottey S, Johnson SA, Crapo PM et al. The effect of source animal age upon extracellular matrix scaffold properties. *J Biomaterials* 2011; 32: 128-136.
47. Yodmuang S, McNamara SL, Nover AB et al. Silk microfiber-reinforced silk hydrogel composites for functional cartilage tissue repair. *Acta Biomater* 2015; 11: 27-36.
48. Freytes DO, Martin J, Velankar SS et al. Preparation and rheological characterization of a gel form of the porcine urinary bladder matrix. *J Biomaterials* 2008; 29: 1630-1637.

49. López-Martínez S, Campo H, de Miguel-Gómez L et al. A Natural Xenogeneic Endometrial Extracellular Matrix Hydrogel Toward Improving Current Human in vitro Models and Future in vivo Applications. *J Frontiers in bioengineering biotechnology* 2021; 9: 156.
50. Pouliot RA, Young BM, Link PA et al. Porcine lung-derived extracellular matrix hydrogel properties are dependent on pepsin digestion time. *J Tissue Engineering Part C: Methods*. 2020; 26: 332-346.
51. Kang H-W, Lee SJ, Ko IK et al. A 3D bioprinting system to produce human-scale tissue constructs with structural integrity. *Nat Biotechnol* 2016; 34: 312-319.
52. Darling NJ, Mobbs CL, González-Hau AL et al. Bioengineering novel in vitro co-culture models that represent the human intestinal mucosa with improved Caco-2 structure and barrier function. *Front. Bioeng. Biotechnol.* 2020; 8: 992.
53. Sirichoat A, Kaewseekhao B, Nithichanon A et al. Proteomic Profiles and Protein Network Analysis of Primary Human Leukocytes Revealed Possible Clearance Biomarkers for Staphylococcus aureus Infection. *Curr Microbiol* 2023; 80: 335.
54. Tyanova S, Temu T, Cox J. The MaxQuant computational platform for mass spectrometry-based shotgun proteomics. *Nat. Protoc.* 2016; 11: 2301-2319.
55. Pang Z, Zhou G, Ewald J et al. Using MetaboAnalyst 5.0 for LC–HRMS spectra processing, multi-omics integration and covariate adjustment of global metabolomics data. *Nat. Protoc.* 2022; 17: 1735-1761.
56. Szklarczyk D, Santos A, Von Mering C et al. STITCH 5: augmenting protein–chemical interaction networks with tissue and affinity data. *Nucleic Acids Res* 2016; 44: D380-D384.
57. Ge SX, Jung D, Yao R. ShinyGO: a graphical gene-set enrichment tool for animals and plants. *Bioinformatics* 2020; 36: 2628-2629.
58. Bourguin PE, Pippenger BE, Todorov Jr A et al. Tissue decellularization by activation of programmed cell death. *Biomaterials* 2013; 34: 6099-6108.
59. Kasravi M, Ahmadi A, Babajani A et al. Immunogenicity of decellularized

- extracellular matrix scaffolds: a bottleneck in tissue engineering and regenerative medicine. *J Biomed Mater Res* 2023; 27: 1-24.
60. Barbulescu GI, Bojin FM, Ordodi VL et al. Decellularized extracellular matrix scaffolds for cardiovascular tissue engineering: Current techniques and challenges. *Int. J. Mol. Sci.* 2022; 23: 13040.
 61. Brown M, Li J, Moraes C et al. Decellularized extracellular matrix: New promising and challenging biomaterials for regenerative medicine. *Biomaterials* 2022; 121786.
 62. Biehl A, Martins AMG, Davis ZG et al. Towards a standardized multi-tissue decellularization protocol for the derivation of extracellular matrix materials. *Biomater. Sci* 2023; 11: 641-654.
 63. Saldin LT, Cramer MC, Velankar SS et al. Extracellular matrix hydrogels from decellularized tissues: Structure and function. *Acta Biomater* 2017; 49: 1-15.
 64. Tsou Y-H, Khoneisser J, Huang P-C, Xu X. Hydrogel as a bioactive material to regulate stem cell fate. *Bioact. Mater* 2016; 1: 39-55.
 65. Balestrini JL, Gard AL, Gerhold KA et al. Comparative biology of decellularized lung matrix: Implications of species mismatch in regenerative medicine. *Biomaterials* 2016; 102: 220-230.
 66. Elliott MJ, De Coppi P, Speggiorin S et al. Stem-cell-based, tissue engineered tracheal replacement in a child: a 2-year follow-up study. *The Lancet* 2012; 380: 994-1000.
 67. Baiguera S, Del Gaudio C, Kuevda E et al. Dynamic decellularization and cross-linking of rat tracheal matrix. *Biomaterials* 2014; 35: 6344-6350.
 68. Batioglu-Karaaltin A, Karaaltin MV, Ovali E et al. In vivo tissue-engineered allogenic trachea transplantation in rabbits: a preliminary report. *Stem Cell Rev Rep* 2015; 11: 347-356.
 69. Zhong Y, Yang W, Yin Pan Z et al. In vivo transplantation of stem cells with a genipin linked scaffold for tracheal construction. *J. Biomater. Appl* 2019; 34: 47-60.
 70. Kokubun K, Pankajakshan D, Kim MJ, Agrawal DK. Differentiation of porcine mesenchymal stem cells into epithelial cells as a potential therapeutic

- application to facilitate epithelial regeneration. *J Tissue Eng Regen Med.* 2016; 10: E73-E83.
71. Kobayashi K, Suzuki T, Nomoto Y et al. A tissue-engineered trachea derived from a framed collagen scaffold, gingival fibroblasts and adipose-derived stem cells. *Biomaterials* 2010; 31: 4855-4863.
 72. Yang Q, Peng J, Guo Q et al. A cartilage ECM-derived 3-D porous acellular matrix scaffold for in vivo cartilage tissue engineering with PKH26-labeled chondrogenic bone marrow-derived mesenchymal stem cells. *Biomaterials* 2008; 29: 2378-2387.
 73. Gong YY, Xue JX, Zhang WJ et al. A sandwich model for engineering cartilage with acellular cartilage sheets and chondrocytes. *Biomaterials* 2011; 32: 2265-2273.
 74. Shin YS, Lee BH, Choi JW et al. Tissue-engineered tracheal reconstruction using chondrocyte seeded on a porcine cartilage-derived substance scaffold. *Int J Pediatr Otorhinolaryngol* 2014; 78: 32-38.
 75. Mohamed MA, Fallahi A, El-Sokkary AM et al. Stimuli-responsive hydrogels for manipulation of cell microenvironment: From chemistry to biofabrication technology. *Prog. Polym. Sci* 2019; 98: 101147.
 76. Elliott MJ, Butler CR, Varanou-Jenkins A et al. Tracheal replacement therapy with a stem cell-seeded graft: lessons from compassionate use application of a GMP-compliant tissue-engineered medicine. *Stem Cells Transl Med* 2017; 6: 1458-1464.
 77. Adamo D, Galaverni G, Genna VG et al. The growing medical need for tracheal replacement: reconstructive strategies should overcome their limits. *Front. Bioeng. Biotechnol* 2022; 10: 846632.
 78. Ravindra A, D'Angelo W, Zhang L et al. Human Bronchial Epithelial Cell Growth on Homologous Versus Heterologous Tissue Extracellular Matrix. *J Surg Res* 2021; 263: 215-223.
 79. Marinkovich MP, Keene DR, Rimberg CS, Burgeson RE. Cellular origin of the dermal-epidermal basement membrane. *Dev. Dyn* 1993; 197: 255-267.
 80. Kim YS, Majid M, Melchiorri AJ, Mikos AG. Applications of decellularized

- extracellular matrix in bone and cartilage tissue engineering. *Bioeng. transl. med* 2019; 4: 83-95.
81. Yamaya M, Finkbeiner W, Chun S, Widdicombe J. Differentiated structure and function of cultures from human tracheal epithelium. *Physiol. J* 1992; 262: L713-L724.
 82. Bhat M, Toledo-Velasquez D, Wang L et al. Regulation of tight junction permeability by calcium mediators and cell cytoskeleton in rabbit tracheal epithelium. *Pharm. Res* 1993; 10: 991-997.
 83. Maurer J, Walles T, Wiese-Rischke C. Optimization of Primary Human Bronchial Epithelial 3D Cell Culture with Donor-Matched Fibroblasts and Comparison of Two Different Culture Media. *Int. J. Mol. Sci* 2023; 24: 4113.
 84. Xiaojun W, Yan L, Hong X et al. Acetylated α -tubulin regulated by N-acetylseryl-aspartyl-lysyl-proline (Ac-SDKP) exerts the anti-fibrotic effect in rat lung fibrosis induced by silica. *Sci Rep* 2016; 6: 32257.
 85. Jacob JT, Coulombe PA, Kwan R, Omary MB. Types I and II keratin intermediate filaments. *Cold Spring Harb. Protoc* 2018; 10: a018275.
 86. Smirnova N, Schamberger A, Nayakanti S et al. Detection and quantification of epithelial progenitor cell populations in human healthy and IPF lungs. *Respir. Res* 2016; 17: 1-11.
 87. Ostrowska-Podhorodecka Z, Ding I, Norouzi M, McCulloch CA. Impact of vimentin on regulation of cell signaling and matrix remodeling. *Front. Cell Dev. Biol* 2022; 10: 869069.
 88. Feng Z, Wagatsuma Y, Kikuchi M et al. The mechanisms of fibroblast-mediated compaction of collagen gels and the mechanical niche around individual fibroblasts. *Biomaterials* 2014; 35: 8078-8091.
 89. Cox TR, Erler JT. Remodeling and homeostasis of the extracellular matrix: implications for fibrotic diseases and cancer. *DMM* 2011; 4: 165-178.
 90. Davenport EA, Nettlesheim P. Regulation of mucociliary differentiation of rat tracheal epithelial cells by type I collagen gel substratum. *Am. J. Respir. Cell Mol. Biol* 1996; 14: 19-26.
 91. Cheng F, Shen Y, Mohanasundaram P et al. Vimentin coordinates fibroblast

- proliferation and keratinocyte differentiation in wound healing via TGF- β -Slug signaling. CELL BIOLOGY 2016; 113: E4320-E4327.
92. Sorrell JM, Somoza RA, Caplan AI. Human mesenchymal stem cells induced to differentiate as chondrocytes follow a biphasic pattern of extracellular matrix production. J Orthop Res 2018; 36: 1757-1766.
93. Twomey J, Thakore P, Hartman D et al. Roles of type VI collagen and decorin in human mesenchymal stem cell biophysics during chondrogenic differentiation. J Eur Cell Mater 2014; 27: 237-250.
94. Gadjanski I, Spiller K, Vunjak-Novakovic G. Time-dependent processes in stem cell-based tissue engineering of articular cartilage. Stem Cell Rev Rep 2012; 8: 863-881.

